THE UNIVERSITY OF CHICAGO

TBX5A FUNCTIONS IN ANTERIOR LATERAL PLATE MESODERM SPECIFICATION AND MIGRATION IN ZEBRAFISH EMBRYOS

A DISSERTATION SUBMITTED TO
THE FACULTY OF THE DIVISION OF THE BIOLOGICAL SCIENCES
AND THE PRITZKER SCHOOL OF MEDICINE
IN CANDIDACY FOR THE DEGREE OF
DOCTOR OF PHILOSOPHY

COMMITTEE ON DEVELOPMENT, REGENERATION, AND STEM CELL BIOLOGY

BY
LINDSEY MEGAN FONG MAO

CHICAGO, ILLINOIS
MARCH 2019

To the LORD, who brought me out of darkness and gave me a new identity and purpose, without whom, I would not have life and freedom today. When I dedicated my life to Jesus in January 2015, I did not withhold giving my career and productivity to him. Instead, I gave more than I knew I was capable of due to the power of the Holy Spirit inside me.

"Concerning this, I pleaded with the Lord three times to take it away from me. But He said to me, 'My grace is sufficient for you, for power is perfected in weakness.' Therefore, I will most gladly boast all the more about my weaknesses, so that Christs power may reside in me. So I take pleasure in weaknesses, insults, catastrophes, persecutions, and in pressures, because of Christ. For when I am weak, then I am strong."

2 Corinthians 12:8-10, HCSB

Table of Contents

List of Figures

List of Tables

ACKNOWLEDGMENTS

In general, this dissertation would not have been able to be completed without the help of others. Mainly, my gratitude is directed to the Lord, whom I have already dedicated this piece of work to. To elaborate, God saved me during graduate school and opened Himself up to me to learn about Him and to start a relationship with Him. Through my daily striving to know Jesus more and more, I have found fulfillment in my life. Without fulfillment, I would never have been able to rationalize why I was at UChicago in the first place. Without knowing why I am here, I would never have been able to establish a life here. Yes, all the glory to God, who has worked in each of the following relationships and resources I mention below.

Thank you to my adviser, Robert Ho. You have provided me with generous academic guidance throughout my time here. I greatly appreciate your experimental expertise and I would not have been able to complete such a technically difficult project without your help and critical eye. Through these last stages of my program, you have made yourself available for working through my data for hours at a time–I really appreciate that. I also thank you for supporting my goals in and outside of the lab and for writing the tens of recommendation letters that have progressed me onward in my career.

Thank you to my faculty committee members, Akira, Vicky, and Ivan. Each of you have contributed to the academic excellence of this dissertation. By providing suggestions at my committee meetings, you have improved the quality of my science and the way that I present it. By criticizing my person and preparedness, you have helped me build resilience, strength, and faith.

Thank you to my labmates: Haley, Chris, Alana, Adam, Erin, and Stephanie. Haley–you have been an incredible mentor to me. In fact, you are the main reason why I joined the Ho lab to begin with. I have always appreciated your honesty and willingness to share with me the good, the bad, and ugly. Chris–your willingness to help with experiments late into

the night has saved me so many times. I am thankful for your quiet presence and gentle support. Alana–out of the whole lab, conversations with you have sharpened my scientific mind the most. Your enthusiasm in entertaining crazy science ideas and troubleshooting various hypotheses has made the dark exploration period of grad school fun and exciting. I have greatly appreciated going through the job search process with you and thank you for the companionship and bar-setting in that regard. Adam–thank you for the wide range of supports you provide the lab... the fish care and confocal maintenance being the most crucial and the puzzle supply being the most destressing. Erin–as my forever grad school companion, I definitely could not have done all of this without you. Thank you for your help in data acquisition, coding help, pace-setting, proof-reading, and ultimately, companionship through these 5.5 years. Just like real twins, we experienced a formative time in our lives together (in the womb, you might say), and I'm sure that the relationship will last onwards. Stephanie– thank you for being my cheerleader, giving me you can do its and checking up on me. Also your fish cartoons really help relieve the stress.

Outside of the lab, I have had a lot of help from other support networks on campus. Thank you to the academic and career support networks within my Molecular Biosciences cohort, the Chicago Center for Teaching, UChicagoGRAD, and the National Center for Faculty Development and Diversity.

Ive experienced life changing transformational growth thanks to the spiritual communities of Intervarsity Christian Fellowship and Hyde Park University Bible Fellowship. Emotional and spiritual support is extremely important in grad school. I can seriously say that these ministries saved my life. Ultimately, of course, all the honor, gratitude, and glory goes to God.

Lastly, I will thank my family. I recognize its not easy sending your child across the country for almost 10 years of study. But what youve taught me and instilled in me growing up is the importance of choosing to walk my own path, expanding my options, and enjoying

the process. I definitely could not have accomplished all that I have if it werent for you. Thank you to my husband, Tim. These last couple of months has been really difficult. Youve led us as a family, leaping us into the unknown of rural Illinois, because you have huge faith in what I can accomplish, which I sometimes lack. Thank you for cooking and doing the dishes, taking care of the moving and packing at home, and supporting my frail emotions these last few months. I love you.

ABSTRACT

The mechanisms behind fate specification are of great interest to developmental biologists. By understanding how organs form and take shape in the developing embryos, we can better understand how mutations and environmental factors impact congenital birth defects. Patients with Holt Oram Syndrome (HOS) carry a mutation in TBX5 and exhibit forelimb and cardiac septal defects. Often, the forelimb defects are more severe in the left arm than the right. Also, considering that the septum primum is a left-sided structure in the developing heart, the role of TBX5 in left-right patterning is particularly important.

tbx5a is expressed in the anterior lateral plate mesoderm (ALPM) in zebrafish, which consists of several precursor fates: cardiac mesoderm; the pericardial sac; pharyngeal arches; and the peritoneum. At 18 hours post fertilization (hpf), the cells of the lateral ALPM undergo migration anteriorly and laterally. Both homozygous mutation in *tbx5a* and Tbx5a-deficiency result in forelimb and heart looping defects, similar to patients of HOS. Studying the process of fate specification and function of *tbx5a* in the ALPM of zebrafish was the goal of my dissertation.

I elucidate a single-cell resolution fate map of the lateral ALPM at 18 hpf. I demonstrate that the ALPM is not organized into segregated fate regions but gives rise to precursors of intermingled fates. I discover an asymmetrical contribution of lateral ALPM-derived heart precursors–specifically that twice as many heart precursors arise from the right side as from the left side. I present cell tracking analyses and regional-to-large-scale labeling of the lateral ALPM and find similar left/right asymmetries in migration dynamics and contributions to the larval heart. These findings corroborate the differences found in the fate map and show that the observed asymmetries are dependent upon Tbx5a expression. These data implicate *tbx5a* function in establishing and maintaining cardiac left/right asymmetry and cell specification.

The work in this dissertation expands upon the current knowledge of organ specification

in zebrafish and how *tbx5a* functions in the development of the heart, pericardial sac, pharyngeal arches, and peritoneum. In conclusion, my work culminates in proposing models of progressive specification of the ALPM and of *tbx5a* function that differs across time and precursor fates.

CHAPTER 1

INTRODUCTION

1.1 Cellular Specification in Developmental Biology

Developmental biology is the study of how a single fertilized cell becomes an adult organism. Initially, the single-celled embryo is pluripotent, meaning that it can give rise to all portions of the embryonic tissues to support the growth and development of the organism. Furthermore, the first cleavage divisions give rise to equipotent blastomeres which share the ability to be pluripotent. These cells are called equipotent. However, at some point, the blastomeres become restricted in their potential to give rise to all fates and become unipotential (a single potential or fate). To achieve the wide variety of fates within the adult organism, blastomeres across the embryo will become specified in a coordinated fashion. To give a sense of how important this process is, recent next-generation -omics analyses have determined that there are over 550 distinct cell types within the mammalian brain [1] and 39 distinct cell types within the mammalian retina [2]. That means that over the course of development, not only do neuronal cells need to be distinguished and differentially determined from the cell types of other organs (gut, heart, bone, skin, gonad, respiratory, etc.), but they also must be differentially determined within neuronal precursors to become the wide-variety of cell types in the adult brain. Generally, cells undergo a gradual restriction of cell fate over time. This means that the cells will first become specified as one tissue layer over another. And then the cells will become specified as a particular organ within that tissue layer. And then lastly they will become specified as a particular cell type within the organ. These complex processes are responsible for the organization of the embryo, and ultimately, the function of the organism. Defects in these processes give rise to birth defects and at times, termination of embryonic development. Therefore, studying how organs form and how embryonic cells become specified has implications on human development and health. Next, I will clarify my

terminology with respect to these processes and then discuss possible models by which my tissue of interest, the lateral plate mesoderm (LPM), may develop in the zebrafish embryo.

Specification is the process by which a cell is able to differentiate into a particular fate on its own when removed from its environment. A specified cell will autonomously differentiate, but only in a neutral environment without the presence of other cellular or chemical signals. **Determination** is defined more rigorously than specification. A determined cell will differentiate according to its original environment autonomously even when moved to a different part of the embryo. In order to test whether a cell is specified or determined, an excision experiment must be performed. Classically, specification is a stepping stone towards determination which eventually results in a fully differentiated cell. Due to the progression of differentiated cells that I discuss here, I want to clarify that I will be using "specification" of various fates within this dissertation to describe cells within the LPM that will eventually give rise to a differentiated fate as determined by morphology and position. As additional clarification, I did not perform any excision experiments on my tissue of interest and therefore cannot make definitive statements of cell specification and commitment as discussed in this paragraph. However, I am using 'specified' to represent a less rigorous definition of progression along cell differentiation commitment stages.

There are many processes and models by which developing cells become specified. First, cells may become specified inherently (autonomously) via intracellular factors, often termed "mosaic" development. *Caenorhabditis elegans (C. elegans)* embryonic development is a classic example of this method. Blastomeres of the *C. elegans* embryo invariantly divide along the same axes and differentiate along a predetermined decision tree. Therefore, cells within the *C. elegans* adult body arise based upon a stereotyped lineage that is the same across all organisms within the species. Generally, it is thought that autonomous specification happens before large-scale embryonic cell migration, since the division of cytoplasmic determinants from the egg dictate how the blastomeres will migrate during processes such as gastrulation.

Therefore, cells are specified based upon their initial positions and lineage.

Second, cells may be specified conditionally based upon their context, often termed "regulative" development. In cases where tissues might lose cells, gain cells, grow, or change shape, neighboring cells are able to adapt and regulate to fulfill the need of the entire tissue. The process of vertebrate body axis specification is an example of this. Cells within the organizer determine how the surrounding cells will be specified and therefore migrate. Even if other peripheral (non-organizer) tissues are destroyed or moved to another location, they will still adopt the correct fates in the new location relative to the organizer, resulting in a complete embryo. Of course, there are more possible mechanisms of cell specification, some of which may be combinations of the processes that I have described here. For example, zebrafish blastomeres initially behave conditionally. However during gastrulation, they undergo a cell sorting refinement mechanism that positions the blastomeres precisely into well-defined domains based upon heterogeneous response to extracellular signaling molecules [3].

Still, other models of specification may be playing a role in development and it is important to uncover the specific contexts and factors behind each developmental process. One goal of the field has been to describe the patterns of development and to make experimental perturbations that lend insight into how cells make commitment decisions. These findings are important to the biomedical field especially in light of using human embryonic stem cells (hESCs) and induced pluripotent stem cells (iPSCs) to treat diseases and conditions in the human race. When human biologists use hESCs and iPSCs, they must draw upon what is known about vertebrate development to ethically manipulate the development of cells to meet our medical needs. For example, once induced with cytoplasmic factors, mesodermal cells can autonomously differentiate into a wide variety of hematopoietic, endothelial, mesenchymal, and cardiovascular lineages [4, 5]; and the usage of these techniques would not had been possible without first mapping the fates of the mesoderm [6].

On the cellular level, the different models of cell specification are accomplished by different means. The Central Dogma of molecular biology describes a direction of information starting from genetic regulation, to RNA message, to proteins that accomplish most of the cell's tasks. In differentiating cells in developing embryos, the Central Dogma also applies. That is, regulation of genes ultimately translates into physical cellular changes that affect many processes in development. Next, I discuss four types of proteins that affect embryonic development when regulated. My goal is to introduce the vast number of pathway components that are simultaneously affecting multiple developmental processes in order to better situate my gene of interest, *tbx5a*, within these processes and cell specification. The first type is called **sensors**, which often are signaling receptor molecules that bind to ligands which come from neighboring cells. Sensors have the ability to respond to the environment, which means that they enable the second type, **signal transducers**, that are within the cell. Signal transducers are the cellular intermediaries than translate and amplify the signal they receive from the sensors into the cellular **effectors**, which will enact phenotypic changes in the cell. The roles of effectors are very broad. They may be cytoskeletal components that change the shape or orientation of the cell [7, 8]. They may activate other cellular effectors that will initiate a cellular event, such as division or death [9, 10]. They may cause the cell to interact differently with its neighbors and substrate, which often results in cellular migration changes [11]. The sum of these individual cellular changes may result in large-scale tissue changes. Tissue change that results in the formation of new structures and forms in the embryo is called morphogenesis. Morphogenic processes require coordinated change between cells. Governance by genes in this whole process, and at the level of each type of the cellular pathway components I describe herein, ensures that each individual level is regulated and robust.

Lastly, there is a fourth type of protein within the cell that acts in cell specification. **Selectors** are proteins, generally transcription factors, that are responsible for regulating

genes and result in changed cellular identity. We can think of selectors as downstream of signal transducers and may be upstream of signaling ligands that will interact with sensors on neighboring cells, thereby repeating the cycle of genetic regulation of cellular specification. *tbx5a* falls within this category of selectors. *tbx5a* is a zebrafish transcription factor, and its mammalian homolog, TBX5, is known to specify cardiac fate in mesodermal precursors along with other cardiac selectors [12]. More on the function of *tbx5a* and the mammalian homolog, TBX5, is discussed in Section 1.5 below.

The aim of this section is to introduce possible models by which my tissue of interest, the lateral plate mesoderm (LPM), may be differentiating to give rise to a number of different organs. I will discuss the overall development of this tissue in the next section and then continue on to discuss the role of my gene of interest, *tbx5a*, in these processes. In the following chapters of my dissertation, my investigation on the specification of the anterior lateral plate mesoderm (ALPM) provides evidence for a model of specification that relies on *tbx5a* to accomplish several functions: to establish asymmetrical contributions within the ALPM (Chapter 2); to enable the directed migration of ALPM precursors (Chapter 3); and to regulate the differential contribution of precursors into the heart and other fates (Chapter 4). The model of specification I propose falls in line with the aforementioned models known to developmental biologists. In particular, my findings suggest that the ALPM develops both autonomously and regulatively in a Tbx5a-dependent manner. More specifically the ALPM develops autonomously with respect to the progression towards a single fate over time. And the ALPM develops regulatively or conditionally depending on the migration dynamics. Further discussion of this proposed model of specification and how it contributes to a hypothesized model of organ morphogenesis is in Chapter 6.

1.2 Lateral Plate Mesoderm

The study of the lateral plate mesoderm (LPM) in vertebrates began over one-hundred years ago with anatomical observations of the developing coelomic cavities in mammalian embryos [13, 14]. By studying sections of rabbit and human embryos, these early researchers described how closely the developing pharynx, pericardium, limbs, heart, and peritoneal cavities lie in proximity to each other and how they grow out of each other over time [13, 14]. The tissue as a whole exists in two layers, and the space in between the layers is called the cavity. Over developmental time, the tissue becomes separated into multiple domains as septa form between cavities. For example, the septum transversum separates the pericardial from the pleuroperitoneal cavity [13, 14]. In zebrafish, there are two cavities, the pericardial and the peritoneal. Mammals have two additional cavities for the lungs.

Since these anatomical studies, researchers have labeled embryonic tissues with dyes to experimentally determine the respective anlagen of LPM-derived tissues [15, 16]. From these studies, we know that the LPM gives rise to the coelomic epithelium, which in adults is called the mesothelium. These various nomenclatures for the same tissue are quite misleading. The LPM is defined based upon its position within the developing embryo. The LPM lies lateral to the paraxial and intermediate mesoderm [17]. The name coelomic epithelium is given to tissue that arises from the LPM because of the cavity that forms within, the coelom. However, the name 'epithelium' is not aptly given. The coelomic epithelium is not a true epithelial tissue in that it does not consist of polarized cells with lateral adhesions resting on a basal lamina [18]. Instead, the layers of the LPM/coelomic epithelium consists of active mesenchymally-shaped cells which abundantly populate mesodermal compartments and the vasculature [19, 20], hematopoietic precursors [21], primordial germ cells [22], pericardial sac [18], the mesenchymal cores of the pharyngeal arches [23, 24], cardiac mesoderm [25, 26], peritoneum [18, 27, 28, 29], gut lining [30, 31], and the paired pectoral and pelvic fins [32]. The last term, mesothelium, is often used synonymously with the former terms, LPM and

coelomic epithelium [19, 27, 29, 31]. However, the term mesothelium technically describes the fully differentiated epithelial cell layer in adults and larval embryos. Therefore in my dissertation, I will not be using the term mesothelium synonymously with the LPM and coelomic epithelium.

In my dissertation, I define the LPM as the embryonic tissue identified during somitogenesis stages morphologically as a layer of cells lying lateral to the intermediate mesoderm spanning the anteroposterior axis of the embryo, which I can detect via Nomarski optics. At times, I also identify the LPM via Hand2 mRNA and enhancer trap *Et(Hand2:eGFP)* expression in zebrafish, which is detectable starting around 10 hours post fertilization (hpf) [33, 34] until around 34 hpf. I note, however, that Hand2 expression becomes upregulated within the heart starting around 24 hpf and within the pharyngeal arches starting around 30 hpf (Supplemental Movie 1, Fig. 3.3.1A). As I was interested in following cells that originated from the LPM at 18 hpf, I purposefully elected not to study Hand2-expressing cells that reside in these later upregulated regions.

Wnt/β-catenin and bone morphogenic protein (BMP) signaling prior to gastrulation is responsible for specifying the LPM [35, 36]. BMP-4 promotes the differentiation of the LPM over becoming somitic/paraxial mesoderm in a dose-dependent manner in chicken embryos [36]. Wnt/β-catenin signaling patterns the tissue along the dorsoventral axis such that *wnt8* promotes ventrolateral mesoderm over dorsal axial mesoderm [35]. Initially, the LPM exists as a single dorsoventral layer which gets patterned along the anteroposterior axis by co-linear expression of Hox genes and along the left-right axis by the Nodal-Lefty2-Pitx2 pathways (Section 1.4). Later, in tetrapods, the LPM divides into two layers—the somatic mesoderm, which lies dorsal and next to the ectoderm, and splanchic mesoderm, which lies ventral and next to the endoderm. These two layers are subdivided according to a binary decision in chicken embryos in an anteroposterior order that is independent of somitogenesis [37]. The splanchnic and somatic layers will outline the coelomic cavity, which will separate the inside

from the outside of the embryo. These signaling and developmental processes might also apply in zebrafish development; the most anterior region of the LPM is similarly separated into two-layered somatic and splanchnic sheets by 18 hpf.

Investigation of the zebrafish LPM to date has primary focused on the development of the heart and pectoral fins (Section 1.2.1, 1.2.5) [34, 38, 39]. Furthermore, pelvic fin progenitors are also thought to arise from the LPM during the larval stage [40], although the exact contributions of the LPM to the pelvic fins are currently unknown. The development of other zebrafish LPM-derived tissues has not been explored in a comprehensive manner. Therefore what specific tissues and structures the LPM contributes to is not completely known. This dissertation focuses on the development of the anterior lateral plate mesoderm (ALPM), which lies posterior to the vascular precursors, and anterior to somite 1, the boundary of the pectoral fin precursor field. Furthermore, the LPM undergoes migration starting at 18 hpf where the ALPM, marked by Tbx5a-expressing cells, migrates anteriorly and separates from the pectoral fin precursors, making this time-point particularly interesting in terms of how migration dynamics affect organogenesis and specification [41]. In my dissertation, I have sought to apply mechanisms known and approaches used in studying pectoral fin initiation to better understand specification within the ALPM.

1.2.1 Pectoral Fin Development

Pectoral fin development is separated into three phases: initiation, outgrowth and patterning. Zebrafish pectoral fin initiation relies on a gene regulatory network that starts with retinoic acid (RA) signaling from the somites around the 12-14 hpf stage [42]. RA and Wnt2b induce the expression of secreted protein, Fibin [43, 44]. Fibin activates the transcription of *tbx5a*, which marks the pectoral fin organ field starting around 16 hpf [45, 44, 46].

After the limb bud organ pool is initiated, outgrowth and patterning are regulated by signaling from two structures within the developing fin bud itself: the apical ectodermal ridge

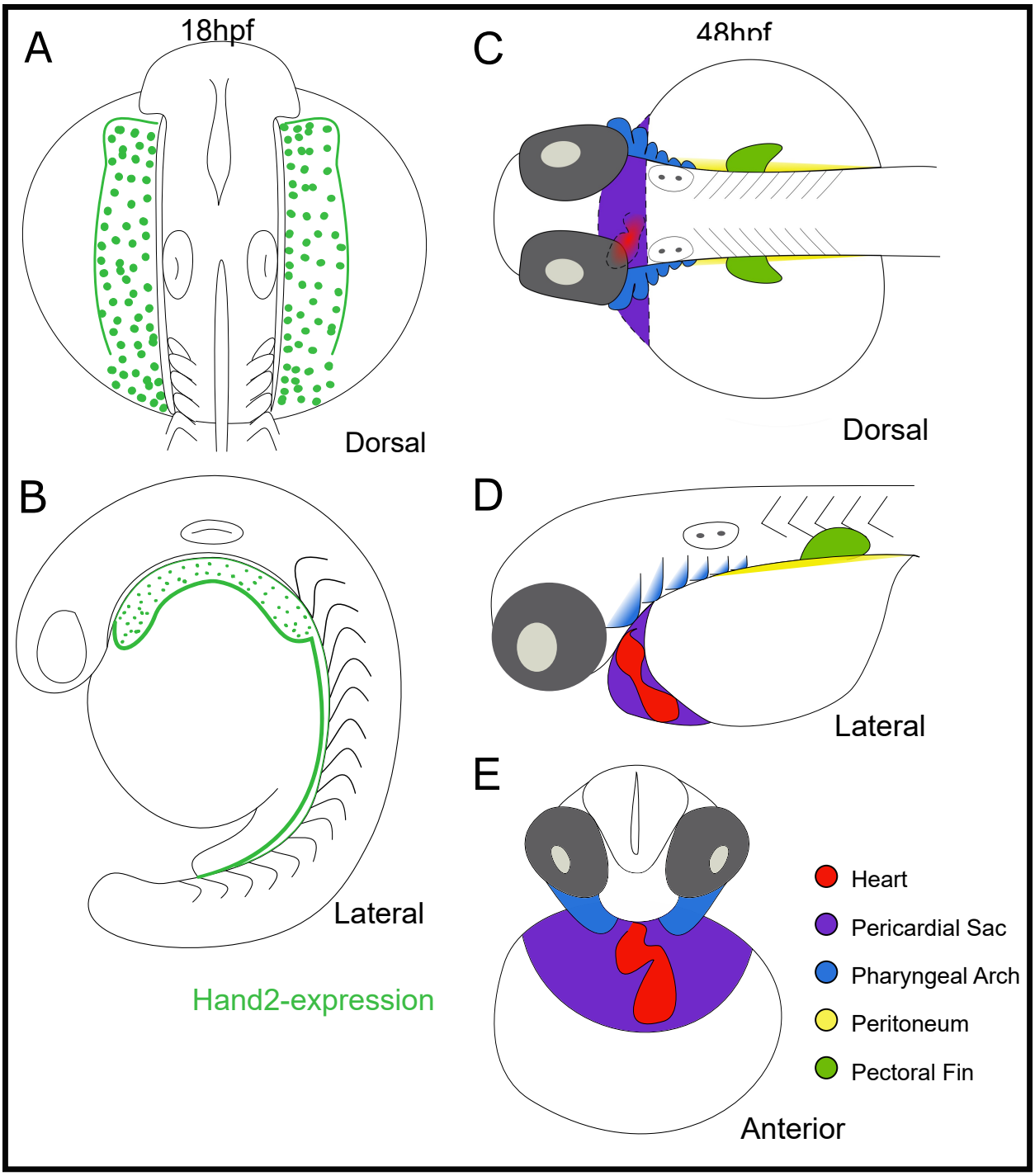

Figure 1.1: **Schematic of the developing anterior lateral plate mesoderm (ALPM).** A, B– Schematics of dorsal (A) and lateral (B) views of the 18 hpf embryo highlighting lateral ALPM tissue in green. Medially localized ALPM precursors which will make up the primary heart tube are not shown and are ventral to the midbrain at this stage. C, D, E– Schematics of dorsal (C), lateral (D), and anterior (E) views of the 48 hpf larva displaying the five LPM-derived tissue types.

(AER) and the zone of polarizing activity (ZPA). In all vertebrates studied to date, growing limb buds require ongoing expression of Tbx5, which serves to activate FGFs (Fgf4/8/10/16) within the AER and Sonic hedgehog within the ZPA [47, 48]. Tbx5 function is both necessary and sufficient for limb outgrowth, as well as to maintain the expression of Wnt and Fgf10 [43]. A dominant negative form of Tbx5 expressed in the prospective chicken limb field represses Wnt and Fgf expression [49]).

Pectoral fin precursors undergo an asymmetric convergence during the initiation phase where the more anterior precursors travel in a more ballistic manner with greater speed and persistence than the more posterior precursors [33]. The result of this asymmetric convergence is that the resulting organ pool becomes more posteriorly localized than the original precursor center of mass. A localized migration cue of Fgf24 expression at the eventual site of the fin bud is responsible for the asymmetric migration. This role for Fgf24 was demonstrated using both loss- and gain-of-function approaches: Fgf24-deficient fin bud precursors fail to migrate, whereas an ectopic source of Fgf protein can rescue the migration [33, 50].

1.2.2 Peritoneum Development

The peritoneum is the lining of the body wall, which is made up of the parietal peritoneum which lines the wall of the peritoneal/coelomic cavity, and the visceral peritoneum, which covers the external surface of abdominal organs. The peritoneum starts to form around 22 hpf in the zebrafish and is fully developed by the adult stage. The developing organ secretes serous fluid which enables the free movement of the peritoneum and intraperitoneal organs. It is hypothesized that the peritoneum and coelomic cavity evolved to 1) allow a larger body size because of the fluid-filled structure, 2) relieve constraint on the outer body wall from the tube-within-tube structure of the gut, 3) accommodate the development and expansion of new internal organs [51]. Thus, the peritoneum is an important structure for the function

of multiple organs and organ systems.

The study of the peritoneum and the coelomic cavity has been severely limited by how thin the tissue is in fish and frogs and by how large and extensive the tissue is in surrounding many organs, such as the pronephros, intestine, swim bladder, spleen, and liver. Development of the chick peritoneum and coelom has been documented by Funayama et al., 1999, where the splanchnic layer expresses HFH8 and the somatic layer expresses IRX8 and PRX1 [37]. These genes indeed have zebrafish homologs that are also expressed in the peritoneum, although not as early as during somitogenesis stages, when we can observe the cellular migrations and developmental processes. HFH8 homolog, Foxf1, is expressed in the zebrafish gut lining starting at 25 hpf [52]. Irx3b is expressed in the pronephric duct, which is part of the pleuroperitoneal region [53, 54]. Prrx1a appears to be the only documented marker of early peritoneum, showing that it is a part of both layers of the LPM in zebrafish as early as 19 hpf [55]. As the peritoneum is derived from the LPM, it is also marked by Hand2 expression and can therefore be seen migrating laterally across the yolk from 18 to 25 hpf using the enhancer trap line *Et(Hand2:eGFP)* [33, 56]. Despite our current knowledge of how the peritoneum develops in chick and the existence of genetic markers in zebrafish, there has yet to be a study on the origins of the peritoneum.

In Q. Mao's doctoral dissertation, she expanded on her findings of how the peritoneal precursors of the LPM migrate and compared the behavior of these cells with migration of the pectoral fin precursors [56]. Q. Mao defines the peritoneum field as the LPM posterior to somite 4, and her fate map indicates somatic peritoneal clones which have an average size of 4 cells and are flattened in shape. She also concluded that the peritoneum precursors exhibit different migration dynamics than the pectoral fin precursors—the posteriorly located tracks have increased scatter and persistence. The work in my dissertation addresses the development of the peritoneum anterior to somite 1, which also does not encompass the entire peritoneal tissue primordium. Nevertheless, by investigating the development of the ALPM

and including the study of all the structures that it contributes to, I show that peritoneum development can be studied further in the zebrafish model system.

1.2.3 Pericardial Sac Development

To the best of my knowledge, the molecular development of the pericardial sac has not been studied in zebrafish, chick, nor mouse, apart from the contribution to the proepicardium that lies within the pericardial sac (see Section 1.3.2). Through studying the anatomy of the developing coelomic cavity, we know that the pericardial sac arises from the LPM and is separated from the peritoneum by septation in the coelom. The pericardial sac itself is filled with fluid and it forms abnormally with edema in more than 500 mutant phenotypes, most likely due to dysfunction in the developing heart. However, there are no known genetic markers that are expressed exclusively in the pericardial sac and therefore it would be difficult to study the molecular mechanisms of pericardial sac development. In this dissertation, I describe a fate map of the ALPM that give rise to the pericardial sac (Chapter 2), analyze the migration dynamics of pericardial sac precursors (Chapter 3), and describe the growth of the tissue over time in relation to the growing heart tube (Chapter 5). In total, I have sought to provide evidence which sheds light into this poorly studied tissue in zebrafish.

1.2.4 Pharyngeal Arch Development

The pharyngeal arches are transient structures within the vertebrate embryo that are made up of all germ layers: ectoderm, mesoderm, endoderm, and neural crest. The arches are organized into seven externally visible tissue bands in the zebrafish embryo that are arranged along the anteroposterior axis (Fig. 1.1C-E, in blue). The anterior arches begin to arise around 30 hpf and each of the posterior arches become visible later in time sequentially until 84 hpf, when they begin to undergo chondrogenesis (formation of cartilage) [57]. Each of the arches will give rise to specific structures within the head and neck: pharyngeal arch 1,

called the mandibular arch, will give rise to the jaw, dentary bone in mammals, middle ear structures, and connective tissues of the tongue; pharyngeal arch 2, called the hyoid arch, will give rise to supports for the jaw; pharyngeal arches 3-7 are also called the branchial arches and they will form the gill and pharynx [58]. Generally, the pharyngeal arches are made up of mesodermal cores that are surrounded medially by endodermal pouches and laterally by ectodermal arches. Neural crest cells migrate into the pharyngeal arches to surround each of the mesodermal cores. The patterning of the neural crest cells establishes dorsoventral axis and differential expression within each arch through BMP and endothelin signaling [59]. The anteroposterior patterning of the pharyngeal arches is established by Hox gene expression and mediolateral patterning is dependent on signaling from medial structures such as the prechordal plate or the forebrain [58]. Since the mesodermal cores of the pharyngeal arches become segmented in an anterior to posterior manner over time and prepatterning exists along the three major body axes, it is possible that the determinants for prepatterning lie within the ALPM prior to 30 hpf, when segmentation is first noticeable [60, 61]. By investigating the fate map and migration dynamics of the ALPM-derived pharyngeal arch precursors, my work begins to test this hypothesis.

A population of mesodermal cells exists that will contribute to both cardiac and pharyngeal arch fates, the cardiopharyngeal mesoderm. Cardiopharyngeal mesodermal cells express Isl2b, Tbx1, and Hand2, which participate in a feed forward circuit with FGF signaling in Ciona [62, 63]. Disruption in the Tbx1 signal from the endoderm, ectoderm, and neural crest will cause the mesoderm to adopt a skeletal fate instead of its typical cardiac muscle fate [64]. Co-expression of Tbx1 and Tbx3 in mouse is also observed in the dorsal pericardial wall [64], suggesting that the pericardial sac shares function or identity with cardiopharyngeal mesoderm. In the cardiopharyngeal mesoderm of mouse, Isl1 functions to delay differentiation of branchiomeric muscles, Nkx2-5 functions to regulate proliferation specifically of the cardiogenic cells, and Tbx1 functions to maintain proliferation and support the differentiation of

cardiac muscle [65, 66]. Altogether, the fact that precursors of both cardiac and pharyngeal (and sometimes pericardial) fate express some of the same genes and require function of those genes to undergo fate specification and proliferation suggest that the precursors might share common origin and at some stage have similar potential. From my fate map analysis of precursors with more than one fate, I am able to add to what is known about precursors within the ALPM that share fate between the heart, pharyngeal arches, and pericardial sac.

1.2.5 Cardiac Development

The entire heart-forming region consists of First Heart Field (FHF) and Second Heart Field (SHF) precursors, which will together develop into both the Primary Heart Tube (PHT) and elaborations to the PHT at the arterial and venous poles, respectively. The SHF was first discovered in chick embryos in 1977 by de la Cruz who observed that cells within the pharyngeal mesoderm gave rise to the outflow tract [67]. Subsequently, SHF in mouse was identified by using LacZ staining under the FGF10 promoter [24]. Molecular markers ISL1 and LTBP3 were discovered to label the SHF in mouse and today the expression of these markers is used to define and follow the SHF in chick and fish [68, 69]. However, these markers are not completely overlapping in zebrafish cardiac precursors, causing a lack of consensus in how the SHF is defined in this model organism. The SHF in zebrafish was first described by Hami et al. (2011) who were able to label cells within the dorsal pericardial wall at 24 to 36 hpf that later contributed to the distal portion of the ventricular myocardium [70]. Hami et al. also observed that Isl1 expression seemed to overlap with the same region and proposed that the SHF was conserved between zebrafish and amniotes [70]. To date, the SHF in zebrafish has primarily been studied by the expression of Isl1, Isl2b, and Ltbp3, or by the lack of FHF markers, such as Draculin [38, 63, 69, 71, 72, 73, 74]. However in comparing the domains of expression between these studies, I found a lack of consensus in molecular definition of the SHF since the expression of each of these markers is visible at

different stages of development and does not morphologically label the same population of cells within the LPM at 18 hpf. Therefore in my dissertation, I chose to classically define the SHF as cardiac precursors that do not make up the PHT by 24 hpf, yet can contribute to the heart at any time thereafter.

The zebrafish heart consists of two major chambers, the atrium and the ventricle. Cardiogenesis begins with the specification of the FHF cardiomyocytes in two lateral populations in the gastrulating zebrafish embryo, which by somitogenesis stages (10-18 hpf) will be positioned on the right and left sides of the embryo. These lateral populations of early cardiomyocyte precursors already exist in at least two layers, the atrial and ventricular precursors, which will correspond to the two chambered myocardium of the zebrafish heart. When individual precursors were labeled with a dye at 5 hpf, they contributed to only atrial or only ventricular precursors, implying that these early precursors are restricted in fate [25]. After gastrulation, these precursors are located within the LPM, and can be visualized by coexpression of Gata4 and Hand2 [75]. The precursors are positioned along the mediolateral axis such that the ventricular precursors are positioned medially (Fig. 1.3A, orange cells) and the atrial precursors are positioned laterally (Fig. 1.3A, blue cells). Nkx2.5 is also expressed within this region, however, the expression domain is only in a medial compartment of the entire heart-forming region that gives rise to both chambers but mostly ventricle [75, 76].

Previous fate map studies of the zebrafish ALPM focused on the cardiac precursors and were conducted from midblastula-stage and 40% epiboly to 26 hpf and from 11 hpf to 44 hpf [25, 75, 77]. Furthermore, although the authors do not explicitly describe the FHF versus SHF, based upon the regions of the heart that their labeled precursors contribute to and the time at which they assess the fates, it appears as if they only observe contributions to the primary heart tube. A general fate map of the entire ALPM, especially the cells lateral to the primary heart tube-forming region, was lacking until my work described in Chapter 2. The primary goal of my dissertation was to generate a more complete fate map of the lateral

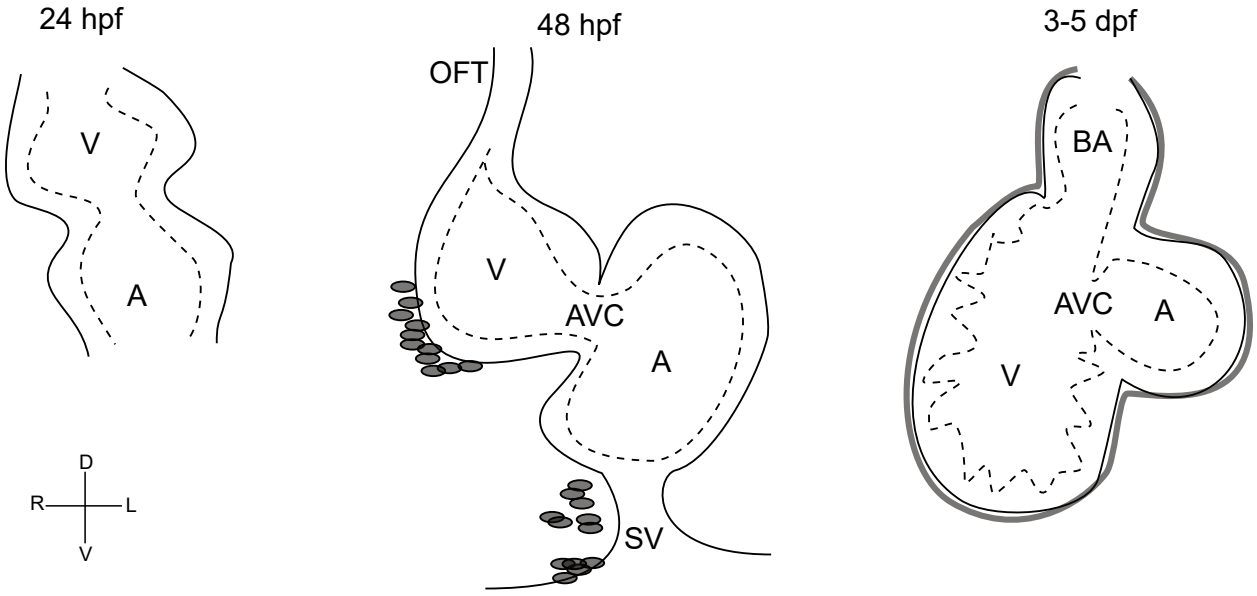

Figure 1.2: **Anatomy of the zebrafish heart.** At 24 hpf, the primary heart tube has formed as layers of myocardial (solid lines) and endocardial (dashed lines) tissues that form into atrial and ventricular chambers. At 48 hpf, the addition of second heart field (SHF) cells into both the arterial pole (from the top) and venous pole (from the bottom, continuous with the pericardial sac) into the primary heart tube has allowed the elaboration of the atrioventricular canal (AVC) in between the chambers, the outflow tract (OFT), and the sinus venosus (SV, also called the inflow tract). At this time, proepicardial cells (grey) have accumulated on the pericardial wall near the arterial pole and at the venous pole. The migration of these cells is further described in Section 1.3.2. At 3-5 days post fertilization (dpf), the proepicardial cells have covered the entire myocardium to become the epicardial layer (grey). The contributions to the OFT have now elaborated into the bulbus arteriosus (BA) and added into the ventricle, causing elaborations of the endocardial cushions (inner dashed lines).

ALPM to determine its composition and organization. Additionally, little is known about the migration dynamics for precursor cells that contribute to the head and heart ALPM-derived structures. Therefore, Chapter 3 describes my attempt to characterize how lateral ALPM precursors differentially migrate into their respective organs. Through investigating the fates and migration dynamics of ALPM, I have sought to answer questions on how fate specification and organogenesis progresses over developmental time. In the next section, I will continue to describe cardiac development with specific emphasis on how the heart adopts

its complex shape.

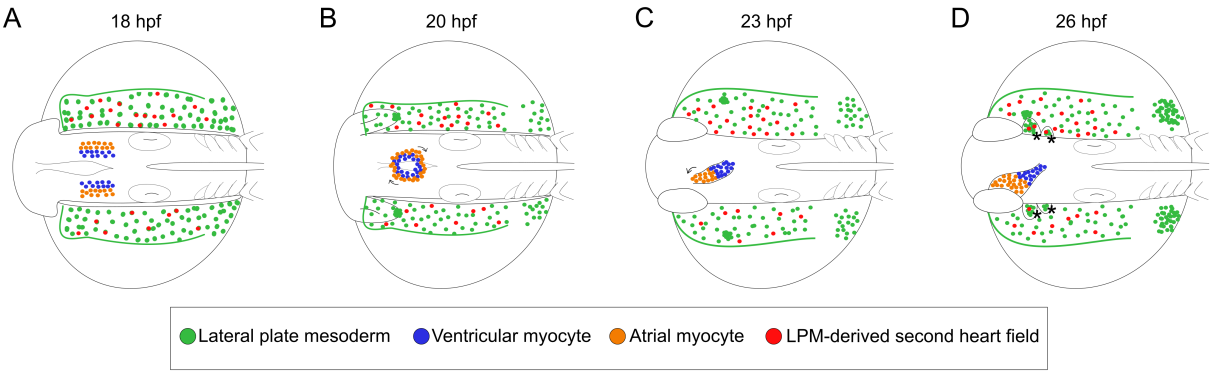

Figure 1.3: **Schematic of early cardiac development.** A–First heart field (FHF) ventricular and atrial cardiomyocytes are positioned medially and ventrally to the lateral plate mesoderm (LPM), which consists of non-regionalized second heart field (SHF) progenitors. B–FHF cardiomyocytes migrate together to form the cardiac cone, which will undergo a clockwise rotation (arrows). Meanwhile, LPM tissue migrates into anterior LPM (ALPM) and pectoral fin precursors. C–Elongation of the cardiac cone forms the primary heart tube, which will undergo leftward jogging of the ventricular pole (arrow). D–Looping of the primary heart tube commences and the ALPM contributes to the mesenchymal cores of the pharyngeal arches (asterisks), which temporarily contain SHF precursors. Dorsal view, anterior to left.

1.3 Heart Morphogenesis

Cardiac development involves many complex morphogenic movements, which are generated by molecular and intracellular changes, individual cellular contributions, movements of entire tissues, and differential expression of genetic factors across the whole embryo. This section will provide details of the overall morphogenic events and how cellular migration and gene expression affect these processes.

1.3.1 Heart Rotation, Jogging, and Looping

The zebrafish adult heart consists of two chambers, the atrium and ventricle. These two chambers are derived from a linear tube heart which needs to undergo septation at the

atrioventricular boundary and asymmetrical looping in the left-right direction. Cardiac precursors are first specified at the lateral marginal zone before gastrulation at 5 hpf [78]. At around 12 hpf, the cardiac precursors exist at the level of the future hindbrain as bilateral populations of mesodermal progenitors in three rows of cells: endocardial precursors medially and the two myocardial precursor rows, pre-ventricular and pre-atrial cells laterally [78]. Around 16 hpf, differentiation of the LPM begins with the migration of CPCs anteriorly and towards the midline [78] (Fig. 1.3A). Expression of *cmlc2*, a marker of heart muscle [79] and Tropomyosin expression slightly later in development (18 hpf), allow the visualization of progressive precursor differentiation [25]. The two groups of cells from the left and right sides of the embryo merge at the ventral midline to form a heart cone by 22 hpf, which sits with its base on top of the yolk cell [25, 78, 80] (Fig. 1.3B). As the left and right populations merge, they also undergo a clockwise rotation that positions the left-originating cardiomyocytes anteriorly and the right-originating cardiomyocytes posteriorly, as shown by timelapse microscopy and mosaic labeling of clusters of cardiomyocytes [81, 82]. Fukui et al. (2018) has recently observed that even caudally-positioned cardiomyocytes within the ALPM contribute to the developing heart cone according to this rotation (left to anterior, right to posterior) [71]. Careful consideration of this rotation with respect to caudal SHF contributions is important in the interpretation of my whole ALPM labeling experiment in Chapter 4.

The heart cone will elongate into a linear heart tube by 24 hpf (Fig. 1.3C). At the same time, the heart cone becomes displaced to the left side. This process, called jogging, is effected by Nodal signaling (Section 1.4). Ocaña et al. propose that zebrafish heart jogging occurs as a consequence of a *prrx1*-mediated right-sided pushing force originating from an actin-rich cable of the ALPM that moves the venous pole to the left side [83]. While the heart cone is elongating and jogging, it also rotates in a clockwise direction. This morphogenic movement is driven by changes in epithelial organization of the cardiomyocytes,

in which more laterally positioned cells have a more cuboidal epithelial shape, whereas more medially positioned cells become more elongated and columnar in shape. This shape change can be seen via the change in localization of apical marker aPKC [84] and is required for the morphogenesis of the heart [85, 86, 87]. In order to elongate, cardiomyocytes on the right side involute and move ventrally toward the anterior, which is independent of Nodal signaling [81, 88, 89]. As this process happens simultaneously with the rotation and jogging of the heart, the right side cardiomyocytes become the ventral side and internal lumen of the heart while the left side cardiomyocytes become the dorsal side of the heart [81, 82, 89, 90]. Eventually, this heart tube will start beating as individual cells become coordinated together and looping will begin around 26 hpf in a right-handed manner, D-loop [78] (Fig. 1.3D). Around 30 hpf, the SHF at the arterial pole contributes to the developing heart. The SHF in general is responsible for changes in heart size and morphology, as it will allow the elaboration of existing atrium and ventricle. It will contribute to structures such as the distal part of the ventricle and outflow tract [79, 91].

Intrinsic and extrinsic mechanical cellular forces also contribute to heart morphogenesis. In chick heart development, morphogenesis is broken down into two stages: that which generates the c-shaped heart and then the s-shaped heart. Each of these stages is controlled by torsion forces that are first exerted on the heart tube by the primitive atria and the splanchnopluere, the membrane that lies against the ventral surface of the heart [92]. Next, contraction forces and differential growth rates combine with the rotation of the heart to create its s-looped form. Each of these forces can be recapitulated with *in silico* and *in vivo* experiments [92].

1.3.2 Cardiac Contributions by Cellular Migration

The migration of myocardial precursors into the heart is a process that has been well studied in zebrafish; and in this section I will summarize the cellular movements and genetic basis

for these movements. The overall migration of the ALPM to generate the heart can be separated into four separate movements depending on the cell type and trajectory of migration. First, medially localized ALPM on the right and left sides migrate toward each other to form the heart cone (Fig. 1.3A-B). There is a long list of mutations that result in a cardia bifida phenotype, where this migration is perturbed, resulting in two separate hearts in bilateral positions [93, 94, 95, 96, 94]. For example, mutations in fibronectin result in cardia bifida, which suggests the role of the extracellular matrix in guiding this migration [94]. The *miles apart* mutation (*mil*) is in a G-protein coupled receptor that binds lysosphingolipid, S1P and also results in *cardia bifida* [96]. Perturbations in transcription factor Yap1 localization also affect the ability of bilateral hearts to fuse. Many endodermal mutations (*sox32*, *sox17*, *gata5*) also affect the ability of the cardiomyocytes to fuse at the midline [93, 94, 95]. Research of these *cardia bifida* mutants illuminates how endodermal cells and the extracellular matrix are necessary for this first aspect of cardiac migration.

Once myocardial cells come together into the heart cone, lamellipodial extensions are required on the leading edge of left-anterior cardiomyocytes of the cardiac cone to involute and extend the cone into the primary heart tube [89]. On the posterior end of the cone, the cardiomyocytes speed up when they move in the left-anterior direction and then slow down again once they reach their destination. This is an example of directed migration when compared to the more constant migration of the cardiomyocytes of the anterior cone [82, 97]. In Chapter 3, I report an analysis of ballistic cell migration, one goal of which was to determine how else cardiac precursors display differential directed migration within the ALPM.

The second movement of cardiomyocyte contribution is from the SHF into the arterial and venous poles of the primary heart tube. A few researchers have observed these migrations of individual cells that come from caudal ALPM into the venous pole [71], from rostral ALPM into the venous pole [83], or gradually into the arterial pole from the midline [38,

66, 74]. These studies report that each of these populations of cells require functioning *fgf8a* [66, 74], BMP signaling [71, 83], and Hippo signaling [71] to enable the migrations of SHF contributions. In general, we still do not know the entire anlage from which these cells continually migrate. One of the goals of my fate map as discussed in Chapter 2 was to determine if there was any specific region within the ALPM from which the SHF arises.

The third movement of cardiomyocyte contribution is of the mesodermal cardiopharyngeal cells. These cells migrate through and become sequestered in the mesenchymal cores of the pharyngeal arches, which express Nkx2.5 [74]. These cells, which express Tbx1, are part of the cardiopharyngeal mesoderm, as described in Section 1.2.4. As part of the cardiopharyngeal mesoderm, these outflow tract precursors stay within the pharyngeal arches between 28 to 72 hpf before migrating into the arterial pole of the heart [74]. The migration itself and cardiac contribution has been observed directly only by Paffett-Lugassy et al. (2017), however the known common ancestry of cardiac and skeletal muscle that I describe in this dissertation fits with this finding in subsequent data chapters [74].

The fourth described movement of cardiomyocyte contribution is of the proepicardium. The proepicardium is the primordium to the epicardium, the outer-most layer of the heart which covers the myocardium, and coronary vascular progenitors. The epicardium functions as a protective layer and is also the source of mitogeneic signals that play a role in organ growth control and repair after injury [98, 99]. Morphologically, the proepicardium can first be distinguished at 48 hpf in zebrafish and it first appears as clusters in two areas: at the pericardial wall near the arterial pole and by the venous pole of the heart (Fig. 1.2). The proepicardial cells from the arterial pole will migrate to cover the outflow tract and form a bridge with the myocardium to the atrioventricular canal [100]. For these cell clusters to move, individual cells must undergo shape changes to protrude into the pericardial cavity. Furthermore, these cells require the functional beating of the heart to migrate and form properly [100]. Several genes (*wt1*, *tbx5a*, *sox9*, *hand2*, and *tcf21*) have been shown to be

required in the migration of the proepicardium over the myocardium [101, 102]. Further elaboration on the left-right asymmetry in proepicardial development is discussed in Section 1.4.

1.4 Left-right Axis Determination

Left-right axis determination is important to internal development of multiple organs despite the fact that most animals show external bilateral symmetry. In humans, heterotaxy occurs in patients who have partial reversal of left-right asymmetry in a subset of organs that can result from defects in embryonic development [103, 104] and laterality birth defects occur in at least 1 in 10,000 births [105]. The importance of correct laterality of internal organs might be to improve organ packaging within a body of limited space [106]. In order to study left-right axis determination in vertebrate embryos, zebrafish has been used as model system because laterality defects have been discovered in mutagenesis screens [107]. In zebrafish, left-right axis specification begins during segmentation stages with the asymmetrical flow of extra-cellular Nodal protein caused by rotating cilia in Kupffers vesicle [108, 109, 110]. During the process of Nodal flow to the left LPM, at the same stage (10-11 hpf) BMP signaling activity restricts expression of Lefty1, a Nodal antagonist, to the notochord at the midline [111]. Lefty1 and Lefty2 play roles in both the initial setup of the left-right axis during somitogenesis and also in the asymmetrical morphogenesis of the cardiac field later in development [111, 112, 113]. Nodal flow results in the unilateral expression of Southpaw (Spaw), one of the three nodal related genes in zebrafish within the LPM around 14 hpf [114]. Nodal signaling involves interactions with the Tgf-β receptor and phosophorylation of intracellular Smad2 protein. Lefty1 is required to restrict Spaw expression from crossing the midline and keep it unilaterally expressed only on the left side LPM [111].

The Nodal pathway sets up inherent asymmetry within the left LPM, while BMP signaling sets up Prrx1a expression within the right LPM [83, 115, 116]. Downstream of both

of these left and right side pathways is Pitx2, which is activated on the left side and inhibited on the right side [83, 117]. When Pitx2 is activated on the right LPM ectopically in mice, chick and *Xenopus*, looping of the heart and gut is affected [118, 119, 120, 121]. When the gene is deleted in mice, multiple mesoderm-influenced organogenesis events are affected: body wall closure, heart position, pituitary gland determination and proliferation and tooth organogenesis [122, 123, 124]. The effects of Pitx2 mutation are also seen in the ectoderm: forebrain and branchial arch [125, 126]. Pitx2 appears to function in mammalian heart laterality by giving left-right identity to the atria, which will keep the myocardial cells within the arterial pole left-right asymmetric across the respective to the body axis [122]. Therefore, Pitx2 appears to be the propagating signal of left-right asymmetry within the LPM that functions in the development of multiple mesodermal and ectodermal organs.

After the left-right axis is established and maintained within the LPM, it must be interpreted by and translated into the various organ fields. Among the left-right asymmetric internal organs, heart morphogenesis occurs first in developmental time during cardiac jogging and cardiac looping. Jogging occurs at about 24 hpf when the venous pole of the primary heart tube shifts to the left side. Cardiac looping then occurs at about 36 hpf when the linear heart tube forms a D-loop that places the ventricle to the right of the atrium. The laterality of the heart appears to be independently controlled from that of the gut [61, 107, 115]. Perturbations in genetic determinants in the TGF, BMP and retinoic acid signaling pathways result in the reversal, absence, or randomization of the direction of cardiac jogging and looping [114, 127, 128], although the two morphogenic processes are not always coupled [129]. In a forward genetic screen, 21 mutations were found to affect the direction of jogging and/or looping of the heart in zebrafish [127]. Many of these genes were involved in signaling pathways, namely BMP and Shh signaling [127]. Despite the conservation of these genetic determinants of cardiac looping among vertebrate species, the mechanism of how these genes enable cellular changes that result in asymmetric morphogenesis is still unknown.

There are a small handful of observations that lend insight into how left-right asymmetry in cardiac development may contribute to the proper morphogenesis of the zebrafish heart. Firstly, chamber formation itself is asymmetric across the left-right axis. When the bilateral populations of cardiomyocytes converge at the embryonic midline, the atrial and ventricular precursors must arrange themselves such that firstly the emerging tube becomes linearly compartmentalized into atrial versus ventricular precursors, and secondly that the entire tube is directionally positioned to the left side (jogged). In order to accomplish these morphogenic movements, the right side involutes ventrally and the left side does not involute [89]. At the same time, the left side precursors migrate faster and more directionally to result in a net leftward displacement of the entire heart tube (jogging) [97]. Both the asymmetric involution and directed migration and dependent on Nodal signaling [87, 97].

Second, the continual additions to the heart from the ALPM also exhibit left-right asymmetry. The caudal portion of the ALPM will migrate into the venous pole asymmetrically across the left-right axis such that the right side undergoes a more direct migration across the midline than the left side [71]. Once at the venous pole, the level of contribution by 26 hpf from the right or left side is regulated by the Hippo pathway [71].

Third, the contribution of the proepicardium also exhibits left-right asymmetry. Accumulation of the proepicardium at 48 hpf is localized to the right side of the pericardial sac and the inflow tract (Fig. 1.2). Invasion of the proepicardium onto the myoepicardium comes from the right side where a cellular bridge is formed [100]. Furthermore, when a marker of proepicardial cells, *wtip*, is knocked out, cardiac looping fails, suggesting the importance of the proepicardium in left-right morphogenesis of the heart [130].

Fourth, after the formation of a looped heart, there is differential expression within the chambers across the left-right axis. Guerra et al. (2018) conducted an RNA-seq analysis comparing the right versus left atrium in zebrafish adult hearts and found two sets of genes that were either only expressed on the left atrium or the right atrium [131]. Interestingly, *pitx2*

was expressed on the left atrium, suggesting that continual expression of this left-determining gene is continually necessary in adulthood for left-right asymmetry [131]. Altogether, there are multiple levels of left-right asymmetrical regulation of heart morphogenesis.

Lastly, the mouse ortholog of my gene of interest, *TBX5*, is involved in left-right asymmetry of LPM-derived tissues in several ways. First, *PITX2C* is a downstream target of TBX5 in mouse [132]. Second, loss of TBX5 function affects the left side more severely than the right side in mammalian limb development [133, 134]. Third, the septum primum in mice expresses PITX2, which is affected in atrial septal defects found in individuals affected by *TBX5* mutation [135]. In the next section I will discuss the structure and function of *tbx5a* and how it relates to the development of the ALPM in zebrafish.

1.5 Tbx5a

In my introduction chapter thus far, I have noted how investigating the specification of multiple organs within undifferentiated tissue addresses many important fields of study within developmental biology (Section 1.1). I next outlined the development of various organ primordia that arise from the LPM (Section 1.2), and then I highlighted the importance of genetic regulation in governing these processes, in particular heart development (Section 1.2.5) and the specification of the left-right axis (Section 1.4). In this section, I seek to provide a review of current literature on one particular gene, *tbx5a*, which acts as a selector within the LPM. The function of *tbx5a* within the ALPM is the focus of my dissertation, and so the review that I provide herein will inform all subsequent chapters of this work.

1.5.1 Tbx5 Expression in zebrafish and amniotes

The T-box gene family are defined by a conserved T-box DNA binding domain of about 180 amino acids. T-box genes typically function in vertebrate mesodermal development [136]. TBX5 in tetrapods is expressed in various embryonic structures including the heart, eyes,

and forelimbs. In amniotes, TBX5 is uniformly expressed in the cardiac crescent during initial heart development and is later expressed in a posterior to anterior gradient in the linear heart tube [137]. Once the heart loops, TBX5 is expressed in the left ventricle and the left side of the ventricular septum [137]. The zebrafish orthologs of *TBX5* are a pair of duplicated paralogs, *tbx5a* and *tbx5b*. The expression of Tbx5a in zebrafish is similar to that of TBX5 in amniotes; *tbx5a* is expressed in the developing heart, eyes, and forelimbs/pectoral fins [41]. In particular, the expression pattern of *tbx5a* transcript seems to overlap with the ALPM from 10-20 hpf until formation of the heart cone [41, 138]. The expression of a new transgenic zebrafish line constructed from a bacterial artificial chromosome containing *tbx5a* (*Tg(tbx5a:eGFP)*) continues to be expressed in the ALPM up until 30 hpf and is upregulated in the pericardium and the entire heart until 50 hpf [83]. The continual expression of *tbx5a* implicates function in these tissues for at least this time period.

The paralog of *tbx5a*, *tbx5b*, was more recently discovered by the phylogenetic analysis Albalat et al. (2010) using alignment to the human TBX5 protein [138]. *tbx5b* transcripts are not visibly detectable via chromogenic whole mount *in situ* hybridization until 17 hpf, and then are only detected in the eye and heart. Furthermore, the *tbx5b* expression in the heart becomes restricted to just the ventricle around 36 hpf. *tbx5a* functions in pectoral fin initiation and looping of the heart [33, 139, 140]. *tbx5b* functions in pectoral fin pattering and jogging of the heart [140]. Although the two paralogs function in similar tissues and have similar evolutionary origins, the functions of *tbx5a* and *tbx5b* are not completely redundant; the addition of one paralog's mRNA cannot rescue the knockdown phenotype of the other [140]. Therefore, it is likely that the two paralogs' functions may sum up to the complete function of Tbx5 as seen in amniotes. As of now, the function of *tbx5b* has not been well studied. Erin Boyle Anderson investigates the function of both paralogs in her dissertation, "The role of the Tbx5 paralogues in zebrafish development". My dissertation does not address *tbx5b* function. For a complete picture of how *TBX5* functions in vertebrates, future

researchers will need to extensively assess how *tbx5b* functions within the entire ALPM. And so, my work lays out the beginnings of how future investigators may compare how the ALPM develops in Tbx5b-deficiency in comparison to the wildtype and Tbx5a-deficiency that I describe (more on this in Section 6.5).

1.5.2 Holt-Oram Syndrome and heartstrings mutant

Mutations in human *TBX5* result in Holt-Oram Syndrome (HOS), which is characterized by forelimb malformations and cardiac septation defects [141]. In particular, haploinsufficiency of TBX5 results in HOS, which implies that *TBX5* function is dosage-sensitive [141, 142]. In zebrafish, a recessive mutation in *tbx5a* affects the formation of pectoral fins and the proper morphogenesis and function of the heart [139]. *heartstrings* (*hst*) mutants do not form pectoral fin buds and initially form a heart that later fails to loop and deteriorates over time [139]. While the *hst* heart deteriorates, it also has a slowed heart beat and extrudes cells into the pericardial sac that also expands and swells in edema [139, 143].

Many subsequent studies of *tbx5a* function have used morpholinos against the *tbx5a* transcriptional start site [33, 41, 73, 144, 145]. Pi-Roig et al. (2014) conduct experiments comparing apparent discrepancies between morphant versus mutant phenotypes of *tbx5a*, the major discrepancy being that the morphant exhibits a laterality phenotype in the direction of heart looping while the *hst* mutant does not [140]. They find that the *hst* mutant allele behaves like a hypomorph, in that it does not behave like a complete loss-of-function allele that they create [140]. Additionally, transcriptional compensation between the *tbx5a/b* paralogs occurs only in the mutants and not in the morphants [146, 147]. Therefore, it seems reasonable to assume that studying the morphant phenotypes might provide a more accurate depiction of how each *tbx5a/b* paralog functions than studying the mutant phenotypes currently available. In this dissertation, I use the Tbx5a morpholino to study the function of *tbx5a*. This method is also logistically superior to using the *hst* mutant, since every mor-

phant embryo shows a phenotype, whereas only 1 in 4 offspring from a heterozygous mating pair will be homozygous for the mutation.

1.5.3 Tbx5a Function in Precursor Specification in the Pectoral Fin and Heart

Since Tbx5a is expressed in the pectoral fins and heart and also is required for the proper formation of these organs, it is logical to ask how molecularly and cellularly *tbx5a* accomplishes this task. As a transcription factor, Tbx5a binds to DNA in dimers, which provides insight into how the *TBX5* phenotype is dosage-sensitive in humans and zebrafish [139, 141]. Crystal structure of the Xenopus TBX5 protein shows that it binds in the form of a homodimer, which interacts with both the minor and major groves of DNA [148]. By using antibodies against mammalian TBX5, researchers have identified co-occupants of TBX5 binding sites on cardiogenic genes [149, 150]. The co-occupation of TBX5 with other transcription factors such as Gata4, or Nkx2-5, activates transcription of downstream target gene activity to specify cardiomyocyte fate [151, 152, 153, 154]. In non-cardiac cell types, TBX5 can bind DNA as a transcriptional repressor to inhibit non-cardiomyocyte gene expression and fate [155, 156]. In pectoral fin precursors, Tbx5a is required to initiate expression of *fgf24* which subsequently activates *fgf10* expression and is also sufficient for the initiation of the pectoral fin [43, 50]. Later in development, TBX5 is necessary for the continued outgrowth of the forelimb and to maintain expression of FGFs in the forelimb mesenchyme [157]. In summary, *TBX5* function is required in both forelimb and heart precursors to initiate developmental programs that will specify that particular organ fate. The next subsections will discuss particular cellular and physiological functions of TBX5 in mouse and how it relates to my work studying *tbx5a* in zebrafish.

1.5.4 Tbx5a Function in Cellular Migration

The ability of TBX5 to affect cellular migration of LPM-derived cells has mainly been studied in amniote heart cells *in vitro*. More specifically, the function of *TBX5* in active migration processes is best described in the migrating proepicardium in mouse [158, 159, 160]. Using canine and quail cells, Hatcher et al. (2001) observed that overexpression of TBX5 resulted in inhibition of myocardial growth and proliferation [158]. A later publication by the same group describes the effect of both TBX5 overexpression and knockdown in perturbing proepicardial cells' abilities to spread over the heart, contribute to coronary vessels, and progress the leading edge of migrating cultured proepicardial explants over collagen-coated dishes [159]. Another further experiment demonstrates that *TBX5* function is required in the myocardium over which the epicardial cells migrate but does not assess whether *TBX5* function is required in the epicardial cells themselves [160]. Altogether, these experiments show that TBX5 is required in a dose-dependent manner for the migration of epicardial cells. However there are currently no experiments studying the effect of *tbx5a* on cell migration in zebrafish hearts.

In Q. Mao's doctoral work, she investigated the cell migration of the LPM adjacent to somites 1 to 4 and found that *tbx5a* is required for the convergent migration of the pectoral fin precursors [33, 56]. More specifically, anteriorly-positioned LPM cells were more affected in their displacement, speed, and persistence than posteriorly-positioned LPM cells [56]. Q. Mao's work suggested that *tbx5a* affected pectoral fin cell motility through regulation of *fgf24*; however, the same mechanism may not apply in the ALPM [33, 56]. Q. Mao did not study the LPM cells anterior to somite 1, and therefore I became interested in studying *tbx5a* function on cell migration in the ALPM.

CHAPTER 2

SINGLE-CELL RESOLUTION FATE MAP OF THE LATERAL ALPM REVEALS *TBX5A* FUNCTION IN THE DEVELOPMENT OF FOUR TISSUES

2.1 Preface

Much of the work described herein is included in a manuscript currently under review with the following title, "Fate mapping analysis of anterior Lateral Plate Mesoderm reveals *tbx5a* function in left-right asymmetry and cell specification of cardiac precursors." This manuscript was authored by Lindsey M. F. Mao, Erin A. T. Boyle Anderson, and Robert K. Ho. Boyle Anderson contributed to the fate mapping experimentation and editing of the manuscript. The 24 hpf fate map was not included in this manuscript and the text in this chapter has been adapted for this dissertation.

2.2 Abstract

The ALPM gives rise to the heart, pericardial sac, pharyngeal arches, and peritoneum. Generally, it is unknown how these four tissues arise out of the undifferentiated ALPM. By conducting a single-cell resolution fate map of the lateral ALPM, I have been able to provide insight into how the ALPM is patterned. I find that the ALPM at 18 hpf is not organized into regions according to fate along either the mediolateral or anterioposterior axes. However, I do find a significant difference between the number of cardiac precursors on the right and left side (right side lateral ALPM has twice as many cardiac precursors than the left). This left-right asymmetry is affected (made symmetric) in the Tbx5a-deficient fate map. These differences in laterality are only seen among the cardiac precursors, which allows me to make inferences regarding how *tbx5a* function is required for specification of second

heart field cells.

2.3 Rationale

Lineage tracing of individual blastomeres in zebrafish shows that cardiac precursors within the anterior lateral plate mesoderm (ALPM) can migrate toward the midline to form the primary heart tube (PHT) [25]. The cardiac precursors that give rise to the PHT are called the First Heart Field (FHF) and cardiac precursors that later add onto the PHT through the venous and arterial poles are called the Second Heart Field (SHF). While the medially migrating ALPM contributes to the FHF, cells of the lateral ALPM migrate anteriorly to give rise to several fates including parts of the SHF, the pericardial sac, pharyngeal arches, and the peritoneum. We define the anteriorly migrating region of the ALPM to include those cells at 18 hours post fertilization (hpf) that are located lateral to the paraxial and intermediate mesoderm, posterior to the vascular precursors, and anterior to the boundary of the pectoral fin precursor field at somite 1 [33]. Previous fate maps of the ALPM focused on the cardiac precursors and were conducted in midblastula-stage, 40% epiboly and 11 hpf embryos and followed cells to 26 hpf and 44 hpf [25, 75, 77]. A general fate map of the lateral anteriorly-migrating ALPM was lacking until my study. I sought to establish this fate map to bring insight into how the ALPM precursors undergo specification over time. Fate mapping of the pectoral fin field of LPM cells adjacent to the anteroposterior positions of somites 1 and 4 at 16 hpf shows that the cells retain their relative anterior-posterior positional identity in the eventual pectoral fin bud [33].

Q. Mao et al. (2015) found that the LPM-derived pectoral fin precursors maintain a **topological** relationship to each other along the anteroposterior axis, meaning that anteriorly labeled precursors give rise to anterior portions of the pectoral fin bud and posteriorly labeled precursors give rise to posterior portions [33, 56]. I hypothesized that the ALPM may be patterned similarly, and so I evaluated not only the fates of ALPM precursors, but

also the relative positions and substructures that precursors gave rise to in constructing my fate map.

It is not completely known what structures the ALPM eventually form within the linear heart tube or multi-chambered larval heart later in development. It is also unknown what other structures besides the heart might be derived from the ALPM. We assume that SHF precursors reside in the ALPM since the timing of the developing heart coincides with the anterior migration of the lateral ALPM (Fig. 1.3). However, this assumption had not been directly tested through a comprehensive analysis of the ALPM. In my study, I sought to find patterns in the spatial composition of the ALPM with regard to fates and maintenance of topological relationships.

Furthermore, I was interested in understanding how *tbx5a* functions in the specification of the ALPM. In Tbx5a mutant and morphant embryos, the linear heart tube still develops and beats (although with a slower rate), therefore the Tbx5-expressing cells of the ALPM must be necessary for development of the heart beyond the stage of PHT formation [38, 161]. Additionally, in the Tbx5a-deficient embryo, the *tbx5a*-transcribing anterior LPM cells are more spread out and mis-migrate [41]. The fates of these mis-migrating cells are unknown, though Q. Mao hypothesized that they may become peritoneum cells [56]. If *tbx5a* functions to maintain the identity of a particular fate within the ALPM, for example, SHF cardiomyocyte, then Tbx5-deficient cells might take on other ALPM fates, such as peritoneum. If *tbx5a* functions to maintain ALPM identity, then the Tbx5a-deficient cells might take on a non-ALPM fate, such as vasculature, or might undergo programmed cell death. To distinguish between these different possibilities of *tbx5a* function, I fate mapped the 18 hpf ALPM when the function of *tbx5a* is abrogated.

2.4 Results

2.4.1 The ALPM exhibits extensive overlap between organ-specific fate map regions

Q. Mao et al. (2015) reported that the single-cell resolution fate map of the LPM adjacent to somites 1 through 6 gave rise to mainly the pectoral fin bud [33]. Two other fates were observed to arise in this fate map area: cardiac and peritoneum. In my fate map, I sought to assess the fates of the lateral ALPM tissue using similar methods. A visual representation of my fate mapping method is shown in Fig. 2.1.

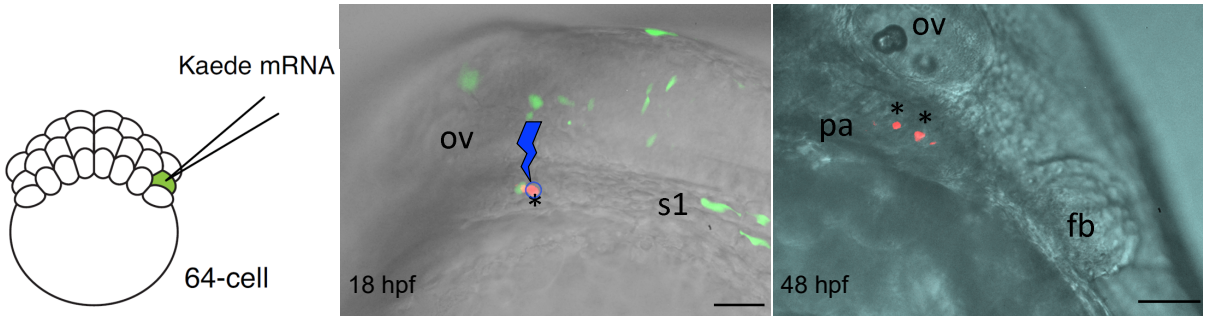

Figure 2.1: **Schematic of fate mapping methodology.** At the 64- to 128-cell stage, individual blastomeres were microinjected with Kaede mRNA. The resultant embryo at 18 hpf expressed green unphotoconverted Kaede in a random mosaic pattern. At 18 hpf, I closed the fluorescence pinhole of the microscope down onto a single isolated green cell that resided within the ALPM. Through the pinhole, schematized as the blue circle, I exposed a single green cell to 405 nm UV light to irreversibly photoconvert a cell from green to red fluorescence, asterisk. In this particular example, a cell posterior to the otic vesicle (ov) and anterior to somite 1 (s1) was phtoconverted on the left side of the embryo. At 48 hpf, I searched for the red fluorescent cell(s) and recorded the fate, position within the organ, and number of cells derived from the single precursor. In this particular example, two photoconverted cells resided in the posterior pharyngeal arches. Scale bar 100 μm.

I injected single blastomeres in 64- to 128- cell stage embryos with Kaede mRNA to create random mosaic-expression. I then photoconverted the Kaede from green fluorescence to red in individual ALPM cells that were positioned lateral to the intermediate mesoderm and

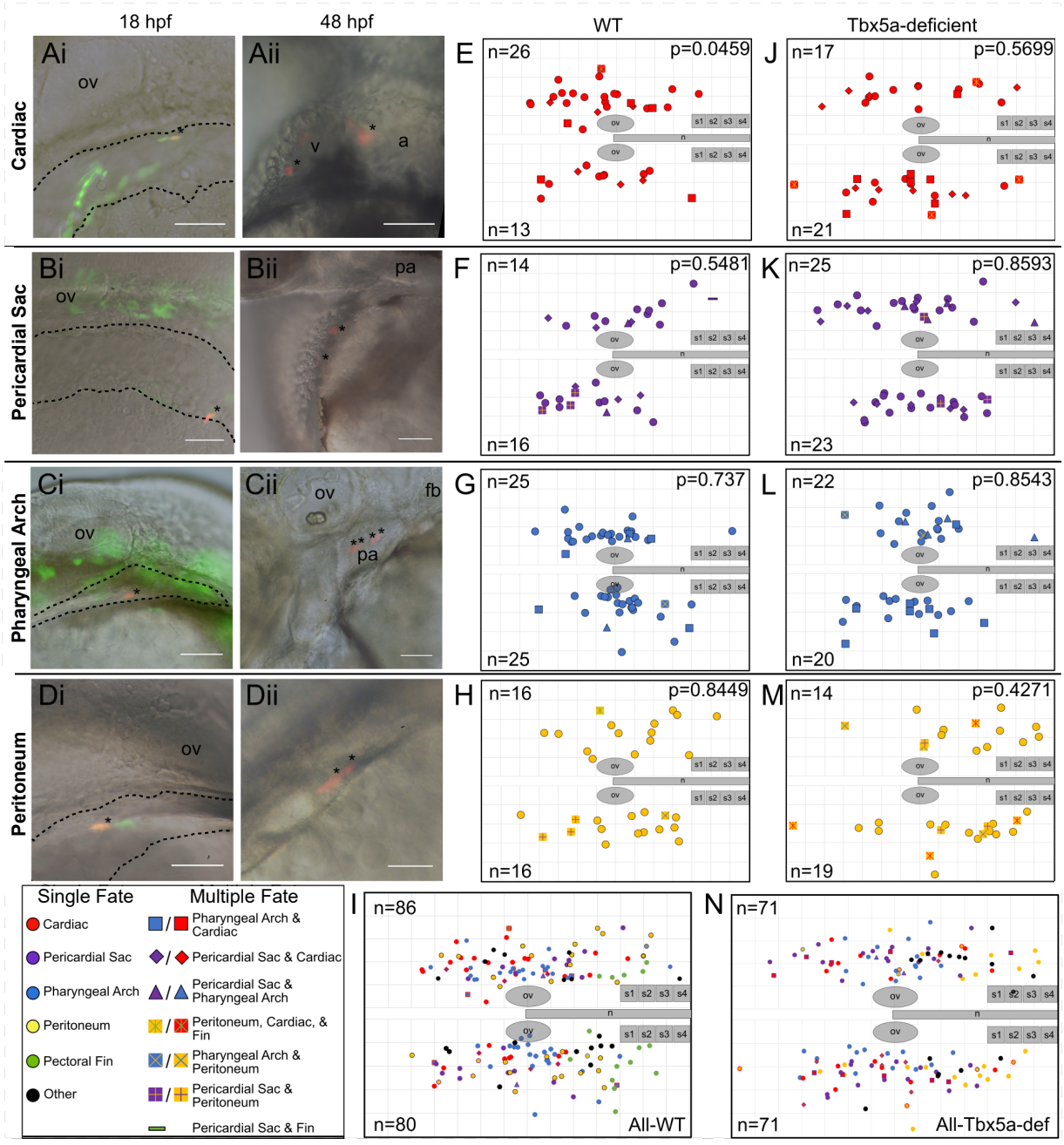

Figure 2.2: **Single-cell resolution 18 hpf fate map of WT and Tbx5a-deficient ALPM.** (Cont. on next page)

Figure 2.2: (Continued) A-D Examples of labeled wild-type single cells within the ALPM, dashed outline. The asterisk marks a single cell photoconverted to express red fluorescent Kaede, whose starting position was measured based upon the anteroposterior and mediolateral distance from the otic vesicle. Ai- Lateral view of the 18 hpf embryo. Aii- Ventral view of the same embryo at 48 hpf. Asterisks mark resultant clone in the heart. Bi, Bii- Lateral view of pericardial sac clone. Ci, Cii- Pharyngeal arch clone. Di, Dii- Peritoneum clone. E-N Dorsal view fate map of ALPM cell fates at 18 hpf (E-I wild-type, J-N Tbx5a-deficient), showing the four fate categories: E, J-cardiac; F, K-pericardial sac; G, L-pharyngeal arch; and H, M-peritoneum. I, N- Summary fate map of all labeled single cells within the ALPM. Circles denote unipotent clones, other shapes denote multipotent clones, refer to legends for identity. N counts represent the number of precursors from the right or left ALPM that gave rise to that particular fate. P-values determined by comparing the number of left and right progenitors using the Fishers Exact test. v, ventricle; a, atrium; fb, fin bud; ov, otic vesicle; pa, pharyngeal arches; n, notochord; s1, somite 1. Grid length and scale bar: 100 μm

anterior to somite 1 at 18 hpf. Using the otic vesicles as relational landmarks at all stages of development, we constructed a fate map consisting of 166 labeled single cells (Fig. 2.2I). We classified labeled cellular clones into six identity groups according to the location and morphology of the photoconverted cells at 24 and 48 hpf: (1) cardiac (Fig. 2.2A, E, n=39), cells which gave rise to myocardial and sometimes endocardial tissue (Fig. 2.3), but did not contribute to the PHT (Fig. 2.4); (2) pericardial sac (Fig. 2.2B, F, n=30), cells which gave rise to either the caudal- or rostral-most tissue surrounding the heart; (3) pharyngeal arch (Fig. 2.2E, G, n=50), cells which gave rise to the mesenchymal cores of all six pharyngeal arches, but mostly lied within the mandibular and first hyoid arches; (4) peritoneum (Fig. 2.2D, H, n=32), cells which gave rise to the tissue laterally positioned over the yolk sac or surrounding the intestinal track; (5) pectoral fin (n=17), cells which gave rise to the mesenchyme of the pectoral fin bud; (6) other (n=18), cells which consisted of non-ALPM (somitic or intermediate mesoderm, midline, and eye) clones. The lateral ALPM at 18 hpf therefore gives rise to at least four mesodermal fates: cardiomyocytes, pericardial sac, pharyngeal mesenchyme, and peritoneum.

The total area fate mapped at 18 hpf ranges from 500 μm anterior to the otic vesicle, at the level of the posterior midbrain, to 600 μm posterior to the otic vesicle, adjacent to

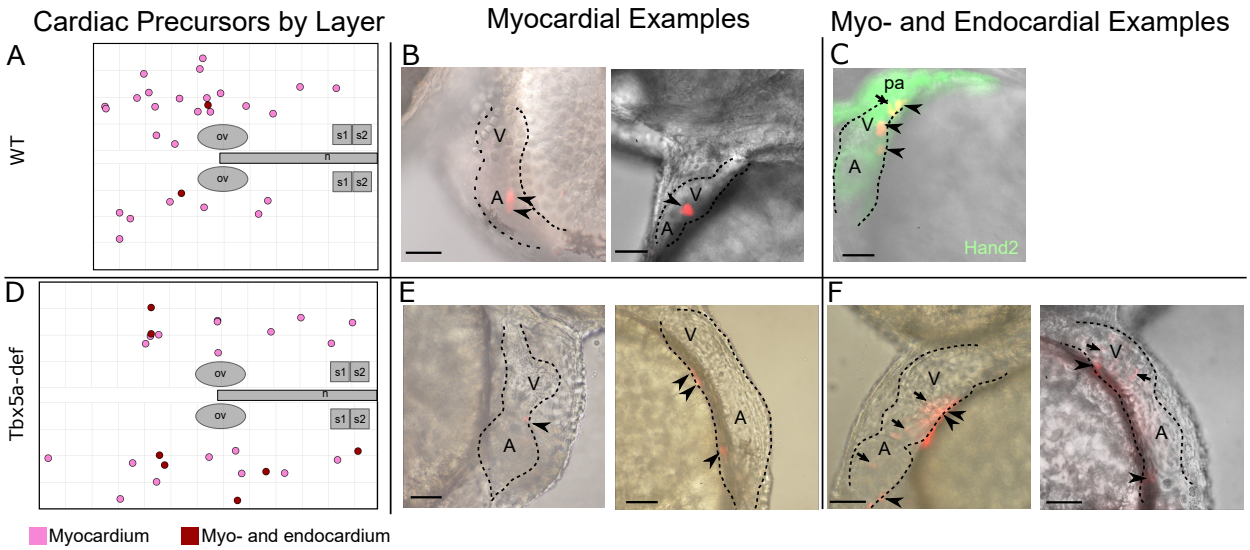

Figure 2.3: **Cardiac precursors within the ALPM give rise to myocardial and infrequent endocardial cells.** A- Twenty-seven (27) photoconverted wildtype clones gave rise to only myocardium (pink), while two (2) gave rise to myocardium and endocardium (burgundy). B, C, E, F- Examples of larval hearts at 48 hpf, outlined with dashed lines, lateral view. B- Wildtype cardiac precursors that gave rise to only myocardial cells, which display a cuboidal morphology (arrowheads). C- Wildtype cardiac precursor that gave rise to myocardium as well as endocardium cells, which in general are smaller and more elongated in morphology than myocardium cells (arrow). Hand2 expression marks the larval heart and pharyngeal arches at 48 hpf. D- Nineteen (19) phtoconverted Tbx5a-deficient clones gave rise to only myocardium (E arrowheads), while seven (7) gave rise to myocarium and endocardium (F arrows). ov-otic vesicle; n- notochord; s1- somite 1; A- atrium; V- Ventricle; pa- pharyngeal arch. Scale bar 100 μm.

somite 3. In the mediolateral direction, the ALPM extends from the medial end of the otic vesicle to about 300 μm lateral of the otic vesicle, a region which was determined by the morphological edge of the ALPM as observed by Nomarski optics (Fig. 2.2Ai-Di, dashed outline). Most labeled precursors in wildtype embryos gave rise to a single fate, though a small number of labeled precursors gave rise to two fates (Fig. 2.5 Rows 6–15), and one precursor gave rise to three fates. In addition to giving rise to cardiac fate, six precursors also gave rise to pericardial sac fate (Fig. 2.2E, F diamonds; Fig. 2.5 Row 6), five precursors also gave rise to pharyngeal arch fate (Fig. 2.2E, G squares; Fig. 2.5 Row 7), and one precursor also gave rise to peritoneum and pectoral fin fate (Fig. 2.2E, H six-pointed cross; Fig. 2.5 Row 16). In addition to giving rise to pericardial sac fate, two precursors also gave rise to pharyngeal arch fate (Fig. 2.2F, G triangles; Fig. 2.5 Row 10), three precursors also gave rise to peritoneum fate (Fig. 2.2F, H plus in square, Fig. 2.5 Row 11), and one precursor also gave rise to pectoral fin fate (Fig. 2.2F dash; Fig. 2.5 Row 12). In addition to giving rise to pharyngeal arch fate, one precursor gave rise to peritoneum fate (Fig. 2.2G, H X in square; Fig. 2.5 Row 13).

Fates within the 18 hpf lateral ALPM occupy overlapping regions that cannot be distinguished by their centers of mass nor by their confidence ellipses (Fig. 2.6), except for the pectoral fin-forming region of the fate map, which lies adjacent to somite 1 through 4 [33]. Although the confidence ellipse around pectoral fin clones overlaps with the others, the center of mass is still distinguishable from those of other fates (Fig. 2.6). Despite no statistically significant regionality within any of the fates, slight trends exist along the anteroposterior and mediolateral axes (Fig. 2.7). Cardiac precursors arise from positions slightly more anterior than posterior to the otic vesicles (Fig. 2.7F red bars). Pericardial sac precursors arise from slightly more lateral than medial positions (Fig. 2.7C purple bars). Pharyngeal arch precursors arise from slightly more medial than lateral positions (Fig. 2.7C blue bars). Peritoneum precursors arise from slightly more posterior and lateral positions (Fig. 2.7C,

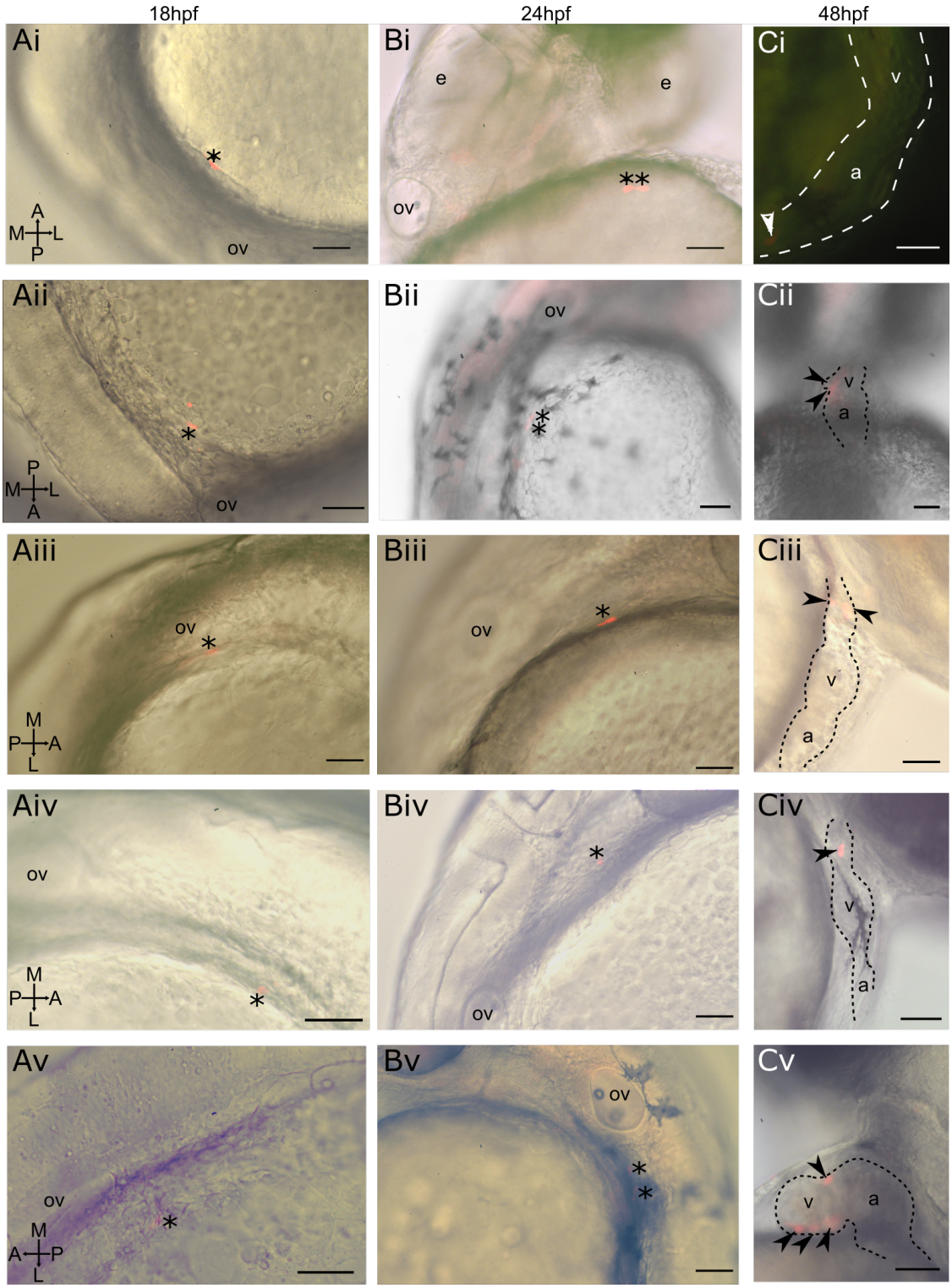

Figure 2.4: **Photoconverted ALPM cardiac precursor clones do not contribute to the primary heart tube at 24 hpf.** (Cont. on next page)

Figure 2.4: (Continued) i-v Displaying five (5) of thirty-nine (39) examples of wildtype embryos. A- Lateral view of 18hpf embryo. Asterisk marks a single cell photoconverted to express red fluorescent Kaede. B- Lateral view of same embryo at 24 hpf. Asterisk marks uncaged heart precursor outside of the primary heart tube, currently out of view on the left side of the embryo. C- Lateral view of same embryo at 48 hpf. Asterisk marks uncaged heart precursor within the larval heart.

F yellow bars). Pectoral fin precursors arise nearly exclusively from the most posterior region of the fate map (Fig. 2.7F green bars). I also found no topological conservation, or spatiotopic arrangement, of original anteroposterior or mediolateral position within the four separate ALPM organ fields at 48 hpf, unlike what has been previously reported for the pectoral fin-forming region [33]. For example, pharyngeal arch precursors that were labeled more anteriorly within the lateral ALPM did not consistently give rise to the most anterior (mandibular or hyoid) arches but formed clones that were equally distributed amongst the mesenchymal cores of pharyngeal arches 1-6 (Fig. 2.2Cii).

Before conducting this fate map, I hypothesized that there might be particular regions within the lateral ALPM that give rise to specific regions of the larval heart. Previous studies in zebrafish report SHF contributions to the outflow tract, inflow tract, and ventricle from anywhere between 28 and 72 hpf [38, 74, 66, 73]. Therefore, I recorded the region of the larval heart that each cardiac clone contributed to by 48 hpf. Just as there are no specific areas of my 18 hpf fate map that give rise to any one specific fate (Fig. 2.6), there are also no specific areas that give rise to any specific region of the heart. More specifically, there was no correlation between the starting positions of the fate map and the location nor identity of cardiomyocytes at 48 hpf. Examples of labeled cardiomyocytes that end up in various chambers of the heart can be seen in Fig. 2.4. In Fig. 2.4i, an anteriorly positioned labeled precursor on the right side at 18 hpf gave rise to the inflow tract. In Fig. 2.4ii, a more posterior and lateral precursor on the left side at 18 hpf gave rise to the atrioventricular junction. In Fig. 2.4iii, a precursor located close to the otic vesicle on the right side at 18

Row #		Fate at 48hpf					Number of Clones
	Clone Fate	Heart	Pericardial Sac	Pharyngeal Arch	Peritoneum	Fin Mesenchyme	
1	Single	x					27[a]
2			x				18
3				x			42[b]
4					x		27[a]
5						x	15
6	Double	x	x				6
7		x		x			5
8		x			x		0
9		x				x	0
10			x	x			2
11			x		x		3
12			x			x	1
13				x	x		1
14				x		x	0
15					x	x	0
16	Triple	x			x	x	1
17	Total Clone #	39	30	50	32	16	148
18	% of all	26%	20%	34%	22%	11%	
19	# of multipotent	12	12	9	5	2	
20	% of total	8%	8%	6%	3%	1%	13%
21	% of fate	31%	40%	18%	16%	13%	

a. 1 also made vasculature.

b. 1 also made blood.

Figure 2.5: **ALPM wildtype clone counts by fate.** Rows 1-16- Each row represents precursors according to their fate(s) at 48 hpf, marked with Xs in the columns. The count at the end of the row (last column) is the number of experiments (labeled precursors) that belong to that fate category. Rows 6-15- Multipotent precursors that gave rise to two fate. Row 16- One multipotent precursor that gave rise to three fates (possible outlier). Rows 17-21- Sums and percentages in each column divided by the total (148) or by the sum in each fate. Note: Clones designated as "other" are not included

hpf gave rise to the outflow tract.

At 48 hpf, the larval heart is made up of myocardium and endocardium. At this time, the proepicardium resides adjacent to the heart and will start its migration in clusters over the myocardium. Therefore, I did not expect to see epicardial cells in my fate map analysis. Currently, there are no studies that describe the relative contributions of myocardium and endocardium to the larval heart. Therefore, I did a visual analysis of the morphologies and

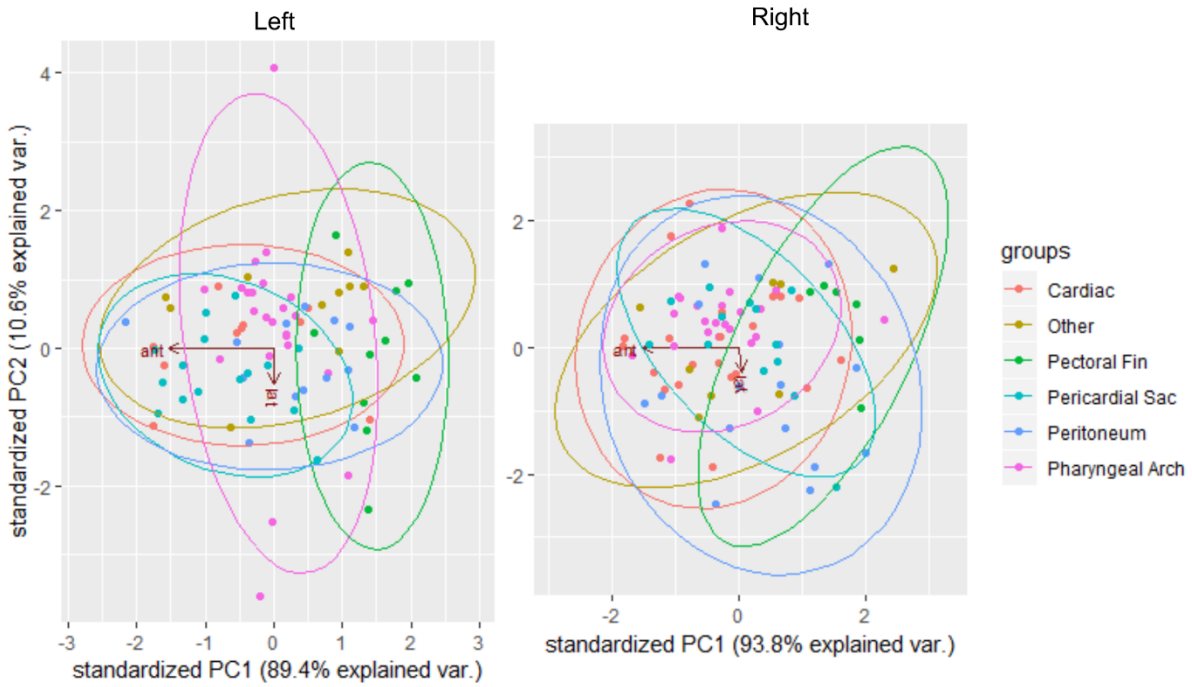

Figure 2.6: **Confidence ellipses of 18 hpf WT fate map points on left and right sides.** 95% confidence ellipses on principle component analyses of anterior (PC2) and lateral (PC1) positions and variance.

positions of cardiomyocytes in my fate map to determine which layer they resided in at 48 hpf. Large cuboidal-shaped cardiomyocytes are myocardial. Smaller and elongated cardiomyocytes are endocardial. Examples of my comprehensive analysis of how the majority cardiac precursors gave rise to the layers of the heart can be seen in Fig. 2.3. Typically, other investigators use myocardial-specific transgenes to visualize and quantify the myocardium. However, this was technically unfeasible given my experimental setup. I could not use transgenic markers for the various cardiac lineages since identification of often a single cell expressing green to red fluorescence was key to the method. The addition of another fluorescent marker would have greatly reduced my ability to observe the fates, morphologies, and positions of single cells in the heart. I considered antibody staining to assess the cell types after photoconversion. However, no antibody exists to distinguish between photoconverted and non-photoconverted Kaede protein. In Fig. 2.3, I analyzed the majority (27 out of 39)

wildtype images of cardiomyocytes (the other photos did not have sufficient resolution due to the movements of the heart), and I found that all cardiac precursors gave rise to myocardium and only two precursors gave rise to both myocardium and endocardium. Therefore, later additions to the heart mostly consist of myocardial contributions.

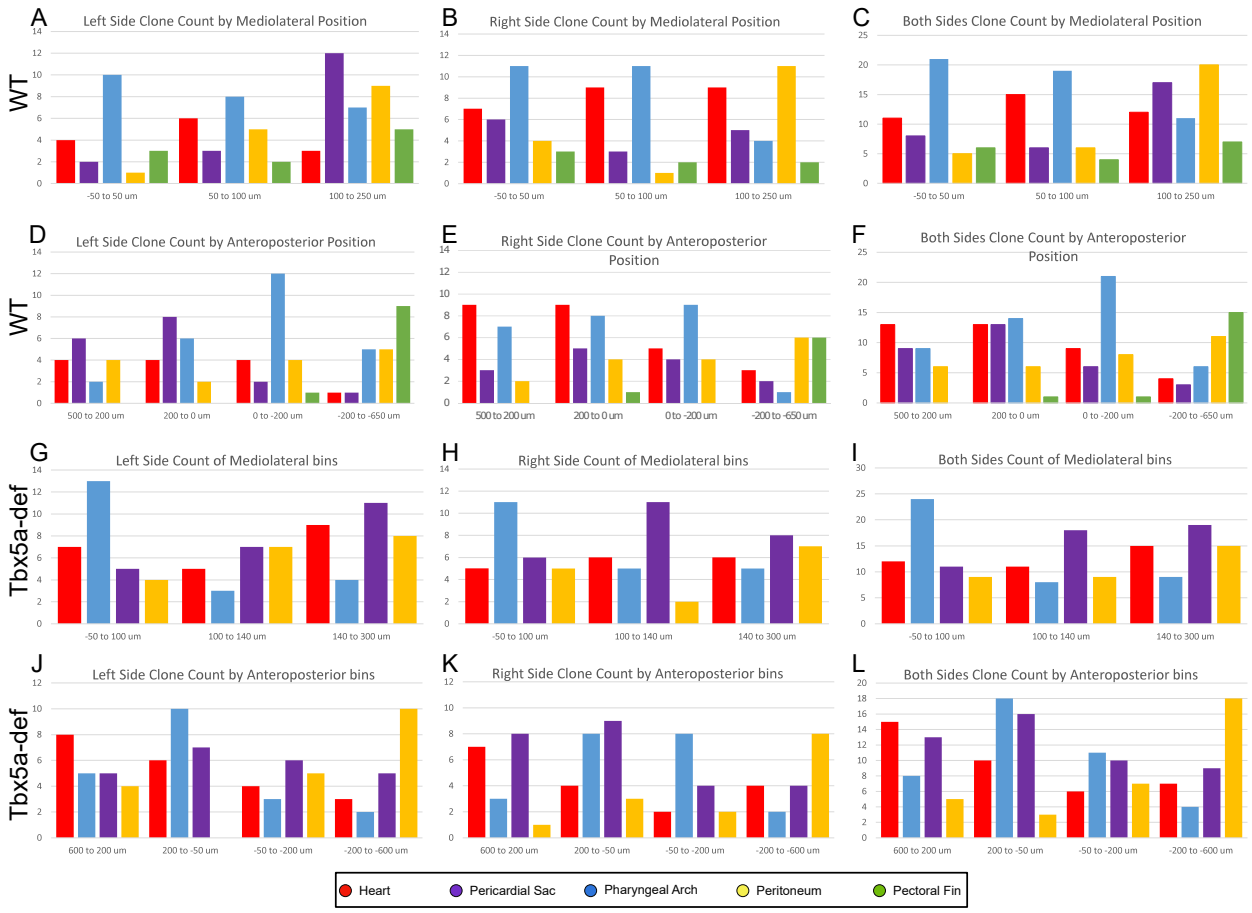

Figure 2.7: **Breakdown of all fate map fates by laterality, mediolateral position, and anteroposterior position.** A-C and G-I- Clone number separate by mediolateral bins of equal number of clones. D-F and J-L- Clone number separated by anteroposterior bins of equal number of clones. A, D- WT clones arising from the left side. B, E- WT clones arising from the right side. C, F- WT clones arising from both left and right sides. G, J- Tbx5a morphant clones arising from the left side. H, K- Tbx5a morphant clones arising from the right side. I, L- Tbx5a morphant clones arising from both left and right sides. red- cardiac clones; blue- pharyngeal arch clones; purple- pericardial sac clones; yellow- peritoneum clones; green- pectoral fin clones.

2.4.2 ALPM fate map at 24 hpf

I followed and imaged the locations of photoconverted precursors at 24 hpf for two main reasons. First, I wanted to make sure that my labeled cardiac precursors did not make up the PHT by 24 hpf. Second, having an intermediate timepoint for the fate map can give more insight into how the cells develop over time. At 24 hpf, labeled precursors still resided in the lateral ALPM and mostly had a clone size of one; i.e. most labeled precursors did not undergo division between 18 and 24 hpf. In the cases where a precursor had divided (as evidenced by two red fluorescent cells), they were always positioned closely apposed to each other, suggesting that the daughters did not migrate apart from each other from 18 to 24 hpf. Therefore, it was easy to measure the locations of photoconverted precursors at 24 hpf relative to the otic vesicle.

The 24 hpf fate map overall shows how the ALPM as a tissue has elongated in the anteroposterior direction by about 100 μm. The slight trends observed in the 18 hpf fate map still exist at 24 hpf (Fig. 2.7): pharyngeal arch precursors are positioned slightly more medially and peritoneal precursors are positioned slightly more laterally. However, it does not appear as if cardiac precursors are positioned slightly more anteriorly. By comparing the final and initial positions relative to the otic vesicle between 18 and 24 hpf, wildtype ALPM precursors do not significantly shift. The average net medial displacement is 12 $\pm$8μm and the average net posterior displacement is 38$\pm$36μm of all precursors, which is approximately the distance of a cell length. The displacements of precursors sorted by fate do not significantly differ from one another. Therefore, the composition and net movements of the ALPM precursors from 18 to 24 hpf do not change significantly. Furthermore, the displacements of individual precursors vary greatly, from a net movement of 10 to about 500 μm. These data indicate firstly that there is still no regionality in precursors by fate at 24 hpf; secondly that individual precursors do not maintain topological or nearest neighbor organization; and thirdly that the ALPM precursors at 18 hpf remain within the ALPM at

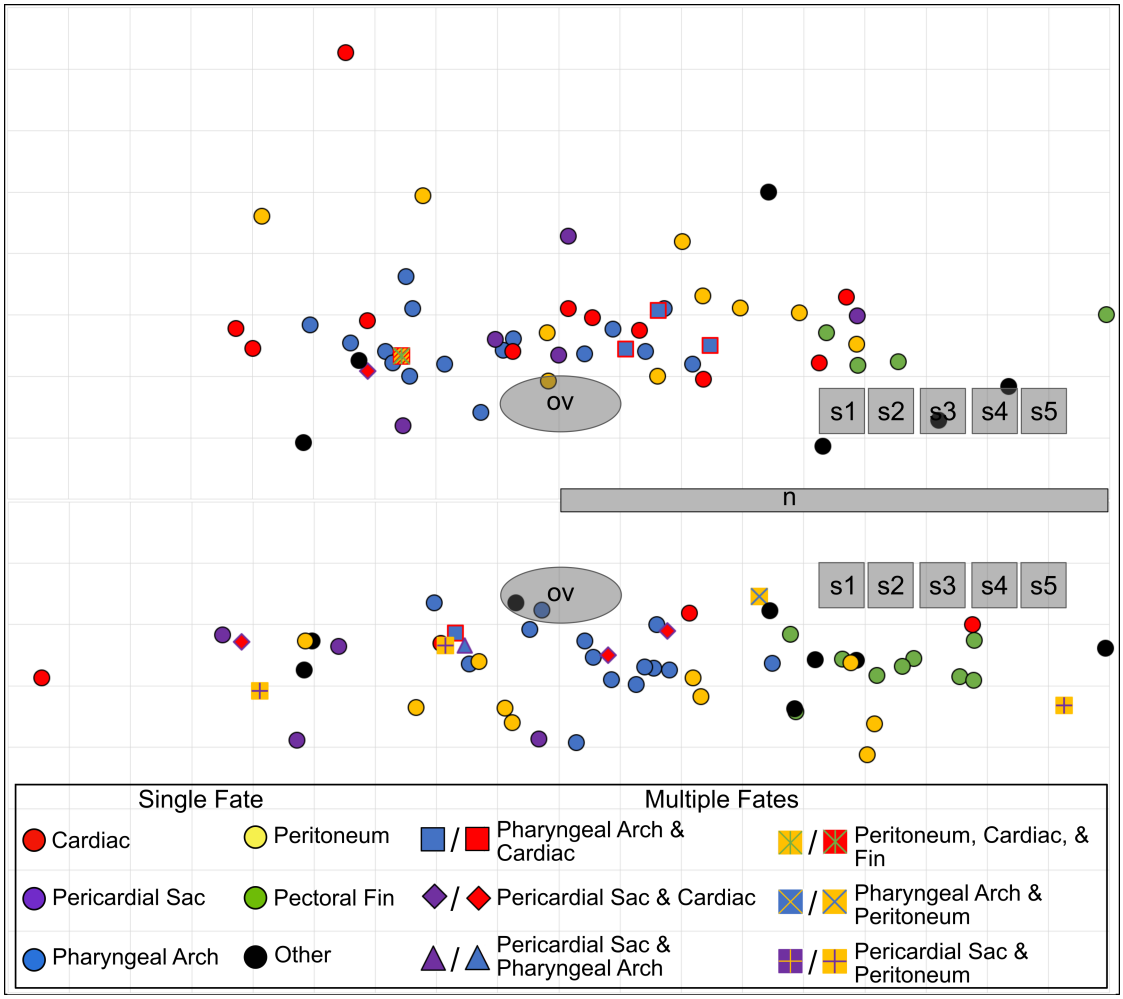

Figure 2.8: **24 hpf fate map of wildtype ALPM.** Summary fate map of all labeled single cells within the ALPM at 18 hpf. Positions were measured based upon the anteroposterior and mediolateral distance from the otic vesicle at 24 hpf. Circles denote unipotent clones, other shapes denote multipotent clones, refer to legends for identity. v, ventricle; a, atrium; fb, fin bud; ov, otic vesicle; pa, pharyngeal arches; n, notochord; s1, somite 1. Grid length and scale bar: 100 μm

24 hpf.

2.4.3 Left-right asymmetries between early cardiac precursors

Within the wildtype fate map data, I found that twice as many cardiac precursors arose from ALPM cells on the right side of the embryo than from the left (Fig. 2.2E, Fisher's

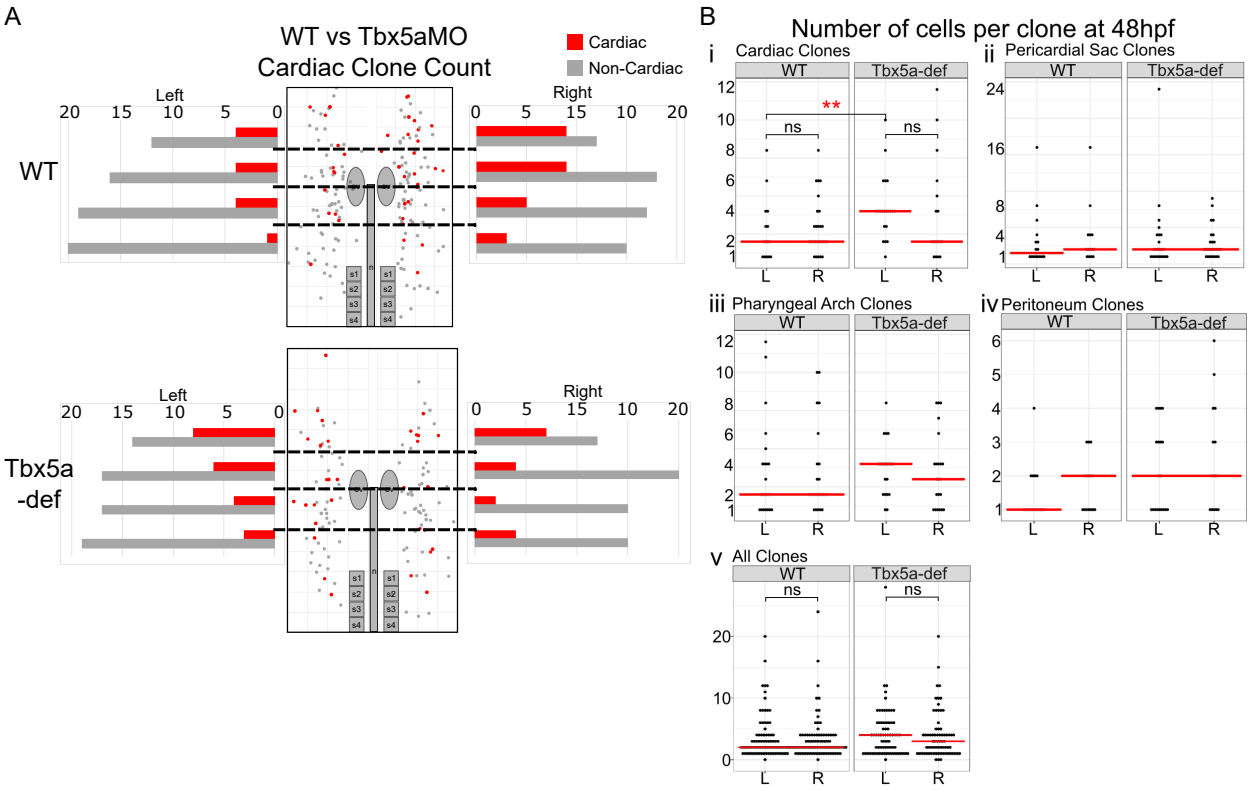

Figure 2.9: **Cardiac precursor asymmetries are affected in Tbx5a morphants.** A- Graphical representation of precursors deriving heart versus non-heart fates arising from AP regions of equal bin size of 20 precursors per side. B- Number of cells per clone at 48 hpf reflects the amount of proliferation of ALPM between 18 hpf and 48 hpf. The red bar represents the median. Statistics performed using the Kruskal-Wallis rank sum test.

Exact Test p=0.0459). This asymmetrical difference was not observed within any other fates (Fig. 2.2F-H). Furthermore, when the fate map is divided into anteroposterior bins of equal total precursor size, I observed that left-right difference in cardiac precursors was larger within anterior bins than within the posterior bins (Fig. 2.9A, Fig. 2.7D, E red bars).

To understand how this right-biased asymmetry contributes to the development of the larval heart, I first assessed how the cardiac precursors proliferated between 18 and 48 hpf. By analyzing the clone size of red fluorescent cells at 48 hpf, I can infer how many times the precursor underwent cellular division. For example, if I observe four red fluorescent cells at 48 hpf, I assume that the precursor divided twice. My assumption does not account for cell

death, since I did not perform a lineage tracing experiment that tracked precursors and their divisions over time. I also observed clone sizes that were odd in number (such as 3 or 5) and that were not part of the exponential sequence (such as 6 or 10). These clone sizes may arise from only one daughter cell undergoing division. In my analysis of clone size, I separated the counts if the precursor gave rise to more than one fate. For example, if a ALPM precursor gave rise to 1 cardiomyocyte and 2 pericardial sac cells, then I recorded the "all clone" size as 3 while the "cardiac clone" size is 1 and the "pericardial sac" clone size is 2. The results of my analysis are shown in Fig. 2.9B. Overall, precursors divided about twice on average and there was no significant difference in the clone size between precursors that arose from the left versus right sides (Fig. 2.9Bv, Kruskal Wallis Rank Sum Test p=0.3055). Within individual cardiac clones, there was no significant difference in the number of progeny arising from the left (average clone size 2.733 cells) versus right side (average clone size 2.926)(Fig. 2.9Bi, p=0.2806). This result indicates that the asymmetry among the number of cardiac precursors between the left and right is not affected by differences in proliferation.

2.4.4 tbx5a *maintains left-right asymmetry in the ALPM*

As *tbx5a* is expressed within the ALPM and functions in heart and forelimb development, I sought to discover how *tbx5a* is involved in patterning the ALPM. I constructed a fate map of the lateral ALPM in Tbx5a-deficient embryos generated using morpholino knockdown, which has been shown to faithfully recapitulate the loss of pectoral fin bud formation displayed in the *heartstring/tbx5a (hst)* mutant phenotype [41, 139]. From 142 labeled single cell precursors, I performed similar analyses to the wild-type ALPM fate map (Fig. 2.2J-N, 2.11). As expected, no pectoral fin clones were observed in the Tbx5a-deficient embryos, as injections of Tbx5a morpholinos have been shown to faithfully recapitulate the loss of pectoral fin bud formation displayed in the *hst* mutant. Overall the Tbx5a-deficient lateral ALPM is wider and longer than in the wildtype, which is measured via *Et(Hand2:eGFP)*

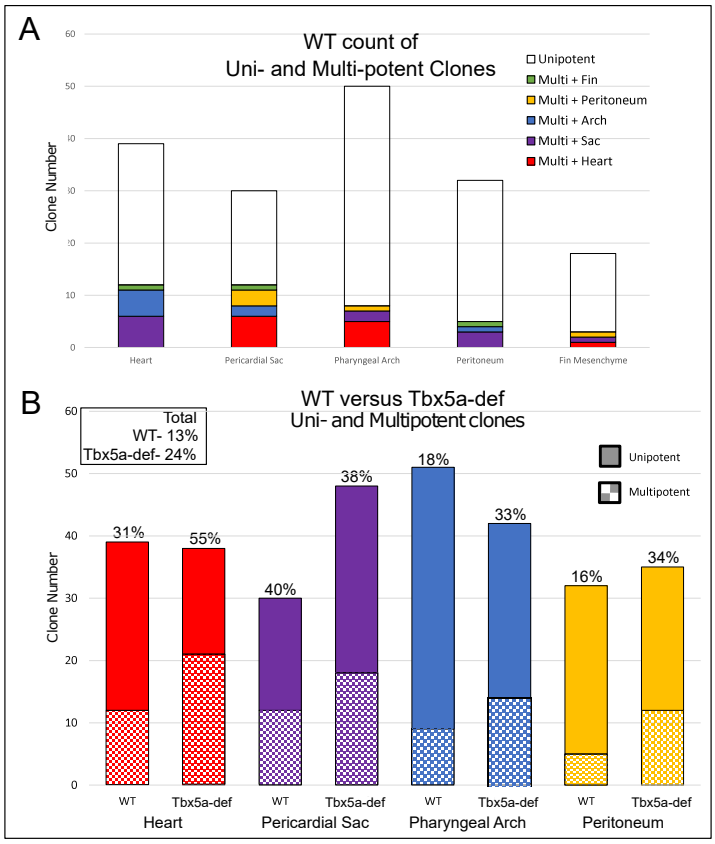

Figure 2.10: ***tbx5a* affects the number of multipotent precursors across all fates.** A- Stacked bar graphs of WT ALPM precursor count. B-Comparison of WT versus Tbx5a-deficient degree of multipotency.

expression and area of the fate map. However, the number of total cells in the tissue is the same between Tbx5a-deficient and wildtype (Fig. 2.2I,N, 3.5C).

Similar to the wildtype, Tbx5a-deficient cardiac precursors also gave rise to myocardium and endocardium of all chambers (Fig. 2.3) and were not found in the PHT at 24 and 48 hpf (Fig. 2.4). In contrast, I found that the Tbx5a-deficient fate map consists of an equal contribution of cardiac progenitors from the left and right sides (Fig. 2.2J). There were no left-right asymmetries in number of precursors for any of the fates (Fig. 2.2K-M). When I broke down the fates by anteroposterior bins, I also found slight trends between the bins , similar to those in wildtype: cardiac precursors arise in slightly more anterior than posterior locations (Fig. 2.7J-L, 2.9A, red bars); pharyngeal arch precursors arise in slightly more

medial than lateral locations (Fig. 2.7G-I, blue bars); peritoneal precursors arise in slightly more posterior and lateral than anterior and medial locations (Fig. 2.7G-L, yellow bars).

Compared to the right-biased contribution from the wildtype cardiac precursors, the Tbx5a-deficient ALPM does not display left-right asymmetry in the proportion of cardiac precursor number (Fig. 2.9A, p=0.4067). I questioned whether this observation correlates with how precursors from each side proliferate in Tbx5a-deficient embryos. Tbx5a-deficient cardiac precursors that arise from the left lateral ALPM have a median clone size that is twice as high as the wildtype (Fig. 2.9Bi, red asterisks p=0.006439), suggesting that *tbx5a* may suppress cardiac cell proliferation on the left side. There is neither significant difference between the right and left average clone size of all ALPM precursors (Fig. 2.9Bv, p=0.1806) nor of the cardiac precursors (Fig. 2.9Bi, p=0.1963) within Tbx5a-deficient embryos. Together, these findings suggest that *tbx5a* normally functions to maintain differences in the left-right distribution and proliferation of cardiac precursors that contribute to the heart.

2.4.5 tbx5a *functions during specification of ALPM organ-specific fates*

tbx5a could maintain left-right differential SHF contribution by a number of different non-mutually exclusive mechanisms. First, *tbx5a* could regulate the specification of cardiac versus other ALPM fates (e.g. pericardial sac, pharyngeal arch, etc.) differently between the right and left sides. Second, *tbx5a* could differentially affect the migration between the right and left sides into potential "organ pools". In order to assess the effect of Tbx5a on cardiac cellular specification, I analyzed the degree of multipotency of the fate map precursors at 18 hpf. In the wildtype fate map, most photoconverted precursors among all fates gave rise to a single unipotent fate. However, a small proportion of wildtype precursors, 13%, gave rise to two fates (Fig. 2.5 Row 20). In the Tbx5a-deficient fate map, however, over half (55%) of Tbx5a-deficient cardiac precursors also gave rise to another fate (Fig. 2.10B, Fig. 2.11 Row 20). These multipotent precursors include cells that give rise to both pericardial sac

Row #	Clone Fate	Fate at 48hpf					Number of Clones
		Heart	Pericardial Sac	Pharyngeal Arch	Peritoneum	Other	
1	Single	x					17
2			x				30
3				x			28
4					x		23
5						x	10
6	Double	x	x				10
7		x		x			7
8		x			x		4
9		x				x	0
10			x	x			2
11			x		x		3
12			x			x	1
13				x	x		3
14				x		x	0
15					x	x	2
16	Triple		x	x		x	2
17	Total Clone #	38	48	42	35	15	142
18	% of all	27%	34%	30%	25%	11%	
19	# of multipotent	21	18	14	12	5	
20	% of total	15%	13%	10%	8%	4%	24%
21	% of fate	55%	38%	33%	34%	33%	

Figure 2.11: **ALPM Tbx5a morphant clone counts by fate.** Rows 1-16- Each row represents precursors according to their fate(s) at 48 hpf, marked with Xs in the columns. The count at the end of the row (last column) is the number of experiments (labeled precursors) that belong to that fate category. Rows 6-15- Multipotent precursors that gave rise to two fate. Row 16- Two multipotent precursor that gave rise to three fates (possible outlier). Rows 17-21- Sums and percentages in each column divided by the total (142) or by the sum in each fate.

and pharyngeal arch fates and an emergence of cardiac precursors which also give rise to peritoneum fates, compared to wildtype. Furthermore, the additional multipotent cardiac precursors in Tbx5a-deficient versus wildtype arise from the left side ALPM twice as often as from the right side ALPM (Fig. 2.2J non-circle shapes). These findings support the hypothesis that *tbx5a* may regulate the specification of cardiac versus other ALPM fates.

2.5 Discussion

2.5.1 Single-cell resolution fate map at 18 hpf identifies lateral ALPM-derived tissues

This chapter describes a single-cell fate map analysis of cells within the zebrafish lateral ALPM. The LPM gives rise to many different organs in the early embryo (Fig. 1.1C-E), and previous studies have usually focused upon the development of a particular organ, such as the heart or forelimb [25, 33, 75, 77]. My goal was to provide an unbiased description of the ALPM using the photoconversion of single Kaede-containing cells to describe the organization of the organ anlagen prior to the laterally- and anteriorly-directed cell migration movements, which begin at 18 hpf. In a previous fate map study of the posterior LPM, the region between somites 1-4 gave rise to mainly the mesenchymal cells of the pectoral fin bud; furthermore, the migrations of these fin precursors proceeded such that they conserved topological arrangement along the AP body axis [33].

In contrast to that study, I observe that the lateral ALPM is not organized into organ-specific regions (Fig. 2.2N, 2.6), and the precursors of four main organs are derived from this area; namely, the heart, pharyngeal arches, peritoneum, and pericardial sac precursors are all interspersed throughout the anteroposterior and mediolateral extent of the lateral ALPM region that we examined (Fig. 2.2N, 2.6, 2.7). The 18 and 24 hpf fate maps are consistent with the hypothesis that ALPM organ precursors are derived from varied locations within the pre-migratory ALPM, stay within the ALPM, but do not migrate in a spatiotopic manner. That is, the displacements of precursors between 18 and 24 hpf are neither correlated with the starting position of cells nor location of the progeny within the formed organ by 48 hpf. Proliferation rates of the ALPM cells are not high between 18 and 48 hpf as most photoconverted cells divided only once or twice during this period (Fig. 2.9B). However, a very high proportion of labeled cells gave rise to unipotential lineages with only 13%

giving rise to clones that contributed to two or more organs (Fig. 2.2, 2.10, 2.5 Row 20). The identification of multipotent precursors at 18 hpf is important for the interpretation of previous studies on this region of the embryo. Therefore, the ALPM is most likely specified towards production of unipotential fates as early as 18 hpf.

In the next subsections, I will discuss how my fate map sheds light onto the development of the following organs.

Second heart field (SHF) cardiac precursors

Within my fate map, labeled cardiac precursors did not contribute to the primary heart tube by 24 hpf (Fig. 2.4). Previously published fate maps observed cardiogenic precursors that give rise to only the first heart field [25, 75, 77]. Here, I report the early identification of the SHF precursors within the pre-migratory ALPM. Although I cannot claim that I have labeled all of the SHF in my fate map, I have mapped a general area from which SHF cells can arise. Q. Mao's fate map of the LPM adjacent to somites 1 through 4 identified precursors that gave rise to the heart by 48 hpf. Both my and her study show that cardiac precursors can arise as posteriorly as the level of somite 1.

Further discussion of cardiac precursors within my fate map that is related to the cardiopharyngeal mesoderm is in the Pharyngeal Arch precursor section below. Further discussion relevant to left-right asymmetries is in Section 2.5.2.

Peritoneal precursors

In previous analyses of the Tbx5a-deficient phenotype within zebrafish [33, 41], it was hypothesized that fin bud precursors that failed to converge into a finbud during migration contributed to peritoneum. Q. Mao (2013) finds ectopically expressed extracellular matrix component, Col6a2, in scattered limb field progenitors in Tbx5a and Fgf24 knockdown [56]. Q. Mao (2013) suggests that upregulation of *col6a2* represents a conversion of pectoral fin

precursors to a default LPM progenitor fate, which is peritoneum [56]. More experiments are necessary to test the validity of this hypothesis of fate switching in the Tbx5a-deficient LPM directly. I demonstrated increases in the number and proportion of peritoneum precursors in the Tbx5a-deficient fate map (Fig. 2.10B). Future experiments can be conducted to label these non-convergent Tbx5a-deficient LPM cells to determine if they indeed give rise to the peritoneum in Tbx5a knockdown conditions. Molecular expression markers *foxf1* and *irx3b* can be visualized in the knockdown to observe the change in splanchic and somatic peritoneal LPM respectively. Additionally, the mismigrating cells must be tracked for longer than 36 hpf, which is when Mao (2013) fixed and stained morphant embryos for Col6a2 expression. I propose assessing Foxf1 and Irx3b expression until at least 96 hpf to capture the entire lateral-ventral movement of the LPM and presumptive peritoneum.

Pharyngeal arch precursors

A previous fate map analysis by Schoenebeck et al. (2007) of Hand2-expressing cardiac progenitors within the ALPM at around 11 hpf observed that labeled cells in over 90% of embryos additionally generated labeled pharyngeal pouch cells [75]. The authors suggested that the pharyngeal pouch cells could have been derived from the anterior endoderm which overlaps the lateral ALPM at this time in development [75]. However, my single-cell labeling technique provides evidence that mesenchymal cores of the pharyngeal arch precursors can arise from within the lateral ALPM rather than solely from endoderm or neural crest [162]. Paffett-Logassy et al. have shown that SHF progenitors that will give rise to the outflow tract migrate through the pharyngeal arches, which is a pathway distinct from the SHF ventricular progenitor trajectory [74]. Therefore, some ALPM-derived clones scored as pharyngeal arch at 48 hpf in my fate map could possibly migrate later to contribute to the SHF after 48 hpf

The lack of spatiotopic migration between 18 and 24 hpf as shown in my fate maps has interesting implications for the patterning of the pharyngeal arch precursors. Current

knowledge of pharyngeal arch patterning is that *hox* gene expression specifies the identity of each pharyngeal arch (1 to 7) during segmentation stages. However, my data suggest that ALPM-derived pharyngeal arches are not prepatterned along the anteroposterior axis at either 18 or 24 hpf. Furthermore, a single photoconverted pharyngeal arch precursor can give rise to cells spread out among multiple different arches. Perhaps the mesodermal cores of the pharyngeal arches are patterned along the anteroposterior axis in a manner similar to that of the neural crest cells–via migration.

Lastly, the seventh pharyngeal arch in zebrafish is anatomically different from the others as it has pharyngeal teeth [61]. Since many pharyngeal arch mutations do not affect the seventh arch, some researchers have postulated that the seventh arch arises from an independent mesodermal origin than the other arches [61]. I observe that my lateral ALPM fate map gives rise to cells that span all seven pharyngeal arches. This finding argues against a theory on the unique origin of the seventh arch.

Pericardial sac precursors

My study also reveals new details on the development of the pericardial sac. At early stages of heart development, the pericardial sac is contiguous with the venous pole [83]. Recent regional-level labeling of the lateral ALPM showed that groups of photoconverted cells can contribute to both the heart and pericardial sac but did not define whether these two fates were derived from the same or different individual cells [83]. This same study confirmed that these pericardial sac cells also express *tbx5a* [83]. My fate map advances these findings by showing that an individual cell within the ALPM at 18 hpf can give rise to both heart and pericardial sac fates (Fig. 2.2E, F-diamonds), and in fact, this shared fate was the most common multipotent lineage found in my fate map (Fig. 2.5 Row 6). There are still many unanswered questions about the development of the pericardial sac that arise from this data. To what extent over time do precursors share fate with the pericardial sac and the heart?

Will the pericardial sac cells contribute to proepicardial cells after 48 hpf? Is the pericardial sac fate the default fate in the anterior regions while the peritoneal fate is the default in the posterior regions? Since the two organs are both derived from the coelomic epithelium and separated by the septum transversum, this is a likely hypothesis. In the future, a search for genetic markers of the pericardial sac will enable evaluation of the molecular development of this tissue.

2.5.2 Left-right asymmetries in the ALPM precursors that give rise to the SHF

Morphological differences between the left and right are not observed in zebrafish until the formation of the PHT around 22 hpf, when medial ALPM rotates clockwise to position left side precursors anteriorly and right side precursors posteriorly with respect to the main body axis [71, 81, 82]. The grossly visible left-right symmetry-breaking event in zebrafish development occurs during cardiac jogging and cardiac looping. Jogging occurs at about 24 hpf when the venous pole of the primary heart tube shifts to the left side. Cardiac looping occurs at about 36 hpf when the linear heart tube forms a D-loop that places the ventricle to the right of the atrium. Perturbations in genetic determinants in the TGF, BMP and retinoic acid signaling pathways result in the reversal, absence, or randomization of cardiac jogging and looping [114, 127, 128], although the two morphogenic processes are not always coupled [129]. Despite the conservation of genetic determinants of cardiac looping, the mechanism of asymmetric morphogenesis is still unknown.

In my fate map, I determined that the cardiac precursors exhibit a left-right differential contribution in wildtype embryos, specifically that twice as many cardiac precursors arise from the right compared to the left (Fig. 2.2E, p=0.0459). I emphasize that these findings may only hold for the non-PHT precursors of the heart, as my labeling methods avoided the early, medially migrating population of ALPM cells [25, 75, 77]. However, this finding is

notable because left-right differences in the number of precursors are not observed for any of the other ALPM-derived fates (Fig. 2.2F-H). Additionally, the difference is more apparent in anterior bins of the fate map, and there were no other changes in anteroposterior distributions between the left and right sides in other fates (Fig. 2.7D, E). The difference does not seem to be compensated by differential proliferation (Fig. 2.9C), though it remains unknown if it could be due to differential programmed cell death. Corroborating my findings, studies in mouse finds that left-right asymmetries emerge in how cardiac precursors, specifically the posterior SHF, migrate and contribute to different aspects of the mammalian heart [163](AND GALLI2008).

Overall, these findings demonstrate that there are differences in the origins of cardiac precursors in the ALPM as early as 18 hpf, before the formation of the heart. In the heart fields of fish and mice, there is an asymmetric expression of non-muscle myosin II on the right side before linear hear tube formation, which could perhaps be setup or propagated by *tbx5a* expression [164, 165]. In the next section, I will discuss the role of *tbx5a* in the asymmetry. As cardiac looping occurs in the same timeframe as the addition of the SHF into the venous and arterial poles of the primary heart tube, I suggest that the asymmetries in ALPM-derived SHF precursors may play a key role in jogging and looping morphogenesis of the heart.

2.5.3 tbx5a *function in cardiac precursors of the ALPM fate map*

Prior to my study, the extent of *tbx5a* function in either zebrafish ALPM as a whole or the later additions to the heart was unknown. It has been reported that Tbx5a-knockdown causes a changed ratio in FHF to SHF cells as measured by Draculin expression in the FHF [73]. However, using genetic lineage tracing of BAC transgenes in zebrafish, Sánchez-Iranzo et al (2018) concluded that *tbx5a*-expressing cells only make minor contributions to the SHF [166]. In fact, the term "SHF" is not consistently defined in zebrafish, hence my avoidance

of using the term here (Section 1.2.5). Likewise, there is no consensus on whether zebrafish *tbx5a* functions in the "SHF" despite the fact that the two domains of *tbx5a* and one of the "SHF" markers *isl1b* expression overlap [63]. However, zebrafish mutants in the "SHF" regulators Isl1 and Isl2b do not result in abnormal *tbx5a* expression [167, 63]. Here I report that Tbx5a knockdown affects the distribution of "SHF" precursors at 18 hpf across the left-right axis, revealing a new function for *tbx5a* in the ALPM.

I show in this chapter that Tbx5a-deficiency affects the lateral ALPM fate map (Fig. 2.2J-N, 2.7G-L, 2.9, 2.10B, 2.11). More specifically, *tbx5a* is required for the left-right asymmetry in cardiac precursors by 18 hpf (Fig. 2.2J). Additionally, the Tbx5a-deficient fate map has proportionally twice as many multipotent precursors as in the wildtype (Fig. 2.10B). *tbx5a* may maintain unipotency of lateral ALPM precursors by individually biasing certain fates over others or by maintaining the progression of development in the tissue by 18 hpf. My results do not distinguish between these two hypotheses, yet, my results show an overall increase in multipotent precursors across all fates in the Tbx5a-deficient fate map, which supports the latter hypothesis. There is, however, weak support for the former hypothesis in that *tbx5a* is specifically involved in the development of cardiomyocyte specification, though not during somitogenesis stages [151, 153, 168, 169].

My fate map results assess *tbx5a* function in the ALPM not only by 18 hpf, but also from 18 to 48 hpf, since I photoconverted and followed precursors between those timepoints. Within this time, Tbx5a-deficient cardiac precursor proliferation is higher than wildtype only for the left precursors and not the right (Fig. 2.9Bi). Put another way, Tbx5a-deficient precursors originating from the left lateral ALPM have a larger clone size by 48 hpf than wildtype precursors originating from the left (Fig. 2.9Bi). I therefore conclude that *tbx5a* is required in limiting the proliferation of lateral ALPM cardiac precursors specifically on the left side between 18 and 48 hpf. Other researchers have also noticed differential *tbx5a* function between the right and left sides. For example, bilateral hypomorphic expression

of TBX5 in just the mouse limb causes more severe phenotypes in the left side versus the right side [134], suggesting that proper levels of Tbx5 are necessary on the left side of the vertebrate body.

Not only do I observe differential distributions of cardiac precursors across the left-right axis, but I also observe them across the anteroposterior axis. Tbx5a is expressed in an anterior-to-posterior gradient in the chick heart tube; however, it has a higher posterior expression in mouse and Xenopus [168, 170]. These observations imply that *tbx5a* might have a function in anteroposterior patterning of the heart. The mouse SHF is divided into two domains: the anterior (aSHF) gives rise to the ventricle and outflow tract (OFT); the posterior (pSHF) gives rise to the atrium and inflow tract (IFT). I observe that Tbx5a-knockdown preferentially affects the number of cardiac precursors arising anteriorly versus those arising posteriorly to the otic vesicle (Fig. 2.9A, 2.7J-L). Taken together, these results suggest that *tbx5a* does not have a role in patterning the cardiac precursors along the anteroposterior axis; yet, *tbx5a* does have a role in maintaining the left-right asymmetrical contribution specifically within anterior compartments of the ALPM. Other authors have postulated roles for *tbx5a* in proliferation, cell death, and migration [158, 159], which may be able to explain these results.

CHAPTER 3

TBX5A AFFECTS CELLULAR MIGRATION DYNAMICS OF ALPM CELLS THAT DIFFER BY LATERALITY OF ORIGIN AND FATE

3.1 Abstract

Migration dynamics of the lateral ALPM precursors at the start of their migration anteriorly away from the pectoral fin precursors have not been studied previously. I hypothesized based upon the results of my fate map (Chapter 2) that ALPM precursors may be specified based upon their migration dynamics rather than their positions at 18 hpf. By performing long time-lapse analysis using Lightsheet microscopy on *Et(Hand2-eGFP); Tg(h2afx:h2afv-mCherry)mw3* embryos, I first identify bilateral cables and bright spots within the ALPM that have not previously been reported in the literature. Second, I show, by conducting cell tracking analyses backwards in time, that ALPM precursors exhibit different migration dynamics depending on what side of the embryo they arise from and what fate they eventually take on. This result suggests that ALPM precursors may be specified based upon the way they migrate between 18 and 24.5 hpf. Lastly, I perform the time-lapse and cell tracking in Tbx5a-deficient embryos and demonstrate that *tbx5a* is required for the ballistic migration of ALPM precursors. Further, I find that Tbx5a knockdown results in pericardial sac precursors becoming left-right asymmetric in their ballistic migration. While in pharyngeal arch precursors, Tbx5a knockdown results in a balancing (becoming symmetrical) of left-right ballistic migration. *tbx5a* function in ALPM precursors differs by eventual fate of the cells, and not according to their anteroposterior position as for the pectoral fin precursors. Therefore, this suggests that *tbx5a* function differs depending on the eventual fate of all LPM precursors.

3.2 Rationale

When I began my dissertation research, how the ALPM precursors become specified was an open question. In Chapter 2, I explored the hypothesis that ALPM precursors may be specified according to their positions prior to their migration at 18 hpf. However, the lack of regionality within the fate map does not support this hypothesis. Instead, ALPM precursors might become specified based upon their migration patterns. In Chapter 3, I explore hypotheses of ALPM specification that involve cellular migration. Perhaps cells at 18 hpf have an inherent directionality or ability to migrate based upon their eventual fate, which will cause cells to segregate into regions later in time. If so, ALPM precursors would have different "profiles" of migration dynamics based upon their eventual fate. Alternatively, precursors at 18 hpf may not have different "profiles" of migration and instead fall stochastically into regions that specify their fate later in development. To distinguish between these two possible methods of ALPM precursor specification, I compare cell tracks along a variety of migration metrics to determine "profiles" of migration that may differ between cells that adopt different fates.

Previous work by Q. Mao et al. (2015) showed that the forelimb precursor cells adjacent to somites 1-4 undergo lateral migration while converging asymmetrically along the anterior-posterior (AP) axis [33]. By tracking the migration dynamics of each group of LPM cells adjacent to somites 1-4, Q. Mao et al. (2015) observed that the cells displayed different speed, scatter, directionality, persistence, and ballistic migration across time depending on their anteroposterior positioning. Furthermore, the cells appeared to converge towards a source of Fgf24 which is expressed at the eventual site of the limb bud adjacent to somites 2 and 3 [33, 41]. During convergence, the forelimb precursor cells maintain a spatiotopic organization with regards to their relative AP positioning. Such spatiotopic organization is consistent with the hypothesis that there is a pre-pattern in the LPM that is set up prior to migration and allows the cells to have a sterotyped migration pattern [33, 41].

TBX5 is known to enable migration of proepicardial cells that will cover the myocardium after 48 hpf [158, 159]. In zebrafish, the role of *tbx5a* in ALPM migration has not been well-studied. Other groups have observed that Hippo signaling affects BMPs, which are a signaling source for ALPM cells to migrate into the heart and are necessary for proper morphogensis of the heart [71, 171]. When other groups observed the migration of the ALPM, they have mostly focused on the medial ALPM which mostly gives rise to the FHF [89, 82, 81, 71, 171]. Mao et al. (2015) reported on the effect of Tbx5a knockdown on the posterior LPM and found that *tbx5a* is necessary for the asymmetrical convergence of pectoral fin precursors along the anteroposterior axis [33, 56]. By analyzing a plethora of cell migration metrics, Q. Mao et al. (2015) found that Tbx5a-deficient posterior LPM cells had altered directionality, decreased displacement, speed, and persistence compared to wildtype [33, 56]. Neither the cellular migration dynamics nor the effects of Tbx5a-deficiency on migration of the lateral ALPM had been studied in zebrafish before my analysis.

3.3 Results

3.3.1 Timelapse microscopy reveals structural features of ALPM development

Based upon our knowledge of how pectoral fin field cells of the posterior LPM migrate to initiate a pectoral fin bud, I wanted to determine if migration of ALPM cells occurs in a similar way. To make this comparison, I first sought to understand how the cells of the ALPM migrate in wildtype embryos and categorize them according to what fates they become and which side of the embryo they originate from. In this chapter of my dissertation, I obtain descriptive dynamics of how these cells behave using similar metrics of migration dynamics to those used in Q. Mao et al. (2015).

I conducted time-lapse microscopy on wildtype embryos of the doubly transgenic line–

Hand2-eGFP enhancer trap and Histone2A-mCherry transgenic line, *Et(hand2:eGFP)ch2; Tg(h2afx:h2afv-mCherry)mw3* over a period of sixteen (16) hours. The enhancer trap line in zebrafish labels the LPM with eGFP, recapitulating the expression of Hand2 [33], and the mCherry transgenic line allows the tracing of individual cells more distinctly. I determined that a long time-lapse from 18 to 34 hpf was able to capture the major morphogenic movements of the heart, pericardial sac, pharyngeal arches and the convergence of the pectoral fin precursors all within the same viewing angle using a Zeiss Z1 Lightsheet microscope. The peritoneum was not visible by 34 hpf anteriorly, and so I do not have any data on peritoneal precursor migration. The Lightsheet microscope proved to be an advantageous tool because of its utilization of selective plate illuminiation microscopy (SPIM), which minimizes photobleaching since the images can be acquired at 10 to 100 times higher speed than confocal microscopy. Furthermore, using multilayered mounting allowed me to use a lower percentage of agarose that applied less physical constraint on the growing embryo (Section 7). Therefore, I am confident that my methods did not perturb the development of the ALPM and my data is representative of an unmanipulated condition.

Between 18 and 34 hpf, *Et(Hand2:eGFP)* expression increases in fluorescent intensity over time in all cells, which is probably due to upregulation (Fig. 3.3.1A). There are two observable structures that have not been described before conducting this experiment. First, there is a bright outline around the lateral perimeter of the ALPM. This "cable" is dynamic, in that it progresses laterally and anteriorly with the migrating ALPM (see Supplemental Movie 1). The cable separates from the posterior LPM at 18 hpf, creating distance between the ALPM and the pectoral fin precursors. The cable curves medially at the anterior end, but it only extends medially until the level of the otic vesicle–it does not meet at the midline with the cable on the other lateral side of the embryo (schematized in Fig. 1.1 as solid green line). In my single-cell photoconversion experiment in Chapter 2, I occasionally saw cable cells expressing Kaede in mosaic embryos. After photoconverting these individual cable cells,

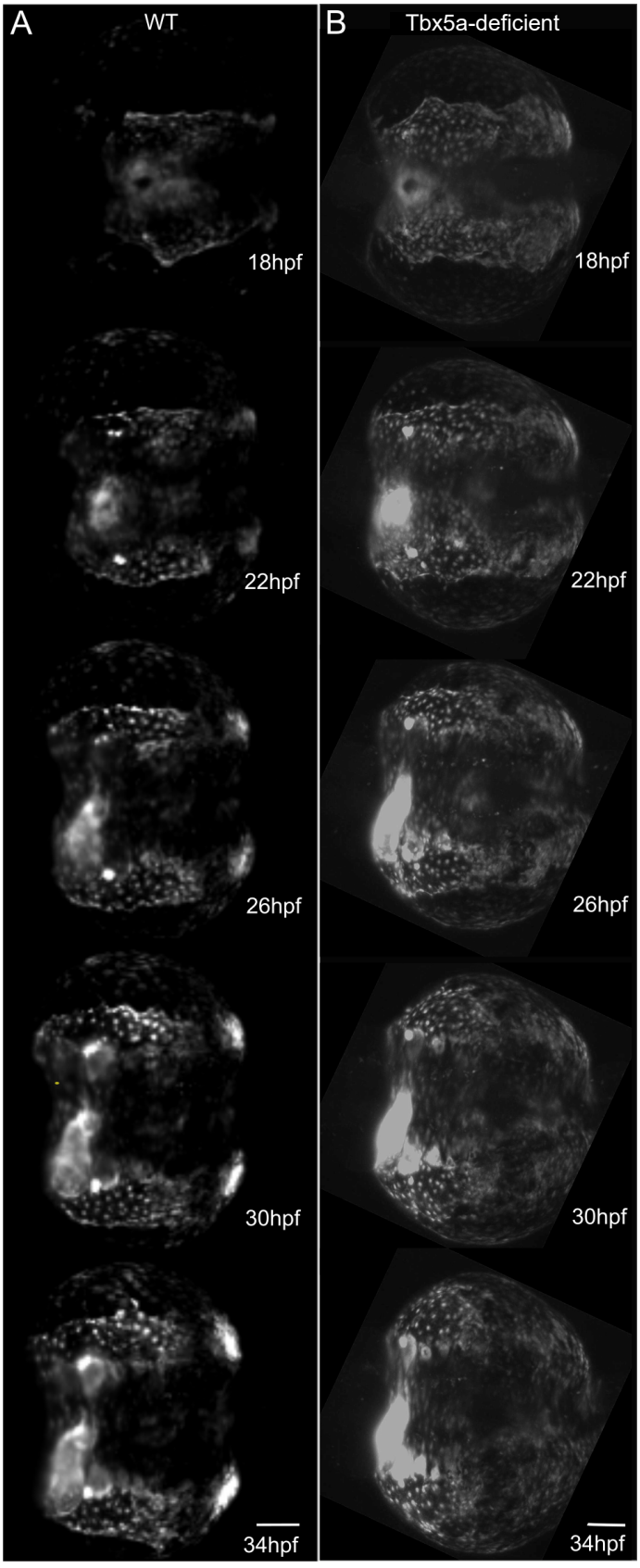

Figure 3.1: **Timelapse of wildtype and Tbx5a-deficient ALPM.** *Et(Hand2-eGFP)ch2* expression using selective plane illumination microscopy. A–wildtype. B–Tbx5a-deficient. Dorsal view, anterior to left. Scale=100μm.

I observed that they can give rise to the percaridal sac (n=2) and the heart (n=1).

Second, I observe two bright fluorescent spots on either side of the embryo that emerge around 22 hpf (Fig. 3.3.1). These bright spots are clusters of around 3-5 cells that are columnar in shape. Cells dynamically join and break away from these spots over time. The spots are located at the dorsolateral anterior corner of the first pharyngeal (mandibular) arch. By 30 hpf, other mandibular arch mesodermal cells have surrounded the bright spots, incorporating them into the first arch.

These observations suggest that there is still much to discover about the morphology and development of the ALPM with regard to the four organs that arise from this tissue.

3.3.2 ALPM precursors have different levels of ballistic migration based upon their laterality of origin and final fate

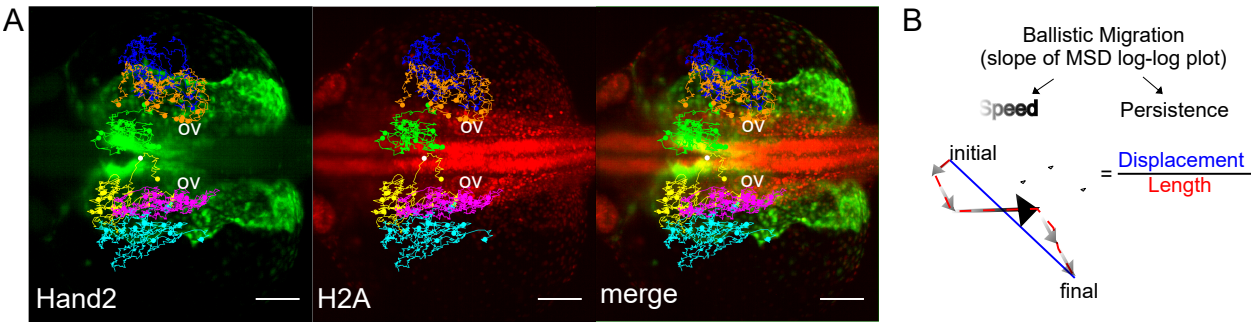

Figure 3.2: **Methodology of backtracking ALPM cell migration.** A– Cell tracks of Hand2-expressing wildtype ALPM, colored by their fate at 34 hpf and laterality side of origin (White-reference point for drift correction; Green-cardiac precursors from the right; Yellow-cardiac precursors from the left; Orange-pericardial sac precursors from the right; Magenta-pericardial sac precursors from the left; Blue-pharyngeal arch precursors from the right; Cyan-pharyngeal arch precursors from the left). Background maximum-intensity projection image 20x magnification of Hand2-eGFP; H2A-mCherry embryo at 18 hpf, when time-lapse begins. Dorsal view, anterior to left. Scale bar– 100 μm. B– The degree of ballistic migration can be measured by the slope of the mean squared displacement (MSD) log-log plot and is a factor of the speed and persistence of migration. Speed is denoted by the magnitude of individual displacement arrows and the greyscale gradient level. Persistence is the ratio of net displacement (final minus initial position, blue) and total length (distance traveled, red).

In order to assess the "profiles" of migration dynamics in the ALPM, I analyzed time-lapse images of the entire ALPM from 18-34 hpf using *Et(hand2:eGFP)ch2; Tg(h2afx:h2afv-mCherry)mw3* fish, which allowed us to visualize how individual cells in the ALPM contribute to each of the four fates (Fig. 3.3.1, Supplemental Movie 1). I first tracked cells backward in time and categorized them based upon which organ field they resided in at 34 hpf and on which side of the embryo they had arisen from (Fig. 3.2A, Supplemental Movie 3). I chose to track the cells manually in three-dimensional virtual stacks since the upregulation of *Et(Hand2:eGFP)* throughout the course of the time-lapse movie made it difficult to set intensity thresholds necessary for automated tracking. I did not track peritoneum precursors as they were not within the field of view at this time. Next, the tracks were only analyzed between 18 to 24.5 hpf to capture individual cell movements into their respective organ fields, while avoiding the later large scale morphogenic movements associated with whole organ formation such as jogging and looping of the primary heart tube, for example. I used the DiPer program to calculate indices of directional migration [172], summarized in Fig. 3.2B. This program is an accessible Excel macro that inputs either two- or three- dimensional tracking data and the time interval to calculate the following: mean squared displacement (MSD), directionality, average speed, and velocity correlation. Although the DiPer program calculated all of these metrics, I chose to only use the MSD in my analyses shown because I chose to recalculate directionality and speed using custom R scripts.

The MSD is roughly a measure of the average area a cell explores over time. In 3D space, the MSD would be the average volume, rather than average area. A high MSD could be achieved by the cell by high speed (i.e. a cell is quickly going over the volume, therefore exploring more) or by directionality (i.e. the cell covers a larger volume because it does not retrace its path). In Fig. 3.3A, cardiac, pericardial sac, and pharyngeal arch precursors exhibit different levels of MSD over time. More specifically in wildtype precursors (Fig. 3.3A, pink and cyan lines), cardiac and pericardial sac MSD are higher than pharyngeal arch MSD.

Furthermore, there is left-right asymmetry in MSD over time in only cardiac precursors (Fig. 3.3A, pink higher than cyan). These differences imply that cells behave differently in their migration between 18 and 24.5 hpf depending on what fate they will become by 34 hpf.

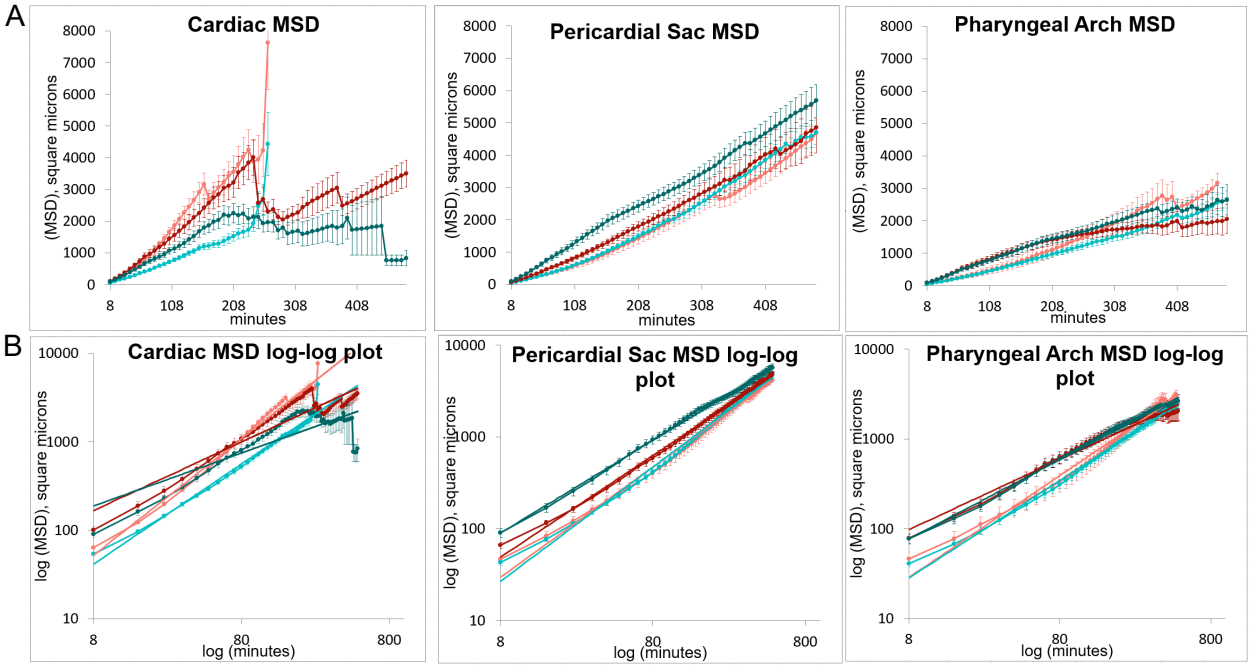

C

MSD log-log trendlines	WT-left	WT-right	Tbx5a-def-left	Tbx5a-def-right
Cardiac	y=3.389x^**1.3158** R^2=0.9887	y=3.9598x^**1.1302** R^2=0.9742	y=33.472x^**0.7742** R^2=0.8676	y=54.273x^**0.5987** R^2=0.6315
Pharyngeal Arch	y=2.7109x^**1.1342** R^2=0.9869	y=2.9531x^**1.0862** R^2=0.9951	y=19.323x^**0.7794** R^2=0.9739	y=12.341x^**0.8808** R^2=0.9947
Pericardial Sac	y=2.429x^**1.2009** R^2=0.9911	y=1.9988x^**1.2454** R^2=0.9925	y=4.8757x^**1.1077** R^2=0.9972	y=11.01x^**1.0084** R^2=0.99887

Figure 3.3: **Derivation of α-value from migration dynamics of ALPM cells.** A- Mean squared displacement (MSD) over time, which was calculated using the DiPer excel macro on cell migration data backtracked in 3-dimensions. This measure approximates how much area the cells explore over time. B- log-log plot of MSD over time overlaid with power trendlines. C- Table of power trendlines and correlation coefficients, R^2 value. The α-value is the exponent of the trendline, in bold.

The slope of the log-log plot of MSD over time is the α-value, which represents the degree of ballistic migration (Fig. 3.2B, 3.3B-C). To calculate this value, I plotted the log-log plot of MSD over time and calculated the exponential trendline (Fig. 3.3B plots, C trendline

equations). In the exponential trendline, the exponent is the slope, meaning that it is also the α-value (Fig. 3.3C, bold number). An α-value of 1 represents random movement and an α-value of 2 represents perfect ballistic movement. The α-value relies on two factors: speed and persistence, where the persistence is the ratio of net track displacement over total distance traveled, or track length (Fig. 3.2B). Overall the ALPM precursors tracked did not have high levels of ballistic migration, as the α-value is around 1.2 averaged for all fates. The group of precursors that had the highest degree of ballistic migration was the cardiac precursors that arose from the left side ALPM, as evidenced by their α-value (Fig. 3.4A, the exponent of the power trendline, α=1.3158). Similar to the MSD measurements, the pharyngeal arch precursors had the lowest α-values. There was a slightly significant difference in the α-values between precursors that originated from the right and left sides: in pericardial sac precursors, the right side had a higher α-value; in pharyngeal arch precursors, the left side had a higher α-value (Fig. 3.4A, pericardial sac p=0.02981, pharyngeal arch p=0.011727).

Ballistic migration is dependent on two factors: speed and persistence (Fig. 3.2B). Persistence is the measure of how "straight" the cell travels over time and is quantified as the displacement (final minus initial position) divided by the track length (total one-dimensional space that the cell explored over time) (Fig. 3.2B). In my analyses, some of the tracks were shorter than others, for example, if I saw the cell become incorporated into the heart at a timepoint earlier than 24.5 hpf. And so, I normalized my values of track displacement and length by the amount of time that the cell was visibly migrating within the ALPM (before it became incorporated into the heart, for example). The y-axis of Track Length and Displacement in Fig. 3.4D-E, has units "microns/timepoint", indicative of the calculated correction. Among the cardiac precursors, the relatively higher ballistic migration compared to pericardial sac and pharyngeal arch precursors is more likely due to higher speed than higher persistence. This is because cardiac speed is higher than pericardial sac and pharyngeal arch average speeds but the cardiac persistence is not (Fig. 3.4B-C).

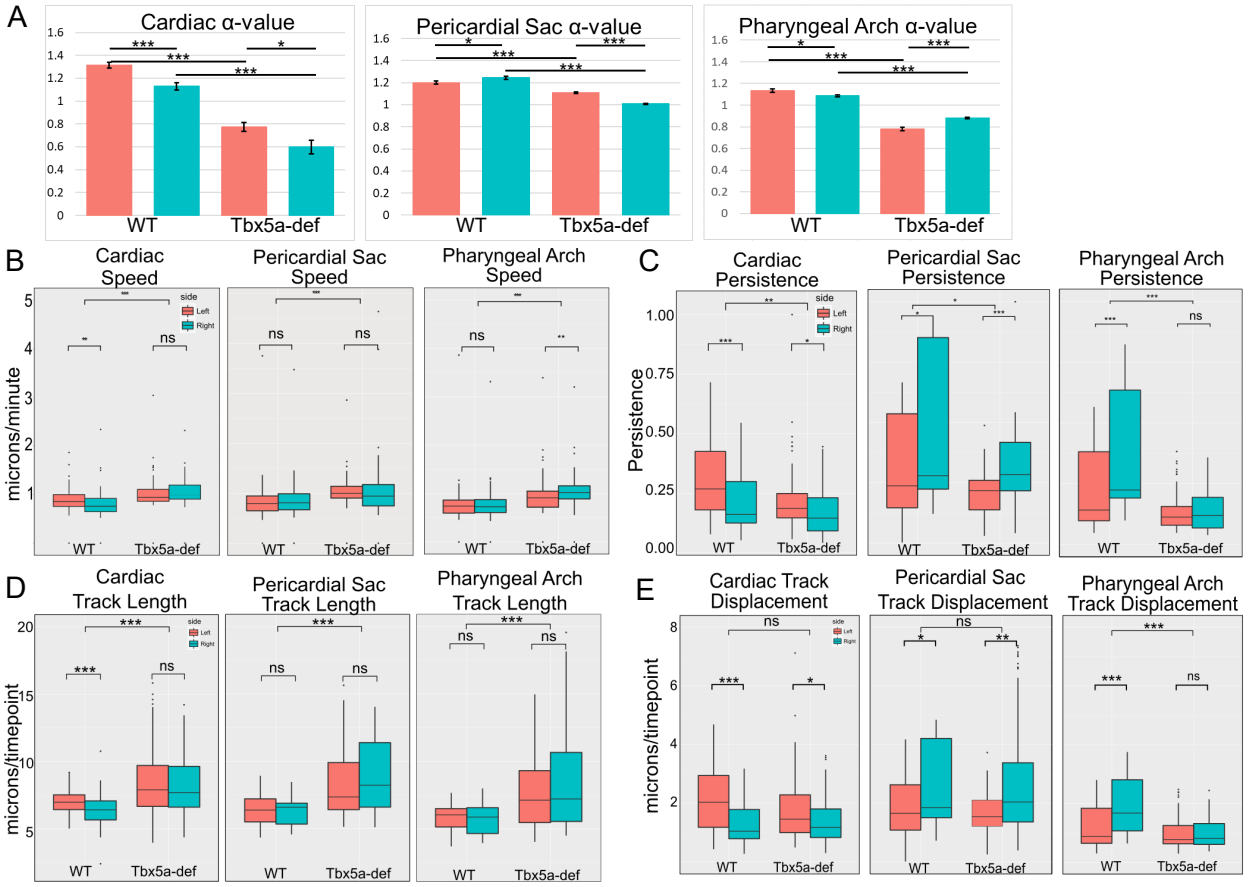

Figure 3.4: **Migration dynamics of cardiac, pericardial sac, and pharyngeal arch precursor cell tracks, comparing WT to Tbx5a MO and progenitors from the left versus the right.** A– log-log plot of MSD over time. Trendlines with correlation R^2 value also shown on the plot. The exponent of the power trendline reflects the α-value, which is an indicator of ballistic migration. B– Average speed. C– Persistence. D–Total track length, normalized by the number of timepoints tracked. E– Net track displacement, normalized by the number of timepoints tracked. Statistics performed using the Kruskal-Wallis rank sum test. 10 cells tracked per group per embryo. N= 6 embryos

Among pharyngeal arch precursors, the relatively lower ballistic migration is more likely due to lower average speed than lower persistence. This is because pharyngeal arch average speed is lower than pericardial and cardiac speed but the pharyngeal arch persistence is not (Fig. 3.4B-C). Overall, these results highlight differences in migration dynamics between precursors of different fates.

Not only did the migration dynamics differ between precursors of different eventual fates, but migration dynamics also differed between precursors from the left and right side of the ALPM. As shown in Fig. 3.4A, the α-value was significantly higher in cardiac precursors from the left than those from the right ($p = 3.49 \times 10^{-5}$). This asymmetry is more likely caused by a higher persistence in left cardiac precursors than by higher speed since the difference is larger among the persistence measures (Fig. 3.4B-C). The higher persistence in left cardiac precursors is more likely due to longer displacement than track length since track length is inversely proportional to persistence (Fig. 3.4D-E). Within pericardial sac and pharyngeal arch precursors, there was a higher degree of ballistic migration (α-value) in precursors from the right than the left (Fig. 3.4A). This asymmetry is most likely due to higher persistence in right side pericardial sac and pharyngeal arch precursors since there is no significant difference within left/right average speeds (Fig. 3.4B-C). The higher persistence of right side pericardial sac and pharyngeal arch precursors more likely comes from a higher displacement than track length since there is no significant difference within left/right track lengths (Fig. 3.4D-E). These results indicate that there are inherent differences in migration dynamics of ALPM precursors correlating with their final fate and laterality of origin.

3.3.3 tbx5a *functions to enable ballistic migration in ALPM cells*

To understand the effect of *tbx5a* on the lateral ALPM cell migration, I conducted time-lapse microscopy in Tbx5a-deficient embryos in the same manner as wildtype embryos, described above. Overall, the development of Tbx5a-deficient embryos mounted in the

Lightsheet microscope was not perturbed or delayed compared to unmounted siblings. The *Et(Hand2:eGFP)* expression in the Tbx5a-deficient embryos also marked the cable and bright spots in similar locations as described in wildtype embryos above. However, the overall mediolateral width of the ALPM increased significantly in size compared to wildtype (Fig. 3.5A-B). The increased width might have significant impact on the migration dynamics of the ALPM precursors, perhaps by increasing the distance which the cells need to traverse to their eventual locations. Despite the increased width, the number of *Et(Hand2:eGFP)*-positive cells was unchanged between the Tbx5a-deficient and wildtype embryos (Fig. 3.5C).

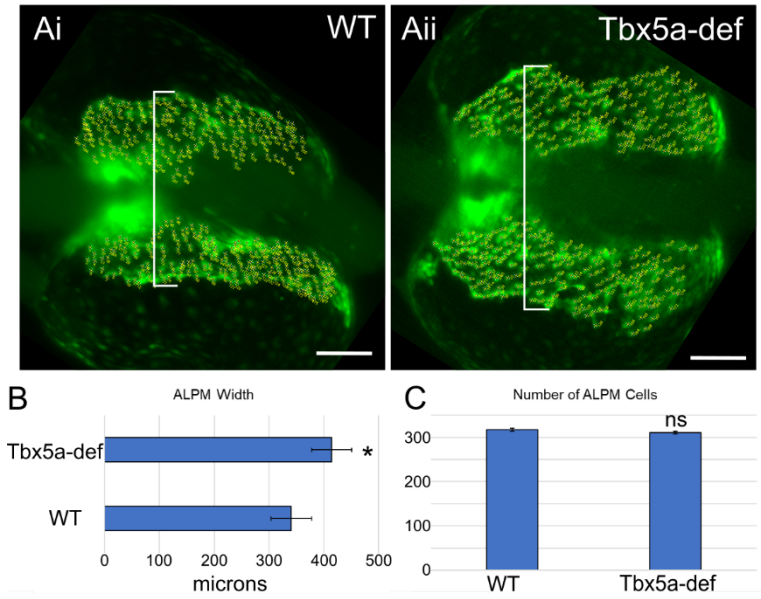

Figure 3.5: **Tbx5a-deficiency affects ALPM tissue width and not cell count.** A- Still images from Lightsheet timelapse comparing WT to Tbx5a-deficient *Et(Hand2:eGFP)ch2* embryos at 18 hpf. Dorsal view, anterior to left. White bracket- width of ALPM measured at the same anteroposterior location, posterior to the medially localized ALPM that will form the heart cone. Yellow numbers and crosshatches- Hand2-expressing cells counted within the ALPM, excluding pectoral fin precursors posterior to somite 1. Scale bar- 100 μm. B- Quantification of the ALPM width. Effect size: Cohens d=1.160309, P=0.02712 using the Wilcoxon rank sum test. C- Quantification of ALPM cell count. Effect size: Cohens d=0.1092772, p=0.4091 using the Wilcoxon rank sum test. n= 6 embryos per condition.

In terms of the migration dynamics, Tbx5a-deficient precursors have significantly decreased measures of ballistic migration in all fates and laterality of origin (Fig. 3.3, 3.4A,

$p = 6.57 \times 10^{-12}$). More specifically, the α-values are at or below 1, which signifies that their migration is less ballistic than random movement (Fig. 3.3C, the exponent of power trendline in bold). The loss of ballistic migration in Tbx5a-deficient precursors is most likely due to the loss of persistence, since migration speed increases in the knockdown condition (Fig. 3.4B-C, $p = 1.595 \times 10^{-5}$). The loss of persistence in Tbx5a-deficient precursors is most likely due to increased track length, as seen by the large effect sizes compared to the wildtype precursors (Fig. 3.4D, cardiac effect size=0.91; pericardial sac effect size=0.99; pharyngeal arch effect size=0.88). Increased track length alongside higher speed and fixed displacement indicate that Tbx5a-deficient precursors meander more than wildtype precursors. These data suggest that *tbx5a* normally functions to enable persistent migration of lateral ALPM precursors that give rise to cardiac, pharyngeal, and pericardial sac.

Cardiac precursors from the left ALPM have higher ballistic migration than precursors from the right in Tbx5a-deficient embryos, just as in the wildtype embryos (Fig. 3.4A, p=0.0154). The laterality difference in migration is maintained despite the changes in other migration dynamics: no laterality difference in cardiac speed (Fig. 3.4B, p=0.1095) and in track length (Fig. 3.4D, p=0.3287). Therefore, the left-right differential ballistic migration in the Tbx5a-deficient embryos is most likely due to the observed difference in persistence (Fig. 3.4C, p=0.01824) and net displacement (Fig. 3.4E, p=0.01924). Together, these data suggest that *tbx5a* functions in maintaining left-right asymmetry in cardiac precursor migration speed and track length.

Tbx5a-deficiency causes the reversal of laterality difference in the ballistic migration of pericardial sac precursors as measured by the α-values (Fig. 3.4A, left greater than right, $p = 1.54 \times 10^{-21}$). This difference is most likely due to the changes in speed, since the persistence is higher in precursors from the right (Fig. 3.4B-C, $p = 3.778 \times 10^{-4}$), which is most likely due to the increase in length, since the displacement is higher in precursors from the right (Fig. 3.4D-E, $p = 2.81 \times 10^{-3}$). Tbx5a-deficiency results in the disappearance of

laterality difference in the ballistic migration of pharyngeal arch precursors displayed in the wildtype (Fig. 3.4A, p=0.01727), which is most likely due to equal measures of persistence (Fig. 3.4C, p=0.4766), length (Fig. 3.4D, p=0.2871) and displacement (Fig. 3.4E, p=0.3691) between the right and left sides. Together, these data suggest that *tbx5a* functions normally to maintain left-right asymmetry in the ballistic migration of pericardial sac and pharyngeal arch precursors.

3.3.4 Undifferentiated lateral ALPM precursors at 32 hpf

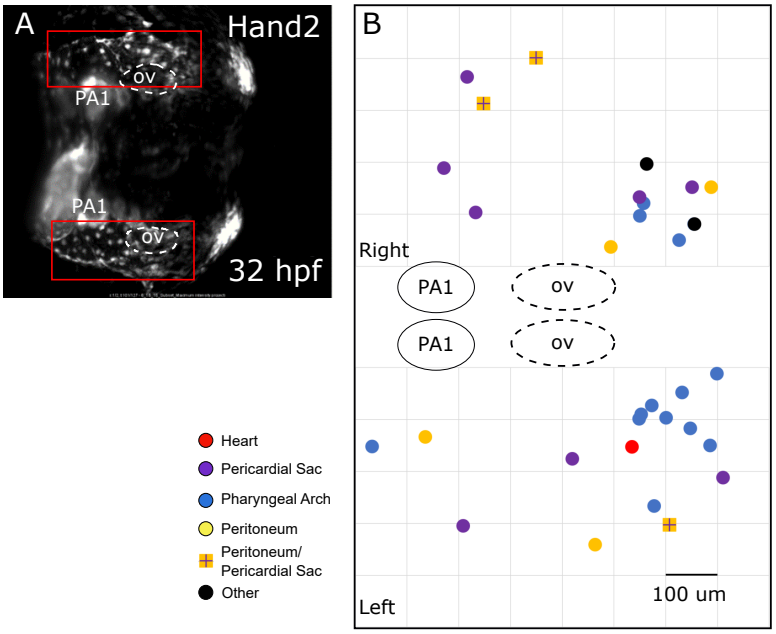

C

Fate at 48hpf	Number of clones	Percent of all clones
Pharyngeal Arch	14	45%
Pericardial Sac	11	35%
Peritoneum	7	23%
Heart	1	3%
Other	2	6%

Figure 3.6: **Single-cell resolution fate map of undifferentiated lateral ALPM tissue at 32 hpf.** A- Maximum intensity projection of *Et(Hand2:eGFP)* expression at 32 hpf. Red boxes outlines many of the undifferentiated lateral ALPM cells that were fate mapped that have yet to make up the heart, pharyngeal arches (PA1), the pericardial sac, nor the peritoneum. ov-otic vesicle. B- Fate map of precursors at 32 hpf colored by fate at 48 hpf according to key. Dorsal view, anterior to the left. C- Table of number of labeled precursors that gave rise to each fate

By the end of the time-lapse movie at 34 hpf, there remain quite a few lateral ALPM precursors that have not visibly made up the heart, pericardial sac, pharyngeal arches, or peritoneum (Fig. 3.6A red boxes). I hypothesized that these undifferentiated precursors were

similar in composition to the fate map at 18 hpf, as that would inform me on the changes in the tissue's potential (and therefore progression of specification) over time. Unfortunately, I could not devise a mounting technique within FEP tubing whereby I could visualize these cells from 32 to 48 hpf. Therefore, I fate mapped the undifferentiated region of the lateral ALPM at 32 hpf using the same technique that I used in Chapter 2. Overall, there are fewer cells within this undifferentiated region, and most of them are located posterior to the otic vesicle. By repeating the experiment in 31 embryos (17 on the left, 14 on the right), I uncover significant differences in the regionality and composition of this fate map.

In general, the undifferentiated lateral ALPM at 32 hpf gives rise to only three out of the four organs: pharyngeal arch, pericardial sac, and peritoneum. I only found one labeled precursor that gave rise to the heart (Fig. 3.6C, 3% of all labeled clones). Furthermore, the vast majority of precursors are unipotential (28/31 = 90.3%) and the multipotential cells are all of one type–that which give rise to pericardial sac and peritoneum (Fig. 3.6B, yellow squares). Unlike the 18 and 24 hpf fate maps, there appears to be regionalization from areas in which only pharyngeal arch precursors arise. Pharyngeal arch precursors arise from posterior and medial locations within the 32 hpf fate map (Fig. 3.6B blue circles).

3.4 Discussion

3.4.1 Advantages and challenges of SPIM in capturing migration dynamics of the ALPM

Extended time-lapse imaging of the lateral ALPM in the developing zebrafish would not have been possible without the usage of the Zeiss Lightsheet and the multilayered mounting technique described in Kaufmann et al. [173]. There are many benefits of the Lightsheet chamber that necessitate its usage: 1) the specimen can be rotated to capture multiple viewing angles; 2) the multiple illumination objectives focus a 2-dimensional sheet of light

onto the embryo, which limits photobleaching and phototoxicity; 3) the entire depth of the embryo can be imaged, which is especially necessary given the curved nature of the ALPM around the yolk. Between 18 and 34 hpf, the tailbud outgrows significantly and extends in length about two-fold. Therefore, the mounting medium needs to be soft enough to allow the growth. When the agarose is too stiff, the tailbud cannot outgrow normally and instead causes pressure against the agarose and malformation of head structures. Furthermore, the pericardial sac of these embryos does not form normally and is instead positioned anteriorly instead of ventrally. Since I was interested in visualizing the development of the pericardial sac and pharyngeal arches, which give rise to head mesenchyme, I had to use a low percentage of agarose. The limitation of low percentage agarose is that it will not hold the embryo in place for over 15 hours. The Lightsheet chamber loads the specimen from above, such that the specimen is suspended in embryo media suitable for normal development. Therefore, a low percentage of agarose would allow the specimen to fall to the bottom of the chamber. However, the multilayered mounting technique positions a plug of higher percentage agarose into the bottom of the FEP tubing, securing the specimen in place. Altogether, these techniques combined allows for an unperturbed visualization of ALPM development over long periods in time at multiple viewing angles.

Backtracking the migration of cells over time is a useful technique when studying a group of cells whose fates can only be identified at a much later stage. Manual backtracking saves time from setting automated thresholds and manually editing such surfaces and tracks. Given the upregulation of *Et(Hand2:eGFP)* expression over time, proper fluorescence intensity thresholds could not be set. And so, manually tracking the cells proved to be the most time-efficient and accurate method. The specific insights of the cell tracking data and how it corroborates the data in Chapter 2 will be discussed in (Section 6.2).

The upregulation of *Et(Hand2:eGFP)*, especially within the beating heart, prevented me from tracking ALPM precursor cells after they entered the heart. Visualizing these heart

cells once they were within the heart would have enabled me to compare migration dynamics of cardiac precursors that gave rise to specific chambers or layers of the heart. Furthermore, it even prevented me from tracking pericardial sac precursors that gave rise to the layer underlying the heart. In order to bypass these limitations, labeling individual cells or cluster of cells and then lineage tracing them using long time-lapse would be necessary.

3.4.2 Features of the lateral ALPM may inform the migration of the tissue

My time-lapse and cell tracking experiments have identified novel features of the ALPM that may lead to further insight into how the lateral ALPM develops. Beginning at 18 hpf, there is a Hand2-positive cable-like structure on the lateral perimeter of the ALPM that does not exist around the pectoral fin precursors (Fig. 3.3.1A). Between 18 to 34 hpf, the ALPM and the cable spread anteriorly and laterally. This movement is similar in nature to the spreading of the enveloping cell layer (EVL) during epiboly, and we could perhaps use what is know about this process to better understand the development of the ALPM. EVL spreading during gastrulation and epiboly is driven by a contractile actomyosin ring that exerts pressure on the embryo by circumferential contraction and a flow-friction mechanism [174]. The friction flow is caused by the retrograde flow of the yolk syncitium that subverts under the EVL, observed by time-lapse microscopy of a fluorescent actin label [174]. Could similar mechanisms of actomyosin cable contraction and flow-friction of the underlying endoderm also apply to the spreading ALPM?

To investigate this, we could use similar experimental methods as Behrndt et al. (2012) on the lateral ALPM [174]. First, we can laser-ablate the cable at various locations and observe the recoil velocity of actin within the cable. A higher recoil velocity would suggest higher tension in that area. Recently, another group has published a BAC-derived transgene of Tbx5a expression that also has a cable-like structure [83]. In the same recent publication, Ocaña et al. photoablated the cable on either the right or left side and observed that the

venous pole of the heart failed to jog to the left side half of the time when the cable was ablated only on the right side [83]. However, they did not measure the recoil velocities immediately following ablation. Furthermore, according to the images in their supplemental figure, the photoablation caused a large hole in the side of the embryo, causing a fair amount of yolk to expel out of the embryo and half of the fluorescently labeled cable to disappear. Based on the results of this experiment, this group hypothesized that the cable exerts a pushing force in the anterior direction that will cause the venous pole of the heart to jog to the left [83]. Future experiments involving the precise ablation and measuring of the recoil velocity should be used to better test this hypotheis. If the cable indeed exerts a pushing force in the right to left direction, then the recoil velocity after ablation would be negative on the right side and higher on the left side (assuming that the cable is also pulling the venous pole on the left side). However, if the recoil velocity is positive on the right side, then it implies that the cable does not exert a pushing force on the right side.

In my *Et(Hand2-eGFP)* time-lapse, I also observed two bright spots on the right and left sides of the lateral ALPM emerging at around 22 hpf in both wildtype and Tbx5a-deficient embryos. The position of the spots is at the dorsal, anterior, and medial corner of the eventual first pharyngeal (mandibular) arch. Other published whole mount *in situ* hybridization expression patterns of Hand2 show similar features [175], suggesting that the observed expression pattern I see is not an artifact of the enhancer-trap line. Furthermore, as to my knowledge, published reports of other transgenes of Hand2 (*TgBAC(Hand2:GFP)* and *Tg(Hand2:GAL4-VP16)*) do not show the same fluorescent expression in these spots that I observe. Therefore, I posit that our lab's *Et(Hand2-eGFP)* line is more representative of Hand2 expression than other published fluorescent zebrafish lines.

The location of the bright spots is also reminiscent of Tbx20 expression, which is expressed in the pituitary gland primordia [45, 176]. Since the pituitary gland develops from the endodermal pharyngeal pouch, it is likely that the Hand2-expressing bright spots are also

expressed in the pituitary gland primordia. Further investigation must be done to confirm that Hand2 and Tbx20 expression overlap in these areas. Of note, the cable and spot features are also labeled by the new Tbx5a-Kaede knock-in construct that I generated (see Appendix A).

3.4.3 tbx5a *functions in the cellular migration of the entire ALPM, with differing functions depending on the fate of the precursor*

By backtracking lateral ALPM cells, I found that ALPM precursors exhibited different levels of ballistic migration according to what lateral side of the embryo they arose from and what organ they were found in by 34 hpf. More specifically, I find that the cardiac precursors from the left side ALPM exhibit the highest degree of ballistic migration that I measured, due to their speed and the longer distance they must travel to the venous and arterial poles. On the other hand, the pharyngeal arch precursors from the right have the lowest degree of ballistic migration that I measured due, to their low speed. These results suggest differential "profiles" of migration according to eventual fate and side of origin between 18 to 24.5 hpf. Since these differences are observed before these precursors become incorporated into their eventual organs, these differential "profiles" suggest that ALPM precursors may be specified based upon their migration patterns.

The Ho lab's previous publication demonstrated that *tbx5a* functioned in the pectoral fin precursors to enable their collective migration to initiate the fin bud [33]. Here, I demonstrate, using similar measures of ballistic migration, that *tbx5a* functions in ALPM precursors differentially between organ precursor fields and between the right and left sides (Fig. 3.4). More specifically, *tbx5a* is necessary for ALPM precursors to exhibit a level of ballistic migration above that of a random walk (Fig. 3.3, 3.4). This change in ballistic migration is mostly caused by increased cell track length in Tbx5a-deficient precursors of all three fates (Fig. 3.4). An increased track length with a fixed net displacement essen-

tially means that the cells meander more. This increased meandering of precursors could be due to cell-autonomous defects that could include inability to recognize the extracellular matrix to migrate over, inability to receive migration signals, and/or dysfunction in cellular and cytoskeletal dynamics. Recent evidence on the non-cell autonomous effects of Tbx5a and its fish paralog Tbx5b shows that these genes can affect the coordination, migration and specification of the ALPM [177], corroborating this finding. Other T-box genes are also involved in mesodermal migration, and the mechanism by T-box 1 and T-box 16 can function is by regulating cell movement through cellular adhesion molecules, protocadherins (BISWAS2010,TAZUMI2010). Perhaps *tbx5a* also regulates protocadherins to deferentially enable migration of the lateral ALPM.

tbx5a functions normally to maintain left-right asymmetry in the ballistic migration of pericardial sac and pharyngeal arch precursors. Knockdown of Tbx5a causes left side pericardial sac precursors to migrate more ballistically than right side precursors and causes pharyngeal arch precursors to show no difference in ballistic migration between the right and left (Fig. 3.4A). Within the pharyngeal arch precursors, I observe that the displacement is lower in the Tbx5a-deficient condition than in wildtype (Fig. 3.4G). It is more likely that this change in displacement is due to a change in the initial positions of the precursors at 18 hpf as opposed to a change in the final positions of the calculated tracks at 24.5 hpf. Pharyngeal arch precursors are more likely to arise from medial than lateral bins in the Tbx5a-deficient condition (Fig. 1G,L, S43G-I, blue bars), and therefore have a shorter distance to travel to medially located pharyngeal arches. Additionally, the entire ALPM tissue has a wider mediolateral width in the Tbx5a-deficient compared to the wildtype condition (Fig. 3.5). Based upon the variety of effects that Tbx5a-knockdown has on each of the organ progenitor fields (cardiac versus pericardial sac versus pharyngeal arch precursors), *tbx5a* functions in different cellular processes depending on the cell-type. Furthermore, the function of *tbx5a* in the more posterior pectoral fin precursors is to enable the anteropos-

terior convergence of precursors, which again is different than the *tbx5a* function in ALPM precursors analyzed here (cardiac, pericardial sac and pharyngeal arch). This conclusion is in concordance with previous observations of how Tbx5 differentially functions between cardiac and non-cardiac cell types in mouse [156].

CHAPTER 4

REGIONAL PHOTOCONVERSION EXPERIMENTS REVEAL HOW THE ALPM CONTRIBUTES TO THE LARVAL HEART

4.1 Preface

The photoconvesion experiment involving the whole left or right side ALPM described herein is included in a manuscript currently under review with the following title, "Fate mapping analysis of anterior Lateral Plate Mesoderm reveals *tbx5a* function in left-right asymmetry and cell specification of cardiac precursors." This manuscript was authored by Lindsey M. F. Mao, Erin A. T. Boyle Anderson, and Robert K. Ho. Other experiments included in this chapter are unpublished.

Rotation student, Jake Henderson, contributed to the photoconversion experiment and data analysis involving quadrants of the lateral ALPM.

4.2 Abstract

In Chapter 2 I observed that single-labeled cells within the lateral ALPM at 18 hpf contribute to the larval heart at 48 hpf (Fig. 2.2). Furthermore, the fate map that I compiled showed a left/right asymmetry in the number of cardiac precursors (Fig. 2.2E). To assess how the lateral ALPM contributes regions within the larval heart, I conducted a series of photoconversion experiments, detailed in this chapter. By photoconverting the entire lateral ALPM on both sides, I found that the majority of cardiomyocytes at 48 hpf arise from the lateral ALPM. By photoconverting just the right or left sides of the lateral ALPM, I found that the left/right asymmetry is retained in contributions to the heart and is dependent upon Tbx5a function. I also found that anterior regions of the lateral ALPM gave rise to more cardiomyocytes than posterior regions. Lastly, by photoconverting small regions of 4-10 cells

within the lateral ALPM, I find that the resolution of the single-cell resolution fate map may be too fine to observe fate patterns that may reside within the lateral ALPM.

4.3 Rationale

In Chapter 2, I investigated whether ALPM precursors were positioned or arranged into regions according to fate at 18 hpf. When analyzing the fate map data, I found that twice as many cardiac precursors arose from lateral ALPM cells on the right side of the embryo than from the left (Fig. 2.2E). Furthermore, the additional cardiac precursors on the right side did not proliferate more than those from the left by 48 hpf (Fig. 2.9B). It remained unknown, however, what structures of the heart the right ALPM contributed to. Furthermore, the differences between right-side-derived and left-side-derived structures of the 48 hpf heart are also unknown. Since I observe more cardiac precursors arising from the right ALPM than the left at 18 hpf, I next questioned whether the right ALPM made up a larger proportion of the larval heart than the left ALPM. I then hypothesized that the greater number of cardiac precursors on the right side contributed more to the larval heart than those on the left side. In the experiments presented in this chapter, I sought to corroborate the left-right asymmetry of cardiac precursors that I found in the single-cell resolution fate map.

Not only did I observe left-right asymmetries in cardiac precursors within the fate map, but I also observed left-right asymmetries in cardiac precursor ballistic migration presentedin Chapter 3. Cardiac precursors originating from the left side had a higher ballistic migration than those from the right side (Fig. 3.4A). Perhaps left side cardiac precursors travel faster and in a more persistent manner to compensate for the fact that there are fewer of them compared to the right side cardiac precursors. Subsequently, I inferred that right side cardiac precursors do not contribute more to the larval heart because they did not migrate as ballistically as those from the left side. If this inference is correct, then I expect to see equal contribution to the heart between the left and right side ALPM.

Next, how does *tbx5a* function in the relative contributions to the larval heart by 48 hpf? The data in Mosimann et al. (2015) imply that *tbx5a* functions to regulate the relative contributions of FHF to SHF [73]. They show that Tbx5a-deficient embryos have a smaller non-Draculin-expressing ("SHF") region than wildtype embryos [73]. If *tbx5a* regulates contribution of "SHF", then I would expect that the number of late-contributing cardiomyocytes from the lateral ALPM would decrease in Tbx5a-deficient embryos.

TBX5 is expressed in an anterior-to-posterior gradient in the chick heart tube; however, it has a higher posterior expression level in mouse and Xenopus [168, 170]. These observations imply that *tbx5a* might have a function in anteroposterior patterning of the heart. The mouse SHF is divided into two domains: the anterior SHF gives rise to the ventricle and outflow tract; the posterior SHF gives rise to the atrium and inflow tract. In my fate map, I observe that Tbx5a-deficiency preferentially affects the number of late addition cardiac precursors arising anteriorly versus those arising posteriorly to the otic vesicle (Fig. 2.9A). This suggests that *tbx5a* has a role in patterning cardiac precursors along the anteroposterior axis. In the next part of this chapter, I assess the relative contributions of anterior or posterior regions of the ALPM to the heart.

Single-cell resolution fate mapping has both benefits and drawbacks. By assessing the fate and clone size of a single precursor, I have been able to make inferences on general regionality, proliferation, and topology of the ALPM at 18 hpf. However, the speckled "salt and pepper" appearance of the fate map might be misleading. Since the whole ALPM has started its migration around 18 hpf, labeling moving cells and recording their positions may not be precise. Also, each cell labeled is in a different embryo, which could cause noise in positions of precursors when they are compared to each other. Therefore, the single-cell resolution fate mapping technique might be too fine a resolution to capture patterns in the whole tissue. As an analogy, a mosaic is a piece of art that is made up of smaller images or pieces. Patterns in the whole picture can be seen at a distance but not when viewed close up.

If the artwork is only viewed closeup, then the image may appear as a random speckling of images and colors. I questioned if my single-cell resolution fate map was taking too myopic a view on the fates of the ALPM. Therefore, in the last part of this chapter, I evaluate the resolution of my fate map through small regional photoconversions of the ALPM at 18 hpf.

4.4 Results

In the following experiments, I injected Kaede mRNA into one-cell stage embryos resulting in animals which express Kaede in every cell. Before photoconversion at 18 hpf, embryos were screened for uniform green expression of Kaede.

At 48 hpf, cardiomyocytes were counted by first taking confocal z-stacks of the heart with z-slices every 2.0 μm. Cardiomyocytes were manually counted as shown in the example in Fig. 4.1.

4.4.1 Photoconversion of the entire lateral ALPM does not give rise to the entire heart at 48 hpf

If the lateral ALPM gives rise to cardiac precursors, as I found in my single-cell resolution fatemap, then how much of the heart does it give rise to? I photoconverted both sides of the lateral ALPM and observed to what extent the heart was populated by photoconverted cells. As I explicitly tried to avoid photoconverting the medial ALPM which gives rise to the primary heart tube, I predicted that photoconversion of the entire lateral ALPM would not give rise to the entire heart. At 48 hpf, I imaged the entire heart and quantified the number of photoconverted and unphotoconverted cells in the heart (Table 4.1). The majority of cardiomyocytes were photoconverted, meaning that they arose from the lateral ALPM. There were no particular regions of the heart that were consistently not photoconverted. Tbx5a-deficient embryos overall had fewer photoconverted cardiomyocytes than wildtype

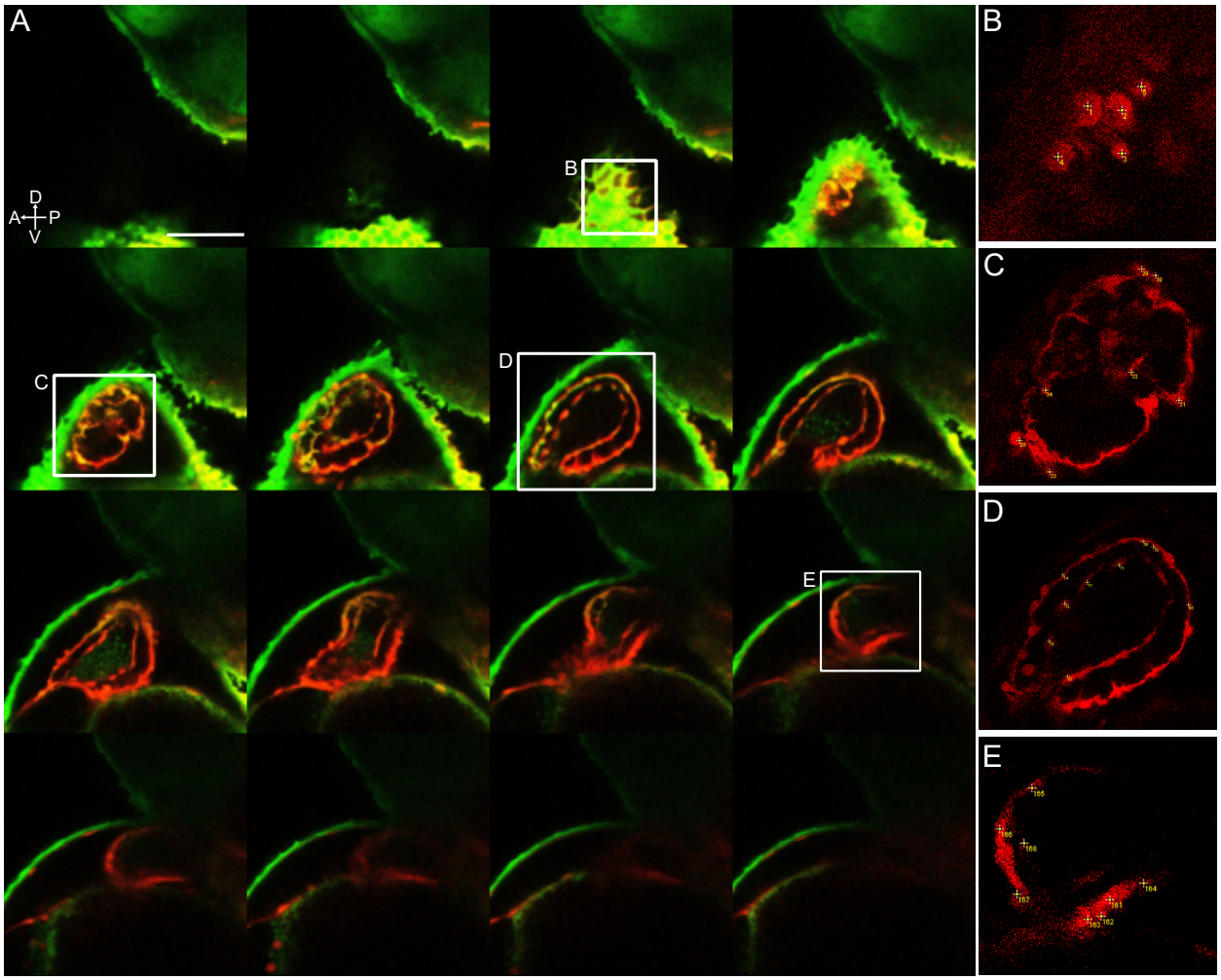

Figure 4.1: **Photoconverted cardiomyocytes counted manually from a z-stack of the larval heart.** A- 48 hpf left lateral side slices of the heart, displaying every fourth stack of 2.0 μm each. Green fluorescece is in every cell of the embryo. Red fluorescence shows right side lateral ALPM-derived Kaede-expressing cells photoconverted at 18 hpf. B-E Insets of the heart showing examples of how cardiomyocytes were counted with numbered points in yellow. This embryo had a total of 185 red fluorescent cardiomyocytes counted, which was verified by the average of three separate manually counted analyses.

embryos, resulting in a smaller proportion of photoconverted cells in the heart (Table 4.1, p<0.0001). This suggests that *tbx5a* may function to maintain the number of lateral ALPM precursors contributing to the heart.

	Mean # Photoconverted	Mean # Unphotoconverted	% Photoconverted	N
Wildtype	154	26	86%	10
Tbx5a-deficient	122	55	69%	7

Table 4.1: **Contribution of both sides of the lateral ALPM at 18 hpf to the heart at 48 hpf.** Difference in Proportion test p<0.0001

4.4.2 Photoconversion of right side lateral ALPM gives rise to more cardiomyocytes than the left

I photoconverted one entire left or right side ALPM by applying UV-light to a region of interest in 18 hpf embryos that had been injected with Kaede transcripts at the one-cell stage (Fig. 4.2A). At 48 hpf, I took confocal z-stacks of the entire heart and manually counted the number of red fluorescent photoconverted cardiomyocytes that were within the larval heart (Fig. 4.1). Overall, the photoconverted red cells gave rise to all previously described tissues from Chapter 2's single-cell resolution fate map, which included the myocardium and endocardium of both heart chambers and the inflow and outflow tracts (Fig. 4.2D-F). Photoconverted lateral ALPM from either the right or left gave rise to equal number of red fluorescence at 48 hpf in the pericardial sac, pharyngeal arches, peritoneum and pectoral fin. Additionally, photoconverted cells that gave rise to these tissues retained their laterality between 18 and 48 hpf; i.e., photoconverted cells that originated from the right lateral ALPM were found on the right side of the 48 hpf embryo. Contributions of photoconverted cells into the heart was not segregated into left versus right sides with respect to the body axis. Instead, heart development proceeds such that medial precursors undergo a clockwise rotation that positions the left side anteriorly and the right side posteriorly [81, 82]. This results in

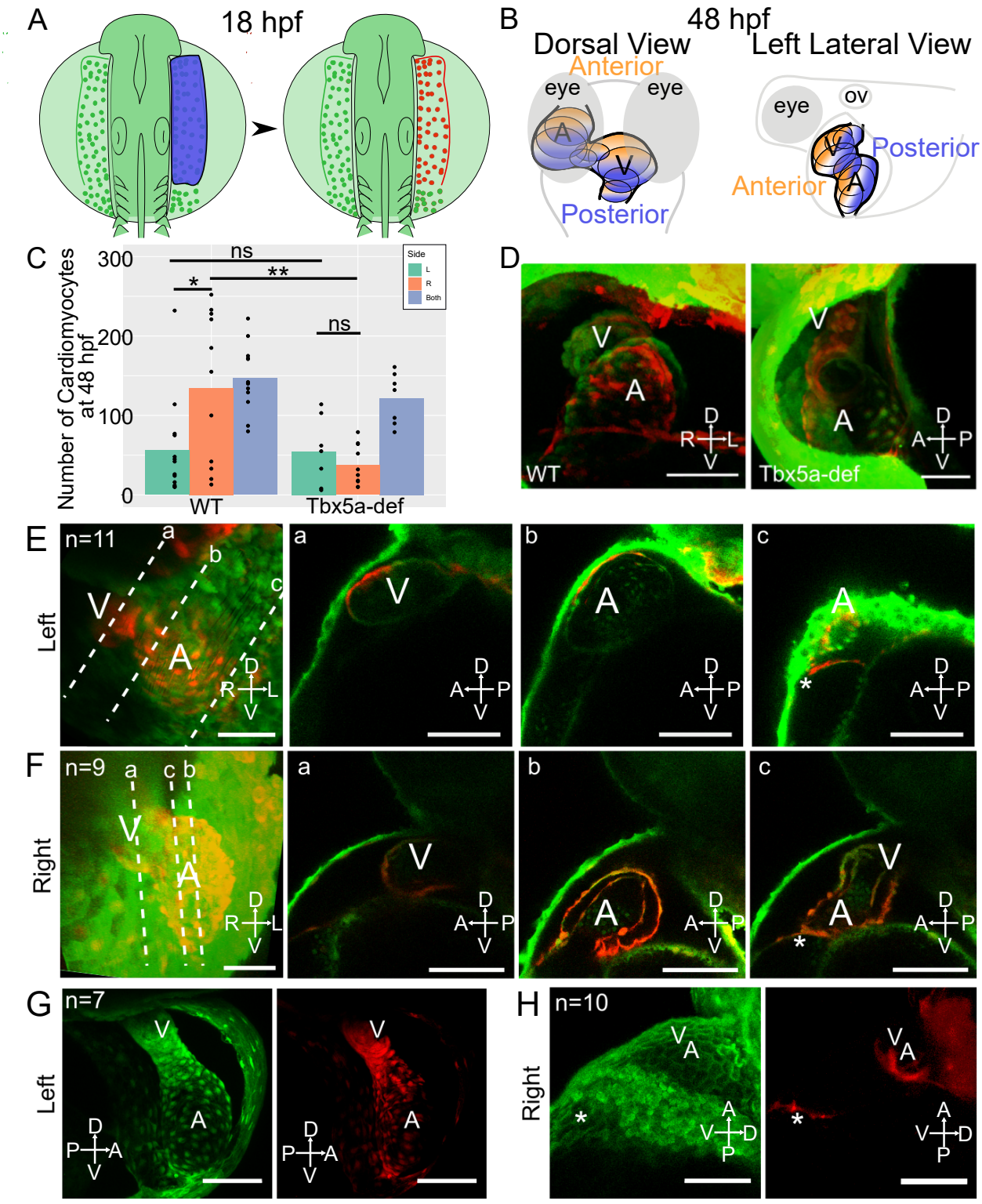

Figure 4.2: **Asymmetric ALPM contributions to the larval heart are affected in Tbx5a-deficient embryos.** (Cont. on next page)

Figure 4.2: (Continued) A- Schematic of dorsal view with right side photoconverted using 405 nm light (shown as blue). B- Schematic at 48 hpf showing anterior (orange) versus posterior (blue) regions of the heart in dorsal and left lateral views. C- Bar plots of mean number of photoconverted Kaede cardiomyocytes at 48 hpf in each experimental condition. Points are counts from each embryo. Statistics performed using the Wilcoxon Rank Sum test. D- 3D projections of larval hearts at 48 hpf in which both sides of the ALPM were photoconverted. E-H- 48 hpf 3D projection of a confocal stack of the larval heart shows the contributions of red fluorescent photoconverted Kaede cells among green fluorescent non-photoconverted Kaede cells, E-F-WT embryos, anterior view. Dotted lines a-c are levels of individual Z-slices through the a-ventricle, b-atrium, and c-connecting region between the venous pole and pericardial sac. E- Heart derived from left side ALPM. F- Heart derived from right side ALPM. G-H- Tbx5a-deficient embryos, G- Heart derived from left side ALPM, anterior view. H- Heart derived from the right side ALPM, left lateral view. A-atrium; V-ventricle; asterisk-venous pole of the heart. Scale bar: 100 μm.

contributions to the heart that are segregated orthogonally/coronally to the body instead of in line with/sagitally to the body (Fig. 4.2B, blue versus orange regions). Recent evidence has shown that later contributions to the heart also segregate along the anterposterior axis between the right and left sides [71]. My large-scale photoconversion experiment resulted in the right side ALPM contributing more to cardiomycytes located in the posterior heart (Fig. 4.2D blue region, Fa-b), whereas cardiomyocytes that originated from the left side were biased towards populating the anterior heart (Fig. 4.2D orange region, Ea-b). Consistent with the left-right asymmetry found within the number of fate-mapped cardiac precursors, photoconverted lateral ALPM from the right side gave rise to more cardiomyocytes than lateral ALPM from the left side (Fig. 4.2C, E-F, effect size 1.14, p=0.0298).

4.4.3 Photoconversion of anteroposterior sections of the ALPM

I showed in Chapter 2 that more cardiac precursors arose from anterior locations of the lateral ALPM than from posterior locations in the 18 hpf fate map (Fig. 2.7F). Furthermore, precursors that arose from the right side in the 18 hpf fate map displayed a larger difference along the anteroposterior axis than precursors on the left side (Fig. 2.7D-E, 2.9A). I next questioned whether these differences in the single-cell resolution fate map translated into

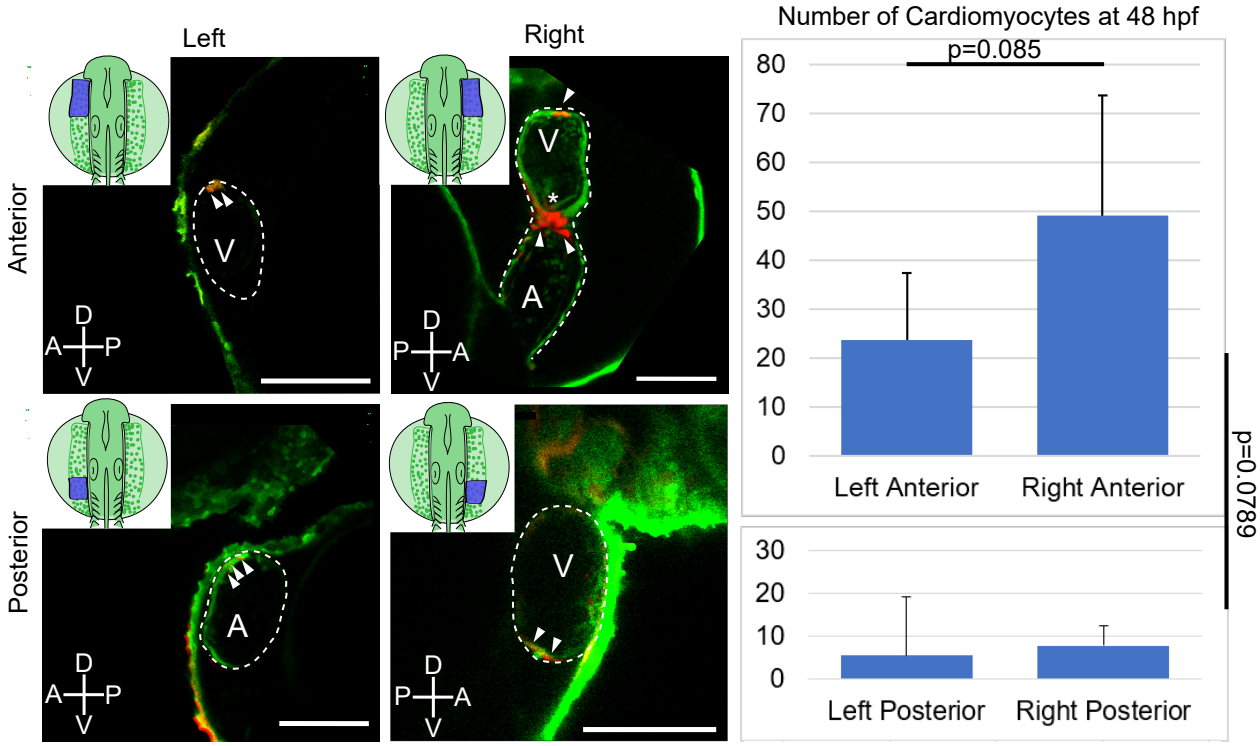

Figure 4.3: **ALPM regions anterior to the otic vesicle give rise to more cardiomyocytes than regions posterior to the otic vesicle asymmetrically along the left-right axis.** Four regions of the lateral ALPM were photoconverted at 18 hpf: left anterior, right anterior, left posterior and right posterior. Dorsal view schematics (anterior up) of each photoconverted region are inset into an example image of a z-slice through the heart at 48 hpf. Blue area represents cells exposed to UV-light, therefore photoconverting them from green to red fluorescent Kaede-expression. Fluorescent z-slices show photoconverted myocardium (arrowheads) and endocardial (asterisk) cells within the larval heart (dashed outlines) at a lateral view. V-ventricle; A-atrium; Compass directions = A-anterior; P-posterior; D-dorsal; V-ventral. Scale bar = 100 μm.
Bar graph of mean photoconverted cardiomyocyte count at 48 hpf per region. Error bars are standard error of the mean. P-values calculated from a Two-Way ANOVA of independent measures comparing left versus right regions (p=0.085) and anterior versus posterior regions (p=0.0789).

differential contributions to the heart by 48 hpf. I photoconverted quadrants of the lateral ALPM along the following boundaries: the right versus left side of the embryo, and cells anterior or posterior to the otic vesicle. The otic vesicle was the landmark used as a reference for all labeled precursors of the fate map, and the center point was the dividing line for the anteroposterior bins. In order to unambiguously distinguish between anterior and posterior regions of the lateral ALPM, I did not photoconvert cells adjacent to the otic vesicle. Dorsal view schematics of the photoconverted region of Kaede-expressing embryos for each quadrant in Fig. 4.3 roughly represent photo-manipulated cells.

Photoconverted red cells from quadrants of the lateral ALPM contributed to the larval heart, pericardial sac, pharyngeal arches, and peritoneum (not pictured) collectively, though not to all fates in all experimental embryos. Occasionally I observed no photoconverted cells in the heart in each of the four experimental conditions (photoconversion of each quadrant). As in the contributions from the whole left or right sides of the lateral ALPM, cardiac contributions of left quadrants were located in the anterior heart while cardiac contributions of right quadrants were located in the posterior heart (Fig. 4.3). There were no particular regions of the heart that anterior versus posterior quadrants contributed to, suggesting a lack of topology along the anteroposterior axis. Similar to the results found in Chapter 2, right side quadrants gave rise to slightly more cardiomyocytes at 48 hpf than left side quadrants (Fig. 4.3, p=0.85). Anterior quadrants gave rise to slightly more cardiomyocytes at 48 hpf than posterior quadrants (Fig. 4.3, p=0.0789). These results corroborate the findings of the single-cell resolution fate map.

4.4.4 Photoconversions of small regions of the ALPM

My single-cell resolution fate map suggests that the lateral ALPM consists of a mix of cell fates within one embryo (Fig. 2.2I). To confirm this hypothesis, I purposefully lowered the resolution of my photoconversion experiment. I photoconverted small regions of 4-10

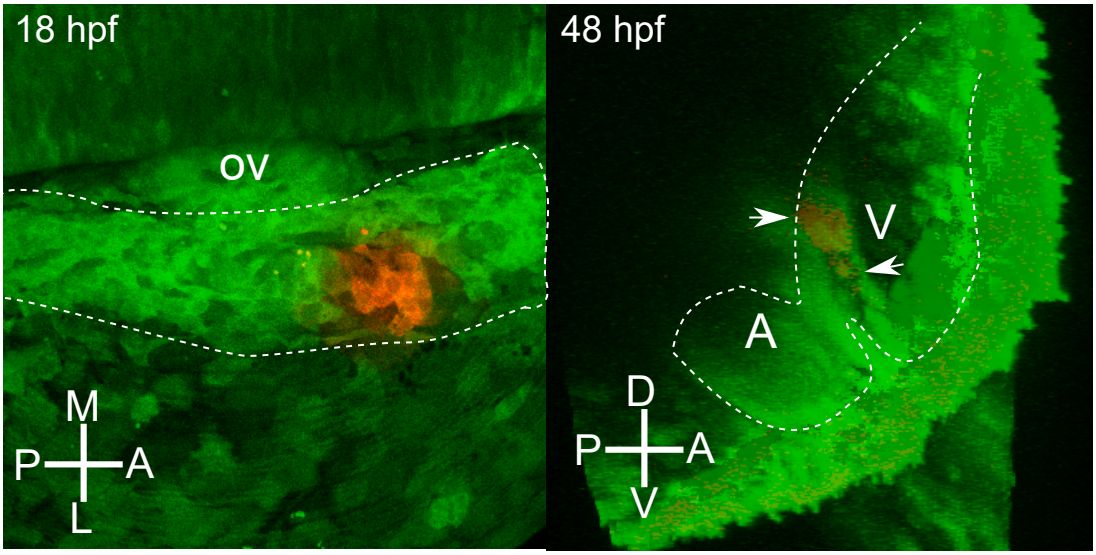

Figure 4.4: **Example of small regional photoconversion contribution to the heart.** Kaede expression in all cells of the embryo. At 18 hpf, a small region of 4-10 cells within the lateral ALPM (dashed outline) were photoconverted from green to red fluorescence. At 48 hpf, the positions and fates of photoconverted cells were assessed. In this example, photoconverted cells resided in just the ventricle of the heart (arrows, outlined with dashed lines). ov- otic vesicle; A-atrium; V-ventricle; direction compass- A-anterior; P-posterior; M-medial; L-lateral; D-dorsal; V-ventral.

cells within the lateral ALPM (Fig. 4.4). If small regions consistently give rise to multiple fates, then the resolution of my earlier fate map is appropriate and the results represent the topology of a single embryo. If small regions mostly give rise to one fate at 48 hpf, then the resolution of my earlier fate map is too fine to capture regionality of the fates in the lateral ALPM. The results of photoconverting small regions of 4-10 cells within the lateral ALPM are shown in Table 4.2. I observed three out of the four previously reported fates at 48 hpf: cardiomyocytes, pharyngeal arches, and pericardial sac. There was no correlation between the positions of photoconverted regions and their fate(s) (not shown). Out of the thirteen (13) small regions, five (5) gave rise to two or three fates. Therefore, 38% of regions are multipotent and reciprocally, 62% of regions are unipotent (Table 4.2, Row 13). This result suggests that the resolution of my single-cell fate map was too fine and not representative of the topology of the ALPM within one embryo.

	Fate at 48 hpf					Number of
Clone Fate	Atrium	Ventricle	PA 1-2	PA 3-7	Pericardial Sac	labeled regions
Single	x					0
		x				3
			x			0
				x		3
					x	2
Double	x		x			1
	x			x		1
				x	x	2
Triple	x		x		x	1
Total Clone #	3	3	2	6	5	13
% of all	23%	23%	15%	46%	38%	
# multipotent	3	0	2	3	3	
% of total	23%	0%	15%	23%	23%	38%
% fate	100%	0%	100%	50%	60%	

Table 4.2: **Number of small photoconverted regions of ALPM according to fate at 48 hpf.** Rows 1-9- Each row represents small photoconverted regions according to their fate(s) at 48 hpf, marked with Xs in the columns. PA-Pharyngeal Arch. The count at the end of the row (last column) is the number of experiments (labeled precursors) that belong to that fate category. Rows 6-8- Multipotent precursors that gave rise to two fate. Row 9- One multipotent precursor that gave rise to three fates. Rows 10-14- Sums and percentages in each column divided by the total (13) or by the sum in each fate.

In addition to assessing fate of photoconverted cells, I also noted the locations within the organ. I found that regions that gave rise to ventricular cardiomyocytes exclusively came from the right side ALPM and did not give rise to any other fate (Table 4.2, Row 2, 14-0%). Atrial cardiomyocytes exclusively arose from regions that also gave rise to other fates (Table 4.2, Rows 6, 7, 9, 14-100%). Photoconverted regions did not give rise to both ventricular and atrial cardiomyocytes. Regions that gave rise to the first two pharyngeal (mandibular and/or hyoid) arches exclusively came from the left side ALPM and always also gave rise to atrial cardiomyocytes (Table 4.2 Rows 3, 6, 9, 14-100%).

4.5 Discussion

4.5.1 Regional photoconversion corroborates the findings of the single-cell resolution fate map

The photoconversion of larger regions of the aLPM in embryos that had been injected with Kaede mRNA at the one-cell stage showed that the early asymmetry in precursor numbers was retained in the larval heart tissues (Fig. 4.2). There were twice as many right side cardiac precursors at 18 hpf (Fig. 2.2E) and the right side contributed about twice as many cardiomyocytes to the larval heart (Fig. 4.2C). The left-right differential contribution in the number of cardiac precursors at 18 hpf correlates with differential composition of the entire right or left ALPM to the heart (Fig. 4.2C). This suggests that there are no compensatory mechanisms between 18 and 48 hpf that will change the relative contributions and numbers of ALPM precursors to the heart between the right and left sides.

By photoconverting left versus right and anterior versus posterior quadrants of the lateral ALPM, I observed differences in the number of cardiomyocytes by 48 hpf that came from each of these quadrants. Right quadrants gave rise to more cardiomyocytes than left quadrants and anterior quadrants gave rise to more cardiomyocytes than posterior quadrants (Fig. 4.3). This result shows that the asymmetries observed from the single-cell resolution fate map at 18 hpf among cardiac precursors corresponds to asymmetrical contributions of cardiomyocytes at 48 hpf among both the left/right and anteroposterior axis.

My study provides evidence that there are inherent asymmetries among the number and contributions of cardiac precursors within the lateral ALPM at 18 hpf, especially between precursors anterior and posterior to the otic vesicle. Guerra et al. (2018) observe that *meis2b* expression in the posterior medial ALPM within the FHF gives rise to the left atrium and controls *pitx2* expression in zebrafish [131]. The authors suggest that anteroposterior patterning within the ALPM controls later left-right asymmetry within the heart [131].

Perhaps *meis2b* is involved in patterning the anteroposterior axis of the lateral ALPM in a similar way.

4.5.2 tbx5a function in contributions to the larval heart across the left/right axis

In Tbx5a-deficient embryos, the lateral ALPM contributes to fewer cells in the larval heart than in wildtype embryos (Table 4.1). This result confirms Mosimann et al. (2015) finding that Tbx5a-deficiency lowers the ratio of SHF to FHF cells in zebrafish [73]. Mosimann et al. (2015) use Draculin expression as a marker of the FHF and extrapolate the ratios of the SHF to FHF cells by absence to presence of Draculin respectively. My investigation does not use molecular markers for FHF or SHF. Since molecular markers can be up- or down-regulated over time, following expression patterns does not necessarily mean that the same cells are being followed over time. I follow cells instead of protein expression, therefore controlling for possible Tbx5a-mediated regulation on Draculin expression. The cells that I follow are later contributions to the heart, which can be termed as SHF. Therefore, *tbx5a* functions to maintain SHF contribution to the heart in zebrafish embryos.

Since there is a correlation between the left/right asymmetries in the precursor number found in the fate map at 18 hpf and in the contribution to the heart at 48 hpf, perhaps the same correlation exists in the Tbx5a-deficient embryos. Indeed, in the Tbx5a-deficiency, the right side lateral ALPM contributes fewer cardiomyocytes such that the contribution is equal to that from the left side (Fig. 4.2C). Therefore, *tbx5a* functions to specifically maintain SHF contributions from the right lateral ALPM to the heart. As TBX5 is known to be downstream of left-right patterning genes in mice (Section 1.4), I propose that *tbx5a* may also be a downstream effector of the left-right patterning pathway in zebrafish cardiac development.

4.5.3 Resolution of single-cell versus small region fate mapping

If the ALPM is composed of domains of single fate, then I would expect to occasionally see small regions of double and triple fate at the boundaries between fate domains. Indeed this is what I observe from photoconverting small regions of 4-10 cells in the 18 hpf ALPM. Therefore, the lateral ALPM at 18 hpf is not composed of a complete intermixing of individual cells by fate.

I found it quite curious that small photoconverted regions did not give rise to peritoneum at 48 hpf, whereas peritoneum derived from single photoconverted cells made up 22% of the fate map (Fig. 2.5, Row 18). Perhaps I did not extensively cover the entire extent of the lateral ALPM in my experimentation. Single-cell derived peritoneum precursors arise from slightly more lateral and posterior locations (Fig. 2.7A-F). The most laterally localized small region reached to around 180 μm lateral to the otic vesicle, which could not cover the lateral extent of the whole tissue (total width = 300 μm on either side). The most posteriorly localized small region reached to around 270 μm posterior to the otic vesicle, which also could not cover the posterior extent of the whole tissue (somite 1 is around 500 μm posterior to the otic vesicle). Not probing the entire lateral ALPM with photoconversion of small regions could explain why I did not observe peritoneum fates.

Photoconversion of small regions of lateral ALPM at 18 hpf was able to identify areas that gave rise to either chambers of the heart or first two versus last five pharyngeal arches (Table 4.2). Previous fate maps of cardiogenic regions of the zebrafish embryo showed that at 5 and 11 hpf, photoconverted cells gave rise to either atrial or ventricular cardiomyocytes and never both [25, 75]. My finding is in line with the other fate maps, suggesting that later additions to the heart are also specified between chambers at 18 hpf. However, my single-cell resolution fate map contained precursors that could give rise to both chambers (Fig. 2.4ii). Perhaps this discrepancy in result is also caused by the smaller extent of the lateral ALPM that I assessed in photoconverting small regions (see paragraph above). If this were the case,

then I predict that cardiac precursors which can give rise to both chambers of the heart reside in more lateral and/or posterior locations within the lateral ALPM at 18 hpf.

Lastly, the occurrence of multipotent small regions lends insight into how the lateral ALPM might be patterned at 18 hpf. For example, first (mandibular) and/or second (hyoid) pharyngeal arch precursors always also gave rise to atrial cardiomyocytes (Table 4.2 Rows 3, 6, 9). This suggests that precursors to the first two arches share fate with atrial precursors. Alternatively, this result could also suggest that the two fate regions are apposed to each other and I consistently labeled the region in between that consisted of both precursor types. More data and a more extensive analysis of these small regions will be necessary to distinguish between these two possible conclusions.

CHAPTER 5

A POSSIBLE ROLE OF THE PERICARDIAL SAC IN HEART LOOPING

5.1 Abstract

The development and role of the pericardial sac in proper morphogenesis has not been studied in zebrafish. Recently, several studies in amniote cardiac morphogenesis have put forth a hypothesis on how mechanical forces can induce heart looping, as reviewed in Desgrange et al. (2018) [178]. This hypothesis, called the growth-induced buckling hypothesis, posits that physical compressive loads on the heart tube are generated by growth differences between the heart tube itself and the pericardial sac. This hypothesis has not been tested in zebrafish cardiac development, and so I sought to provide evidence that might support or oppose it. I measured the heart tube length and four various metrics of pericardial sac growth to determine which metrics were changed in Tbx5a-deficient embryos. I found that the relative growth of the heart tube compared to the growth of the dorsoventral length of the pericardial sac was in line with predicted results from the growth-induced buckling hypothesis. In Tbx5a-deficient embryos, the relative growth rates are decreased, implicating *tbx5a* in regulating pericardial sac growth. However, Tbx5a-deficient embryos did not have significantly more cells within the pericardial sac compared to wildtype embryos. The mechanism by which Tbx5a-deficiency results in increased pericardial sac size and impaired heart looping is, therefore, not likely due to abnormal ALPM specification and so remains unknown.

5.2 Rationale

Theoretically, cardiac looping may occur due to intrinsic factors of the primary heart tube and/or external constraints. Some intrinsic factors, such as an asymmetric distribution of actin bundles [179], myocardial cell shape changes [180], and differing proliferation rates of SHF cells [181] have been observed in chick and mouse experiments. At the same time, extrinsic physical constraints also act in cardiac looping in amniotes. The **growth-induced buckling hypothesis** posits that physical compressive loads on the primary heart tube are generated by the growth differences between the heart tube itself and the pericardial cavity, which holds the heart. The slower growing distance between the ventral-most pericardial sac and the dorsal mesocardium can theoretically provide an external constraint on the heart tube that can drive looping. These forces have been shown via mechanical simulations of rubber tubes to drive the complex helical coiling in the proper direction (D-loops instead of L-loops, [182]). Recently, Le Garrec et al. (2017) used dynamic three-dimensional computer simulations to show the requirement and sufficiency of various *in vivo*-experimentally validated parameters in driving cardiac looping in the mouse [181]. It remains unknown whether these parameters are conserved in other tetrapods.

In chick, physical removal of the splanchnopleure underlying the heart causes an initial suppression on the torsion of the heart tube; however, looping is restored after a several-hour delay [183]. Ablation of the caudal part of the heart does not affect the twisting of the residual rostral part of the heart [184]. The unlooped heart phenotype in Tbx5a-deficient zebrafish embryos is always comorbid with pericardial edema. In my single-cell resolution fate map, I observe that upon knockdown of Tbx5a, the number and proportion of pericardial sac precursors increases (Fig. 2.2F versus K; Fig. 2.10B, purple bars). Further investigation is needed to determine whether the increase in pericardial sac cells identified in the 18 hpf Tbx5a-deficient fate map is responsible for the enlarged pericardial sac at 3 dpf and therefore the alleviation of an external physical constraint on the heart in looping.

5.3 Results

5.3.1 Preliminary data on the correlation between the pericardial sac and heart looping morphologies

I first sought to discover how the physical metrics of morphological growth of the pericardial sac and heart tube changed over time. I imaged the heart region in six hour intervals between 30 and 54 hpf, which is when looping occurs. I measured the length of the heart tube by drawing a freehand line down the midpoints of the heart (Fig. 5.1A line in red heart). This method of measurement is suitable in two-dimensional images since the zebrafish heart adopts a flat S-shape instead of the coiled spiral shape of the mouse heart. The length of the heart tube increased by about two-fold, and mostly from 36 to 43 hpf in wildtype embryos (Fig. 5.1B). To understand the morphology of the pericardial sac over time, I measured four different metrics: lateral length, dorsoventral length, circumference, and area of the pericardial sac. The lateral and dorsoventral lengths are single-dimension measurements that are orthogonal to each other (Fig. 5.1A brackets). The lateral length of the pericardial sac increased by 1.99x from 30 to 54 hpf in wildtype embryos (Fig. 5.1C). The dorsoventral length of the pericardial sac increases by 1.35x from 30 to 54 hpf (Fig. 5.1D). The circumference of the pericardial sac was measured by tracing a line around the two-dimensional anterior view image (Fig. 5.1A bold line around purple). The circumference of the pericardial sac increases by 1.46x from 30 to 54 hpf in wildtype embryos (Fig. 5.1E). Lastly, the area of the pericardial sac is the two-dimensional area within the traced circumference of the pericardial sac, and it increased the most, by 2.99x, from 30 to 54 hpf (Fig. 5.1F).

Next, I compared the growth metrics of the pericardial sac and heart tube to those in Tbx5a-deficient embryos. By observing which metrics differed the most between wildtype and Tbx5a-deficient embryos, I could better understand *tbx5a* function on the pericardial sac and heart looping morphogenesis. In Tbx5a-deficient embryos, the length and growth of the

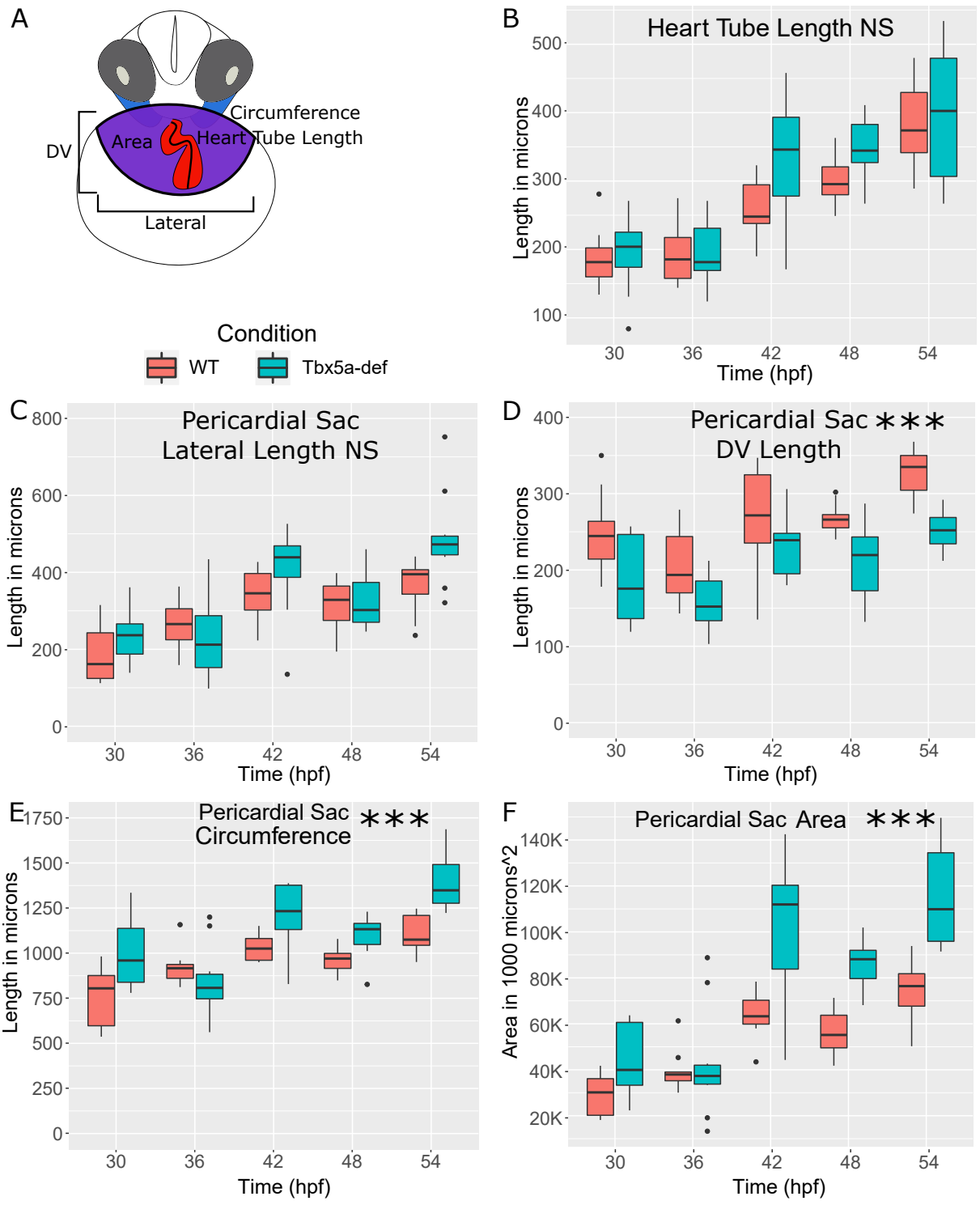

Figure 5.1: **Metrics of growth of the pericardial sac and heart in Tbx5a-deficient embryos.** A- Anterior view schematic of a 48 hpf larval embryo. Purple-pericardial sac; red-heart; blue-pharyngeal arches; grey-eyes. Brackets denote lengths of dorsoventral (DV) and lateral boundaries of the pericardial sac that were measured. (Cont. on next page)

Figure 5.1: (Continued) Bold lines along the middle of the heart and circumference of the pericardial sac made up the remaining measurements. Area was calculated based upon the circumference drawn over the pericardial sac in two dimensions. B-F Box plots of each measurement over time in both WT and Tbx5a-deficient embryos. Asterisks denote statistical significance between WT and Tbx5a-deficient measurements over all times using the Kruskal-Wallis test on total mean measurements. B- Length of heart tube; C- Lateral length of pericardial sac; D- Dorsoventral length of pericardial sac; E- Circumference of pericardial sac; F- Area of pericardial sac measured at an anterior view. n= 10 embryos per condition per time.

heart tube is unaffected (Fig. 5.1B). The lateral length of the pericardial sac is also unaffected when compared between wildtype and Tbx5a-deficient embryos (Fig. 5.1C). However, the dorsoventral length, circumference, and area of the pericardial sac in Tbx5a-deficient embryos are all larger than those in wildtype across all times measured (Fig. 5.1D-F). The increased pericardial sac dorsoventral length, circumference and area in Tbx5a-deficient embryos is not due to an increased growth rate, since the growth rates from 30 to 54 hpf are the same as in wildtype. Instead, the pericardial sac is larger in Tbx5a-deficient embryos at my earliest timepoint measured, at 30 hpf, and remains larger throughout.

The idea behind the growth-induced buckling hypothesis was first posited by Patten (1922), who observed that the growth of the chick heart tube was over three-times that of the distance between the poles (Fig. 5.2A) [185]. The hypothesis itself was named by Bayraktar and Männer (2014) [182]. Patten (1922) proposed that "mechanical compulsion" exerted on the tubes by the limited space between the poles was responsible for looping the chick heart [185]. Since then, studies in axolotl and mouse have also observed similar differential growth between the length of the heart versus pericardial sac (2.64 times in axolotl, 4.4 times in mouse) [186, 181]. However, the same metrics have not been assessed during zebrafish heart looping, and I predicted would be similar to those found in other vertebrate hearts (Fig. 5.2A). The relative growth rates of the zebrafish heart to pericardial sac from 30 to 54 hpf is 3x (Fig. 5.2)B, which is aligned with that found in other organisms. In the Tbx5a-deficient embryos, the relative growth rate is reduced to 2x between the heart

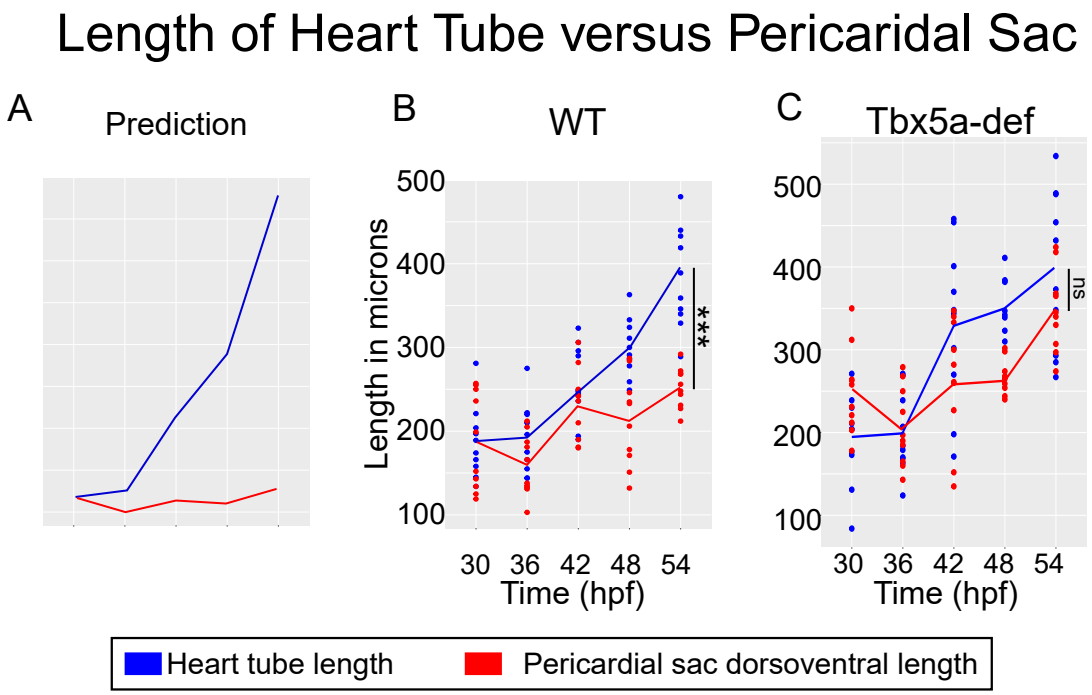

Figure 5.2: **Measures of heart and pericardial sac growth by the growth-induced buckling hypothesis.** Length of the heart tube increases by 4x while the length of the pericardial sac remains constant. B-C Measured lengths of WT (B) and Tbx5a-deficient (C) embryos. Lines through the points denote means. Asterisks denote statistical significance of one-way ANOVA test at 54 hpf between the heart tube and pericardial sac lengths. N=10 per condition.

and pericardial sac and the difference between the final lengths are not significantly different (Fig. 5.2C). This result is expected since Tbx5a-deficient and mutant embryos do not have looped hearts.

5.3.2 At 24 and 32 hpf, Tbx5a-deficienct embryos do not have increased number of pericardial sac cells

I questioned whether the increase of the pericardial sac in dorsoventral length, circumference, and area in Tbx5a-deficient embryos was due to an increase in the number of cells. Furthermore, since much of the increased size of the pericardial sac seems to have arisen before 30 hpf, I wanted to assess the number of pericardial sac cells at an earlier stage. The

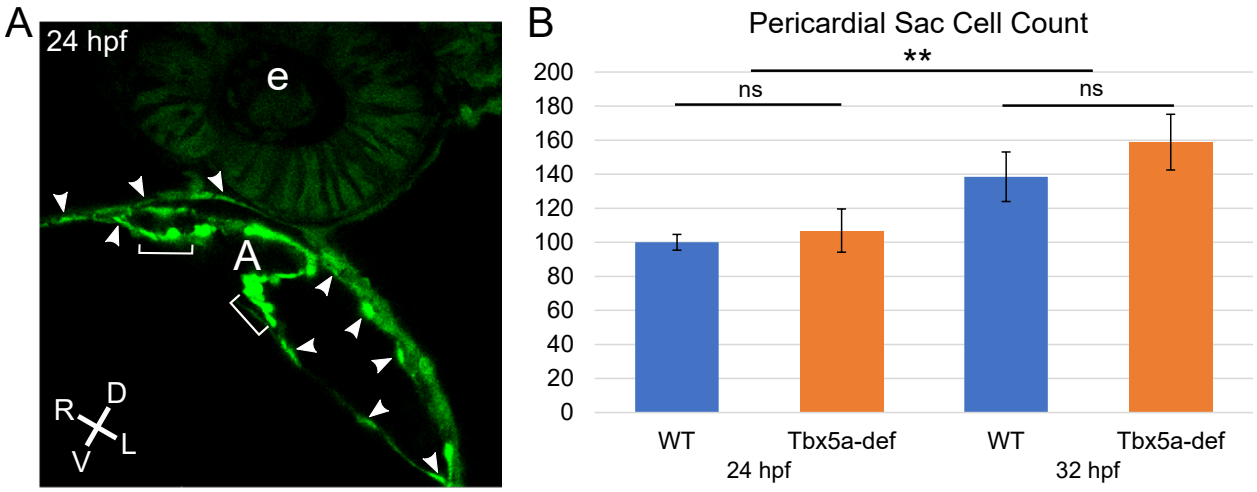

Figure 5.3: **Cell count of pericardial sac cells.** A- Example slice of 24 hpf wildtype embryo with green Kaede expression in every cell, anterior view. Pericardial sac cells in arrowheads. Brackets point to venous pole cells of the heart, not pericardial sac. e- eye, A-atrium. B- Bar graph of pericardial sac cell count. Error bars are standard error of the mean. Statistical comparisons done with a Two-Way ANOVA test for independent measures. N=10 embryos per condition

earliest stage at which I could count the cells was at 24 hpf. In Chapter 2, I observed that there are about twice as many pericardial sac precursors in the Tbx5a-deficient fate map at 18 hpf (Fig. 2.10B). I predicted that I would observe more pericardial sac cells at 24 hpf and especially at the onset of cardiac looping (around 30 hpf).

Currently, there are no molecular markers for the pericardial sac. Therefore, I injected single-cell embryos with Kaede transcript so that every cell expressed green fluorescence. At 24 and 32 hpf, I took confocal stacks of the pericardial sac at 2.0μm intervals. The pericardial sac appears to be a thin single-cell layer that sits underneath the epidermis and hatching gland (Fig. 5.3A arrowheads). While counting pericardial sac cells through the z-slices, I did not count cells of the venous pole of the heart, which are more cuboidal in their morphology (Fig. 5.3A brackets).

The result of counting pericardial sac cells at 24 and 32 hpf in wildtype and Tbx5a-deficient embryos is shown in the bar graph (Fig. 5.3B). The number of pericardial sac cells

increases over time (Fig. 5.3B, p=0.0014), which corroborates the results of the morphological measurements (Fig. 5.1). The number of pericardial sac cells is higher, but not by a statistically significant amount in the Tbx5a-deficient compared to wildtype embryos (Fig. 5.3B).

5.4 Discussion

5.4.1 An increase in pericardial sac cells is not responsible for edema and looping dysmorphogenesis in Tbx5a-deficient embryos

By measuring various metrics of growth of the heart tube and pericardial sac, I found that both organs increase in size over time (Fig. 5.1B-F). Furthermore, Tbx5a-deficiency results in a decreased growth rate of the pericardial sac (Fig. 5.1B-F). Therefore, *tbx5a* function is involved in promoting growth of the pericardial sac between 30 and 54 hpf. I questioned whether *tbx5a* function could contribute to heart looping through regulating the size of the pericardial sac. The growth rate of the heart tube length compared to the dorsoventral length of the pericardial sac decreases in Tbx5a-deficient embryos (Fig. 5.2C). This evidence supports the hypothesis that *tbx5a* functions in enabling growth-induced buckling of the zebrafish heart.

Tbx5a-deficient embryos also have a larger pericardial sac by 30 hpf (the earliest timepoint that I measure in Fig. 5.1). I hypothesized if a larger pericardial sac was caused by the increased number of pericardial sac cells identified in the Tbx5a-deficient fate map at 18 hpf in Chapter 2. Counter to my hypothesize, I found that Tbx5a-deficiency does not result in greater number of cells within the pericardial sac at 24 and 32 hpf. Therefore, it is unlikely that *tbx5a* function in ALPM specification regulates contribution to the pericardial sac. However, it is possible that I did not assess the appropriate time for observing a large difference in the number of pericardial sac cells. Therefore, I recommend counting the

pericardial sac cells at 38 and 48 hpf for future work.

5.4.2 Alternative hypotheses for increased pericardial sac size in Tbx5a-deficient embryos

If the relative growth rate of the heart versus pericardial sac is consistent with the growth-induced buckling hypothesis, yet, there are not more pericardial sac cells in the Tbx5a-deficiency, then what is the mechanism for increased pericardial sac size? The pericardial sac might grow by being stretched from within by internal pressure or intrinsically by cell shape changes such as flattening or rearranging.

Swelling of the pericardium can happen as a consequence of fluid buildup within the pericardial sac. Genetic studies have found mechanisms that link malformations of the zebrafish heart to pericardial edema. First, vascular cadherin protein Cdh5 is necessary for endocardial adhesion to the myocardium and chamber integrity [187]. In Cdh5-deficient zebrafish embryos, the endocardium and myocardium layers separate and increased permeability of the endothelial layer causes leaking [187]. Second, loss of FHF cells being extruded into the pericardial space can increase the size of the pericardium. In Cyp26a1- and Cyp26c1-deficient zebrafish embryos, ventricular cardiomyocytes have disrupted cell polarity and become extruded outward into the pericardial space [143]. In both of these knockdowns, the hearts were not looped, suggesting that Cdh5 and Cyp26 proteins may be involved in the growth-induced buckling hypothesis. It is unknown how mechanistically *tbx5a* functions on or with these proteins. This is an area of further study to better understand mechanisms of cardiac looping.

There could be other mechanisms by which *tbx5a* affects pericardial sac size, and thereby, looping. The following heart phenotypes are characteristic in mutants that cause an unlooped heart and increased pericardial length (including *tbx5a*): slowed heart rate, increased apoptosis, and inability to form valves and sense blood flow [139, 188, 137, 152, 94]. Each of

these phenotypes could be the cause of or result of pericardial edema, but it is currently unknown which causes the other. Further investigation of the function of *tbx5a*, and other genes, could shed light on how the size of the pericardial sac is regulated.

CHAPTER 6

CONCLUSION

6.1 Limitations of this study

In my investigation of ALPM development, I could not assess the difference in potentials and behaviors between the somatic and splanchnic layers. Since the coelomic cavity has not filled at this stage, the somatic and splanchnic layers of the ALPM are so close in proximity that the layers can only be distinguished from each other via careful scrolling between the z-stacks. My analysis in any of the experiments did not assess from which layer tracked cells came from.

In my dissertation, I used Kaede as a cytoplasmic marker and conducted irreversible photoconversion from green to red fluorescence. The benefit of using Kaede was that photomanipulation is fast and non-invasive. However, I was prevented from using other molecular tools in my study. I was unable to use transgenic markers for the various cardiac lineages in the fate map experiment since identification of often a single cell expressing green to red fluorescence was essential to this method. The addition of another fluorescent marker would have greatly reduced my ability to observe the fates, morphologies, and positions of single cells in the heart. It also would have been advantageous to co-stain for molecular markers of the other fates found within the fate map. However, no antibody exists to distinguish between photoconverted and non-photoconverted Kaede protein

6.2 A proposed mechanism of ALPM specification

By compiling the data on the specification and migration of the lateral ALPM between 18 and 48 hpf in this dissertation, I have assembled a multi-component model of how this tissue behaves over time to produce the many resultant fates. Overall, I propose that the tissue becomes specified progressively due to the following processes that are taking place during

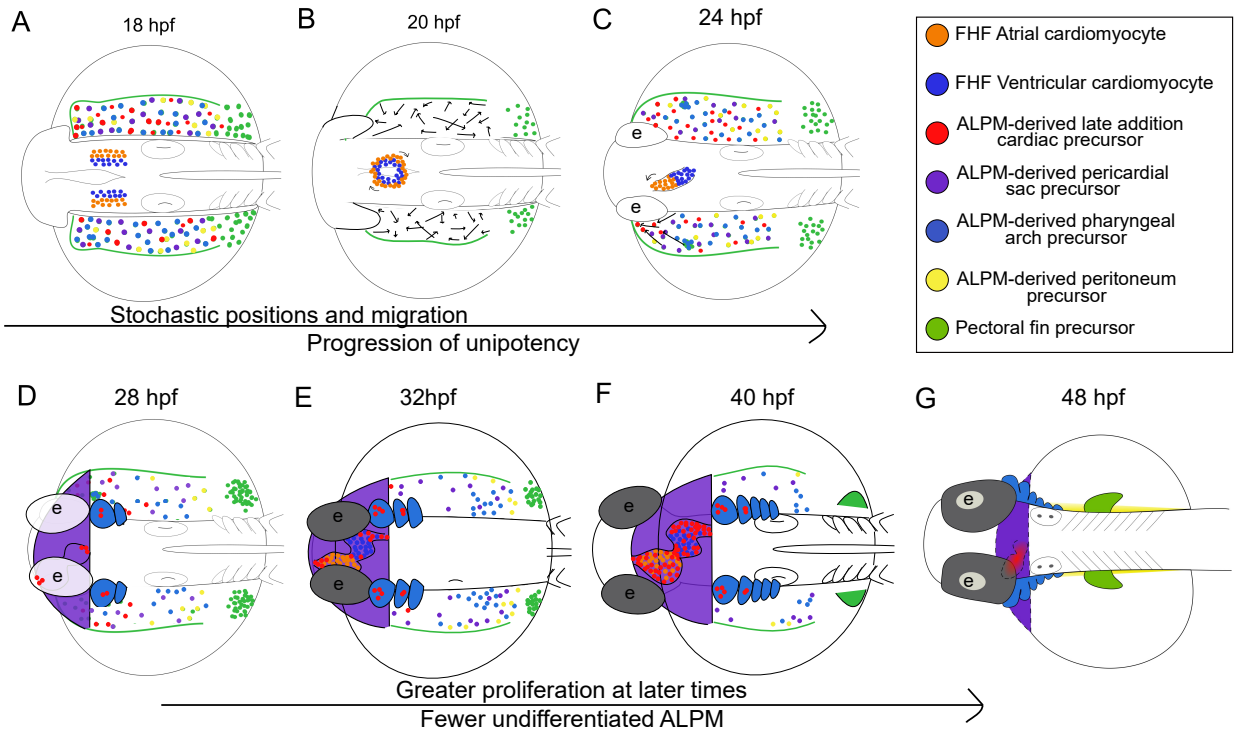

Figure 6.1: **Model of ALPM specification from 18 to 48 hpf.** Over developmental time, specification of the lateral ALPM occurs progressively. Embryo schematics dorsal side up, anterior to the left. Cell fate colored according to legend. A- At 18 hpf, the ALPM consists of medial FHF precursors, lateral precursors with mixed fates, and pectoral fin precursors positioned posteriorly. B- Lateral precursors undergo stochastic rearrangement of positions until 24 hpf (arrows) and are becoming restricted towards unipotency. C- Cardiac precursors on the left migrate more persistently towards the venous pole. D- Around 28 hpf, small pericardial sac (purple) and pharyngeal arches (blue) have formed. Some ALPM-derived late addition cardiomyocytes have contributed to the arterial and venous poles of the heart. D-G From this time until 48 hpf, the number of undifferentiated ALPM will progressively decrease and cells will proliferate when they reach their final location. e-eyes

the relevant stages: stochastic positioning and movements within the undifferentiated tissue; differential directed migration of precursors to the organ field according to the displacement; and differentiation of the anterior ALPM before posterior ALPM. In this section, I will describe in detail my model of ALPM specification and migration over time (Fig. 6.1).

18 hpf marks the time in which the ALPM begins to migrate anteriorly away from the pectoral fin precursors. In Figure 6.1A, the 18 hpf embryo's ALPM precursors are positioned as follows. FHF atrial (orange) and ventricular (blue) precursors are positioned in rows

medially under the midbrain. Pectoral fin precursors (green) are spread adjacent to somites 1-4. Lateral ALPM consists of late addition cardiac, pericardial sac, pharyngeal arch, and peritoneal precursors that are stochastically positioned with slight regionality. All of the precursors are not yet specified as any one lineage, since few can give rise to more than one fate. Cardiac precursors are slightly more anterior and are twice as abundant on the right side than left. Pharyngeal arch precursors are slightly more medial within the lateral ALPM, while peritoneal precursors are slightly more lateral and posterior. Most of the cells are unipotent and will continue to progress towards 100% unipotency over time.

Between 18 and 24 hpf, lateral ALPM precursors stay within the lateral ALPM and undergo stochastic rearrangement (Fig. 6.1B arrows). The whole lateral ALPM tissue is migrating anteriorly away from the pectoral fin precursors. At the same time, the medial ALPM is forming the heart cone and undergoes a clockwise rotation. By 24 hpf, the primary heart tube has formed and is jogged to the left. The lateral ALPM as a whole has remained the same size since 18 hpf. Only a few precursors have undergone cell division and no cells have migrated out of the ALPM to contribute to their final organs. Therefore, the precursors are still not specified as any one lineage, yet remain restricted in fate. Later additions of ALPM-derived cardiac precursors have undergone slight directed migration (Fig. 6.1C arrows to red cells). Right side cardiac precursors have positioned themselves closer to the arterial pole, traveling a shorter net distance than the left side precursors which have positioned themselves closer to the venous pole of the heart. The difference in displacement causes left side cardiac precursors to have the highest amount of directed migration among lateral ALPM precursors.

The mechanism behind cardiac precursor directed migration may involve signaling cues. Perhaps the cardiac precursors are responding to a migration cue similar to how pectoral fin precursors respond to FGFs. Bmp proteins may act as a directional cue for cardiac tube jogging and migration as myocardial cells move towards a Bmp-covered bead [82]. There is

a source of Bmp4 on the right side of the ALPM and in the outflow tract, atrioventricular junction and sinoatrial myocardium by 48 hpf [101]. Bmp proteins can affect adhesion properties of the migrating cells in gastrulation, and so they might act similarly during cardiac migration [189].

After 24 hpf, lateral ALPM precursors will become incorporated into various organs, thereby leaving the ALPM. The pericardial sac forms around the heart ventrally and dorsally (Fig. 6.1D purple). The pharyngeal arches form sequentially from anterior to posterior. Around 28 hpf, the first two (mandibular and hyoid) arches have formed (Fig. 6.1D blue). ALPM-derived cardiomyocytes will have contributed to the arterial and venous poles of the heart and will be sequestered into the pharyngeal arches (Fig. 6.1D red). Heart looping will begin around 30 hpf and the pectoral fin precursors undergo an asymmetrical convergence to form the fin bud adjacent to somite 3 [33].

I propose that the development and specification of the lateral ALPM occurs progressively from 24 to 48 hpf based on the following observations: 1) SHF precursors continuously add to the heart from 24 to 72 hpf [66]. 2) The pericardial sac grows in shape and cell number at least until 32 hpf (Fig. 5.1C-F, 5.3). 3) The pharyngeal arches form from 1 to 7 in the anterior to posterior direction one-by-one over time (Fig. 3.3.1). 4) At 32 hpf, the lateral ALPM contains fewer precursors and is particularly devoid of cells within anterior and medial locations in the tissue (Fig. 3.3.1, 3.6, 6.1E). 4) At 48 hpf, there are no longer any undifferentiated precursors within the lateral ALPM. However, the organs continue to grow after the ALPM-derived precursors contribute due to proliferation. For example, the lateral ALPM is composed of about 50 total precursors per left and right side, 26% of which are cardiac precursors (Fig. 3.3.1, 2.5). However, photoconversion of a whole side will contribute to 60-140 cardiomyocytes (Fig. 4.2C). This difference is reconciled by the fact that cardiac precursors divide about twice between 18 and 48 hpf (Fig. 2.9B).

Some organ precursors progress towards specification at different rates. Cardiac precur-

sors are mostly not found within the 32 hpf fate map (Fig. 3.6), suggesting that cardiac precursors reside within the lateral ALPM for a shorter time (between 24 and 32 hpf) than other precursors. Perhaps this is why cardiac precursors migrate in a more ballistic manner between 18 and 24.5 hpf (Fig. 3.3, 3.4A). On the other hand, pericardial sac and peritoneal precursors remain within the lateral ALPM at 32 hpf and peritoneal and pericardial sac precursors have shared fates with each other, suggesting that they have yet to progress towards a single lineage and therefore specification (Fig. 3.6).

Based upon this model of progressive specification, I would predict that the fate maps of embryos at 28 and 40 hpf would appear similarly as I have drawn in Figure 6.1D and F. At 28 hpf, the progression of later additions to the heart is partly complete. And so I predict that cardiac precursors would exclusive be found anterior to the otic vesicle in a 28 hpf fate map. At 40 hpf, halfway between 32 and 48 hpf, most of the pharyngeal arches have formed. Therefore, I predict that there will be half as many undifferentiated lateral ALPM precursors at 40 hpf than there were at 32 hpf and pharyngeal arch precursors will be positioned posterior to the otic vesicle.

6.3 A proposed mechanism of *tbx5a* function that differs across time in the lateral ALPM

The range in my methodologies allowed me to assay the development of the lateral ALPM along multiple different developmental timepoints. It is important to distinguish between each of these timepoints, as *tbx5a* may function differently across time. First, precursor fates found within my fate map from Chapter 2 are a readout on the specification of the lateral ALPM up until 18 hpf, the pre-migratory stage. Second, my backtracking experiment on migrating lateral ALPM cells from Chapter 3 addresses the next stage, which is from 18 to 24.5 hpf. Third, my assessment of proliferation and contribution to the larval heart via fate mapping from Chapter 2 and large-scale photoconversion from Chapter 4 addresses a wider

window of time from 18 to 48 hpf. In the following discussion, I propose that *tbx5a* has distinct functions on the developing lateral ALPM in each of these time windows.

As a selector, Tbx5a interacts with several other transcription factors to activate and/or repress DNA transcription through acting on enhancers. Currently, the extent of *tbx5a* function in zebrafish lateral ALPM is unknown. It has also been reported that Tbx5a-knockdown alters the ratio of FHF to SHF cells as measured by Draculin expression in the FHF [73]. However, using genetic lineage tracing of BAC transgenes in zebrafish, Snchez-Iranzo et al. (2018) report concluded that *tbx5a*-expressing cells only make minor contributions to the SHF [166]. I show that Tbx5a-deficiency affects the lateral ALPM fate map, migration dynamics, and contributions of precursors to the heart (Fig. 2.2J-N, 2.3, 2.7F-L, 2.9, 2.10B, 2.11, 3.3.1B, 3.3, 3.4, 4.2C, Table 4.1). More specifically, *tbx5a* is required for the left-right asymmetry in cardiac precursors within the first time window, by 18 hpf (Fig. 2.2J). Additionally, the Tbx5a-deficient fate map has proportionally twice as many multipotent precursors as in the wildtype (Fig. 2.10B). *tbx5a* may maintain unipotency of lateral ALPM precursors by individually biasing certain fates over others or by maintaining the progression of development in the tissue by 18 hpf. My results do not necessarily distinguish between these two possible hypotheses (biasing particular fates or maintaining the progression of development), yet, the results show an overall increase in multipotent precursors across all fates in the Tbx5a-deficient fate map, which supports the latter hypothesis. There is weak support for the former hypothesis in that *tbx5a* is specifically involved in the development of cardiomyocyte specification, though only later in developmental time and not during somitogenesis stages [151, 153, 168, 169].

Next, *tbx5a* is required for the ballistic migration of lateral ALPM precursors; more specifically, Tbx5a-deficient cells take a longer track length with faster speed, meaning that they are less persistent than wildtype cells (Fig. 3.4C-G). Both wildtype and Tbx5a-deficient cardiac precursors from the left undergo higher ballistic migration than the right (Fig. 3.4C).

Altogether, *tbx5a* functions within 18 to 24.5 hpf to maintain ballistic migration on both sides of the lateral ALPM. *tbx5a* could be affecting the migration by cell-autonomous defects that could include the recognition of the ECM that is the substrate for migration, inability to receive migration signals, and/or dysfunction in cellular and cytoskeletal dynamics. Also, our lab group and others have observed evidence for non-cell autonomous effects of Tbx5a and Tbx5b that could affect the coordination, migration and specification of the ALPM [33, 140, 177].

Between 18 and 48 hpf, a left-right asymmetry emerges in the Tbx5a-deficient cardiac precursor proliferation that does not exist in the wildtype (Fig. 2.9B). Since Tbx5a-deficient cardiac precursors originating from the left lateral ALPM have a larger clone size by 48 hpf than those originating from the right (Fig. 2.9B), I conclude that *tbx5a* is required in limiting the proliferation of lateral ALPM cardiac precursors just on the left side during this time window. At the same stages of in development, I observe that right side lateral ALPM contribute more than the left side to the larval heart by 48 hpf in wildtype embryos (Fig. 4.2B). In the Tbx5a-deficiency, the right side lateral ALPM contributes fewer cardiomyocytes such that the contribution is equal to that from the left side (Fig. 4.2B). I propose that *tbx5a* changes function over time between 18 to 48 hpf. There is another hypothesis that is non-mutually exclusive to my aforementioned hypotheses that can also explain these observations. *tbx5a* may have separate functions across the left-right axis. Support for this hypothesis includes evidence of involvement of TBX5 in left-right asymmetry, of which there are multiple previous observations. First, PITX2C is a downstream target of TBX5 in mouse [132]. Second, loss of TBX5 function affects the left side more severely than the right side in mammalian limb development [133, 134]. Third, the septum primum in mice which is affected by atrial septal defects similar to HOS patients expresses Pitx2 [135]. As TBX5 is known to be downstream of left-right patterning genes in mice, I propose that *tbx5a* may also be a downstream effector of the left-right patterning pathway in zebrafish cardiac development.

Other authors have postulated *tbx5a*'s role in proliferation, cell death, and migration [159, 158, 188, 190], which may be able to explain these observed results.

Altogether, I suggest a model of *tbx5a* function in the lateral ALPM that proceeds as follows in developmental time. First *tbx5a* acts downstream of Pitx2c to asymmetrically enable more cardiac precursors within the right side lateral ALPM to undergo directed cell migration than the left by 18 hpf. Then *tbx5a* enables the persistent directed cell migration of precursors from both sides into their respective organ fields from 18 to 24.5 hpf. As precursors are migrating between 18 and 48 hpf, when I assessed their fates, *tbx5a* functions to restrict the fates of all lateral ALPM precursors to keep them mostly unipotential. At the same time, *tbx5a* restricts proliferation of cardiac precursors on the left side once they reach the heart. Lastly in this model, *tbx5a* allows the compensation of more cardiomyocytes contributing to the larval heart from the right side lateral ALPM to maintain proper organ size, which might be executed by the Hippo pathway [71]. Further study must be done to determine on which side *tbx5a* function is necessary in these mechanisms and to confirm the order of mechanisms that I propose.

6.4 A proposed mechanism of cardiac looping morphogenesis

Although cardiac jogging is the first visible instance of left/right symmetry breaking in zebrafish development, the left/right asymmetries that I observe in my dissertation research probably do not affect leftward cardiac jogging. Cardiac jogging occurs within just the medial ALPM FHF precursors, which I am explicitly not studying. The differential speeds among left and right FHF as they migrate together to form the heart cone and primary heart tube are sufficient in generating heart jogging [165]. Therefore, I propose that the phenotypes that I observe under Tbx5a-deficiency contribute to lack of heart looping, not heart jogging.

Tbx5a-deficient and mutant *heartstrings* (*hst*) embryos fail to undergo heart looping and die around 6 dpf after exhibiting a slow deteriorating heart beat and severe pericardial edema

[139]. The role of *tbx5a* in heart looping is not understood. There are intrinsic and extrinsic forces that may act within and on the developing heart that will cause looping. As reviewed in Desgrange et al. (2018), the forces behind zebrafish heart looping are not as well understood as chick or mouse heart looping. Intrinsic forces that may act in zebrafish heart looping include differential cell recruitment and/or proliferation between the left/right sides or venous/arterial poles of the heart. My research shows that there is differential contribution to the heart between the right and left lateral ALPM. Furthermore, this differential contribution is correlated with more cardiac precursors residing in the right lateral ALPM than the left. This implies that more cells are being recruited into the heart from the right than the left sides. This difference could be one factor in generating proper cardiac looping (Fig. 6.2A). Experimentation using DiI and DiO labeling of SHF cells as they ingress into the mouse heart showed that more cells ingressed into the venous pole from the right than from the left at E8.5 [181]. Further *in silico* experimentation showed that this asymmetrical cell ingression is required for looping morphogenesis of a growing tube [181]. Likewise, in Tbx5a-deficient embryos, the left/right asymmetrical contribution of cardiac precursors evens out (Fig. 4.2), implicating *tbx5a* in this mechanism. I propose that the differential contribution of cardiac precursors across the left/right axis in zebrafish is responsible for the rightward positioning of the ventricle and posterior heart chambers.

Contribution of the numbers of cardiac precursors is not the only means of cell recruitment. The directed migration of cardiac precursors is also important in cell recruitment. If cells do not get to their destinations fast enough or in a straight path, then there will be fewer cells recruited in a given time. By analyzing cell tracks of migrating lateral ALPM precursors, I found that left side cardiac precursors undergo a more ballistic migration into the heart than right side precursors. The left side cardiac precursors had higher speed and traversed a longer displacement to the venous pole than the right side precursors. It is likely that this left/right migration asymmetry could contribute to heart looping. A greater

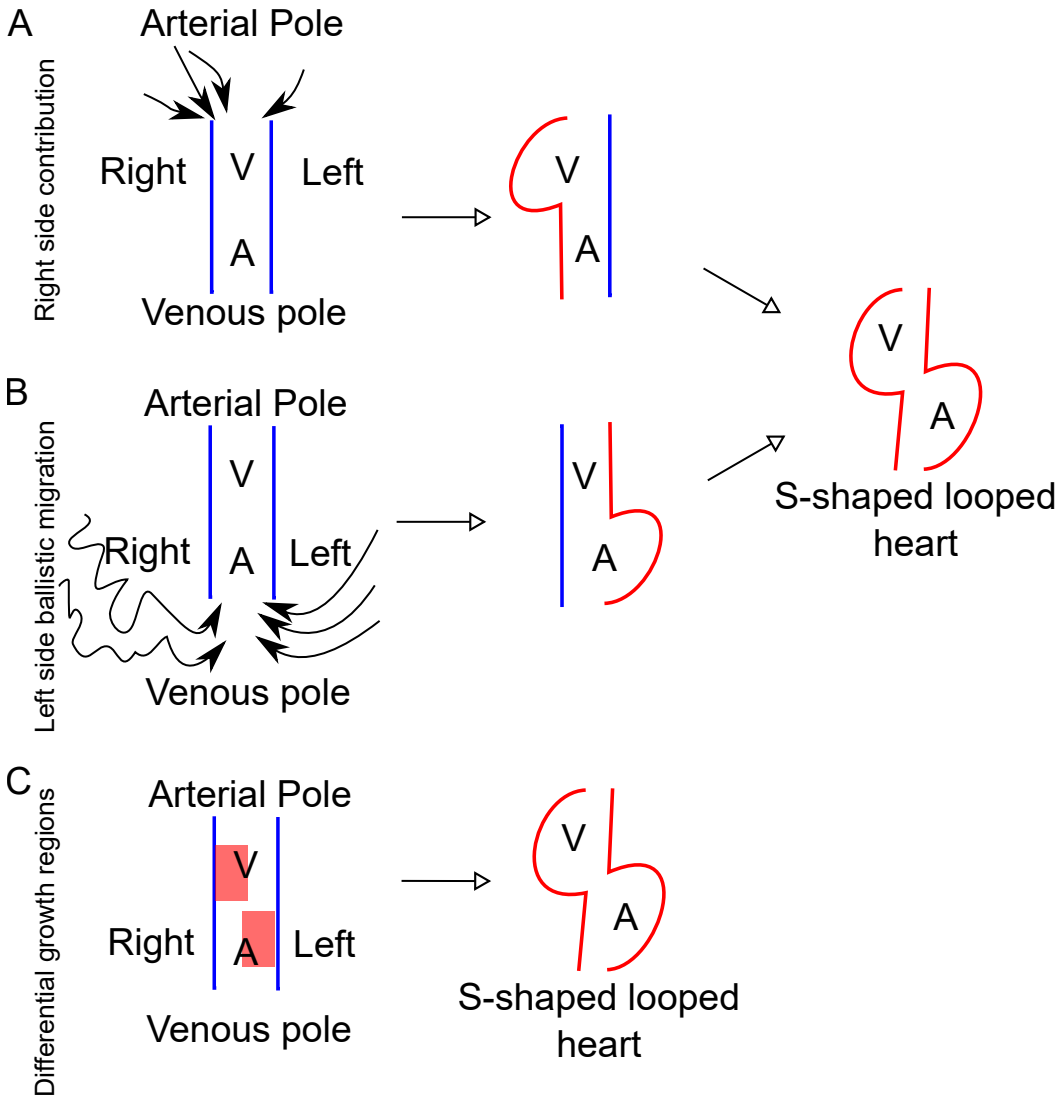

Figure 6.2: **Schematic of the mechanisms contributing to heart looping morphogenesis.** The linear heart tube (blue lines) can adopt a looped morphology by several means. A-B Mechanisms involving intrinsic changes caused by differential contributions to the heart tube. A- Greater contribution of right side cardiac precursors to the arterial pole can cause the ventricle to outgrow towards the right. B- Cardiac precursors migrating more ballistically (straight versus meandering lines) from the left to the venous pole can cause the atrium to outgrow towards the right. C- Mechanism of differential internal growth regions (red boxes) of the heart tube will cause the ventricle to outgrow towards the right and the atrium to outgrow to the left. A-atrium; V-ventricle.

ballistic migration of left cardiac precursors could cause greater cell recruitment on the left side of the venous pole, which could cause the atrium to shape leftwards (Fig. 6.2B straight arrows versus meandering arrows). Tbx5a-deficiency causes both the left and right cardiac

precursors to lose ballistic migration, which would limit the ability of precursors to be recruited into the heart, which may affect heart looping. I thereby propose that differential cell recruitment occurs at both poles of the heart to generate looping. At the arterial pole, *tbx5a* functions to add more cardiac precursors from the right ALPM than the left. At the venous pole, *tbx5a* functions to enable ballistic migration of cardiac precursors from the left ALPM.

Additionally, cardiac looping can be intrinsically generated by differential cell proliferation. Regions of cells within the heart tube may proliferate more than other regions, which would cause the outgrowth of that section of the tube. If the regions are positioned towards the middle of the heart tube on the left and right sides, then this proliferation would result in an S-shaped heart (Fig. 6.2C). de Pater et al. (2009) observe low proliferation within the zebrafish heart tube itself and instead, high proliferation was located at the poles of the heart or within cardiac precursors of the LPM [91]. However, I did not find left/right asymmetry in the proliferation of cardiac precursors in wildtype embryos. Therefore, it is unlikely that differential proliferation in zebrafish contributes to cardiac looping by intrinsic means.

Even though there is no evidence for differential proliferation causing cardiac looping by intrinsic means, proliferation of the heart in general can result in cardiac looping by extrinsic means. The growth induced buckling hypothesis posits that when the growing heart is constrained by the pericardial sac, the external force exhibited can cause the heart tube to loop. I find that the heart tube grows about two-fold in length between 30 and 54 hpf while the dorsoventral length of the pericardial sac only grows by 13%. This difference in growth is not present in the Tbx5a-deficiency, implicating that *tbx5a* functions in a growth induced buckling model of cardiac looping. The mechanism, however, of how *tbx5a* causes the pericardial sac to constrain the growing heart tube is still undetermined. I tested if the additional specification of pericardial fates in the Tbx5a-deficient fate map was responsi-

ble for more cells in the pericardial sac at 24 and 32 hpf. However, I was not able to make that correlation as Tbx5a-deficient embryos did not have statistically significantly more pericardial sac cells than wildtype embryos. Additional experiments need to be conducted to confirm this hypothesis and narrow down the functional tissue and time window that *tbx5a* acts in to affect laterality.

6.5 Future Directions

How does tbx5a *affect the progressive model of specification?*

Additional experiments need to be conducted to confirm the progressive model of specification that I propose. In which tissue and time window does *tbx5a* function to affect laterality? I first propose that *tbx5a* functions in all precursor types to regulate the pace of specification. To test this proposal and determine how long the possible time-delay of specification is in the Tbx5a-deficient fate map, I would first perform fate mapping of the Tbx5a-deficient lateral ALPM at various stages (22, 26, and 30 hpf). In particular, I would assay for the degree of multipotency in each of these fate maps. Firstly, if the degree of multipotency decreases over time, then the Tbx5a-deficient ALPM also undergoes progressive specification. Second, if the Tbx5a-deficient fate map a 22 hpf has a degree of multipotency that matches that of the wildtype fate map at 18 hpf (13%), for instance, then it would imply that the time delay would be four hours. Put another way, this result would imply that loss of *tbx5a* functions to delay fate restriction by four hours.

Is tbx5a *function in the left/right asymmetries cell autonomous?*

I propose that *tbx5a* has different function in the left versus right ALPM. More specifically, I propose that *tbx5a* is necessary on the left lateral ALPM to regulate proliferation of cardiac precursors. In cells of the right lateral ALPM, *tbx5a* functions to maintain increased

contribution to the larval heart. There is an alternative hypothesis which could also explain my results: *tbx5a* may function non-cell autonomously to affect left/right patterning and downstream functions that differ between the right and left sides.

To test these proposed functions of *tbx5a*, future investigators will need to downregulate *tbx5a* function in only one side of the ALPM. This may be experimentally achieved by using the dominant negative transgene of *tbx5a* under the heatshock promoter *Tg(hsp70:dntbx5a)f23* [101]. Expression of *Tg(hsp70:dntbx5a)f23* can be locally induced on just the left or right lateral ALPM by sublethal laser irradiation [191, 192]. If downregulation of Tbx5a on the right side recapitulates the reduced contribution of right ALPM to the larval heart (similar phenotype to global Tbx5a-deficiency), then I would determine that *tbx5a* functions to maintain the asymmetrical contribution in a cell autonomous manner. If instead the left/right differential contributions is similar to wildtype, then I would determine that *tbx5a* functions non-cell autonomously.

What function does tbx5b *have on the progressive specification of the lateral ALPM?*

As paralogs, *tbx5a* and *tbx5b* have overlapping but distinct functions (Boyle Anderson, manuscript in preparation) [193, 140]. Tbx5b-deficient embryos are defective in cardiac jogging, which suggests that *tbx5b* functions in earlier cardiac morphogenesis than *tbx5a* [193, 140]. In her doctoral dissertation, Erin Boyle Anderson calls for including *tbx5b* in studies of *tbx5a* in zebrafish since together the functions of these genes may sum to the function of the amniote *TBX5*. Therefore, I recommend that similar fate map and cell tracking analysis be done using Tbx5b-deficient and doubly-deficient embryos.

Discover intrinsic cellular changes that contribute to tbx5a-*driven morphogenesis*

In this dissertation, I propose that differential cellular contributions and migration can account for heart looping morphogenesis in zebrafish. *tbx5a* is involved in each of these left/right differential mechanisms. However, as a selector gene, *tbx5a* does not enact cellular changes directly. Instead, *tbx5a* must function to change the transcription of DNA that will enable downstream proteins to enact cellular changes in a left/right asymmetrical manner.

For example, Ocaña et al. 2017 found that Palladin, a component of microfilaments that is responsible for cell shape changes, is co-expressed with Tbx5a and Prrx1a in the cable of the ALPM only on the right side [83]. Furthermore, these transcripts are downregulated in Prrx1a-deficient embryos, in which looping laterality is affected [83]. I propose further investigation of the cytoskeletal dynamics of migrating cardiac precursors of the lateral ALPM in wildtype and Tbx5a-deficient embryos.

In a review by Naganathan (2016), actomyosin-driven cytoskeletal changes result in left-right asymmetry and chirality to generate molecular-scale torque. These changes always are cell-autonomous, intrinsic to individual cells that then propagate into an entire tissue to create shape changes [194]. I propose that similar cellular mechanisms are at play within the cardiac precursors of the ALPM that allow the cells to contribute in an asymmetric manner. Since I document that lateral ALPM cardiac precursors from the left side migrate more persistently than those from the right side (Fig. 3.4), I propose that the migratory cells exhibit different directionalities and orientations between the left and right sides. Visualization of the actin cytoskeleton dynamics can assess the orientation of cells along their migration paths.

To visualize the actin cytoskeletal dynamics in live cells, I generated a UAS:Lifeact-GFP transgenic zebrafish line using Tol2 transgenesis and a plasmid construct from the Herzog lab. This construct has been used in zebrafish to visualize the orientations of endothelial cells

in the common cardinal veins and it has shown that active migration can be seen through actin-rich lamellipodia at the migration front [195]. To specifically express the Lifeact-GFP in LPM cells, a Tbx5a-KalTA4 line will need to be generated using a CRISPR/Cas9-mediated knock-in strategy similar to the method in Appendix A. KalTA4 is a sequence variety of Gal4 that is less toxic to fish [196]. Then, comparisons can be made between cell orientation and protrusions during migration of the two fields of cells. A descriptive analysis of changing dynamics in the actin cytoskeleton during migration of the ALPM will suggest mechanisms of how these cells achieve these behaviors.

CHAPTER 7

MATERIALS AND METHODS

Zebrafish husbandry and strains

Zebrafish adults and embryos were raised and maintained in standard laboratory conditions [197] and approved by the University of Chicago Institutional Animal Care and Use Committee. *Et(hand2:eGFP)ch2* was generated by D.G. Ahn and is described by [33]. *Tg(h2afx:h2afv-mCherry)mw3* was a gift from B. Link [198]. *Tg(Nkx2.5::zsYellow)* was a gift from C.E. Burns [69]. Morpholino used against Tbx5a (5-CCTGTACGATGTCTACC-GTGAGGC-3) is as described in [41]. 1.2 ng per embryo was injected into the single-cell stage. Morphant phenotype was confirmed at 3-4 dpf in all experimental animals.

Single-cell photoconversion and fate mapping

Single marginal blastomere at the 64- or 128-cell stage were injected with 100 ng/μL Kaede mRNA. 18 hpf embryos were mounted on glass slides under bridged coverslips. A single lateral ALPM precursor at 18 hpf was photoconverted in each individual embryo for 30 s through a pinhole with 20x objective and light from a 100 W HBO mercury bulb through the DAPI filter on a Zeiss Axioplan microscope. Cell identity was assayed by live morphology and final position of the labeled cells over the described timecourse of these experiments. Lateral views were photographed using a Nikon D5000 camera immediately post-photoconversion and at 24 and 48 hpf. The positions of labeled precursors were measured in ImageJ.

Whole side and regional photoconversion

1-cell stage embryos were injected with 100ng/μL Kaede mRNA. 18 hpf embryos screened with uniform green fluorescence were embedded into 0.3% low-melting-point agarose (Sigma;

A9414) in E3 dorsal-side up. Using an upright Zeiss LSM 710 confocal microscope, a region of interest was drawn around the entire lateral ALPM tissue on either the right, left , or both side(s) in a Z-stack, avoiding as much of the medial ALPM as possible. The region of interest was scanned using the diode 405 nm laser at 5% through the 40x water-emersion objective to photoconvert Kaede into red-fluorescent. Since the same 2-dimensional region of interest was drawn based upon the entire extent of the lateral ALPM tissue, other ectodermal and endodermal tissue in these regions were also photoconverted. These unintended photoconversions did not contribute to the heart as they were neither mesodermal in origin nor location. Confocal stacks were acquired of ALPM-derived tissues after photoconverting the right, left, or both sides of the lateral ALPM at 48 hpf every 2 μm. Using FIJI, 3D stacks were reconstructed and cell counts were obtained by manually scoring red-fluorescent cardiomyocytes by morphology through both rotating the 3D reconstruction and progressing through the z-slices (Fig. 4.1). Double-counting of cells was avoided by only counting the first instance of a cardiomyocyte, which had an average depth of 10 μm through the z-slices. Cell counts were therefore corroborated by two different methods of analysis. Image stacks in which cell counts could not be corroborated between methods due to non-uniform Kaede distribution or movements of the heart through the z-stack were not considered in this analysis.

Time-lapse microscopy and cell migration dynamics

Live imaging was performed using *Et(hand2:eGFP)ch2* heterozygous embryos. Selective plane illumination microscopy (SPIM) was performed using multilayer embryo mounting as described in [173]. Dechorionated embryos were mounted in 0.3% low-melting-point agarose (Sigma; A9414) in E3 containing 200 mg/L tricaine into FEP tubing (Bola, S1815-04, refractive index 1.338, inner diameter 0.8 mm, outer diameter 1.6 mm). FEP tubing was plugged with 1.5% low-melting-point agarose in E3. FEP tubing was suspended into E3 media con-

taining 200 mg/L tricaine, maintained at 28.5°C in the Zeiss Lightsheet Z.1. z-stacks were collected every 8 min with 20x objectives.

Cell tracking was performed manually using the FIJI MTrackJ plugin backward in time. Ten cell tracks were chosen per organ type per laterality side for analysis in Excel. AP position (x), ML position (y), DV position (z) and time (t) were normalized by a reference track created by following the most postero-dorsal position of the heart cone/primary heart tube at the midline over time. The following metrics were calculated from the original four parameters: Instantaneous Speed, Average Speed, Instantaneous Displacement, Net Displacement, Total Length, Persistence, and Mean Squared Displacement. Additionally, DiPer computer program [172] was run on 2-dimensional tracks to calculate the α-value and directionality/persistence. Subsequent statistical analyses were performed in R.

Measurements of the pericardial sac

Images of wildtype and Tbx5a-deficient embryos were taken on Zeiss dissection microscope at lateral and anterior views. Measurements of dorsoventral and mediolateral lengths of the pericardial sac were taken by drawing straight lines across the tissue in ImageJ. Pericardial sac circumference and two-dimensional area measurements were taken by drawing freeform curves around the tissue in ImageJ. Heart tube length was measured by drawing a freeform curve along the midpoints along both chambers of the heart, which is visible via Nomarski optics, at an anterior view of the embryo in ImageJ. The mean measurement across three attempts was recorded. N=10 embryos per condition.

To count the pericardial sac cells, one-cell stage embryos were injected with either 100 ng/μL Kaede mRNA or Kaede mRNA plus Tbx5a morpholino so that all cells contained green fluorescent. 24 hpf embryos were screened for uniform green fluorescence and mounted anterior-side up in 0.3% low-melting point agarose. Using an upright Zeiss LSM 710 confocal microscope, 2 μm z-stack sections were taken in the 488 nm (green) channel. At 32 hpf, the

same embryos were remounted and z-stack confocal images were retaken using the same filter. Using FIJI, pericardial sac cells were counted carefully by progressing through the stack and marking flat elongated cells underneath the hatching gland and epithelium and above the heart. At the border of the venous pole, pericardial sac cells were only scored if they did not have myocardial morphology (columnar and large in volume).

CHAPTER 8

SUPPLEMENTARY MATERIALS

There are three .mp4 files associated with this dissertation.

Movie 1- *Et(Hand2:eGFP)ch2; Tg(h2afx:h2afv-mCherry)mw3* Lightsheet timelapse 18-34 hpf shows the migration of the aLPM into distinct organ fields.

Dorsal view, anterior to the left.

Movie 2- *Et(Hand2:eGFP)ch2; Tg(h2afx:h2afv-mCherry)mw3* Lightsheet timelapse 18-34 hpf shows the migration of the aLPM into distinct organ fields in the Tbx5a deficient condition.

Dorsal view, anterior to the left.

Movie 3- Cell tracks of Hand2-expressing aLPM, colored by their fate at 34hpf and laterality side of origin overlaid on WT *Et(Hand2:eGFP)ch2; Tg(h2afx:h2afv-mCherry)mw3* Lightsheet timelapse 18-34 hpf.

Red-reference point for drift correction; Green-cardiac precursors from the right; Yellow-cardiac precursors from the left; Orange-pericardial sac precursors from the right; Magenta-pericardial sac precursors from the left; Blue-pharyngeal arch precursors from the right; Cyan-pharyngeal arch precursors from the left. Dorsal view, anterior to the left.

APPENDIX A

KNOCK-IN STRATEGY IN MAKING *IS(TBX5A-E2A-KAEDE)* USING CRISPR-CAS9

Rationale

At the time of starting my dissertation research, there was no transgenic zebrafish reporter line for *tbx5a* expression. Therefore, I sought to make a *tbx5a* reporter line. Furthermore, since I was interested in the effect of *tbx5a* on the development and fates of the ALPM, creating a knock-in Tbx5a-Kaede line could meet my aims. I intended to use this line to photoconvert Tbx5a-expressing cells that lie within the lateral ALPM.

CRISPR-Cas9 technology was gaining traction at the time I began my dissertation research. Specific targeting of genomic regions with precision could create knock-out mutants in zebrafish for the first time. However, the usage of CRISPR-Cas9 for knock-ins was barred by unknown requirements for homologous recombination in zebrafish and apparent locus-specific effects (CRISPR-Cas9 knock-in was more effective at some genes than others, even using the same methods). There was great debate over whether homology arms should be added to exogenous DNA to mediate homologous recombination over non-homologous end joining mechanisms. Furthermore, how large should those homology arms be to achieve the best yield?

My attempts and approaches in creating a knock-in of Kaede into the *tbx5a* locus were based upon a new report at the time. Li et al. (2015) reported that targeting intronic sequences through non-homologous recombination resulted in maintenance of endogeneous gene integrity [199]. However, the design of the donor plasmid still contained flanking arm sequences of 670 to 1300 bp [199]. Since I was interested in the precise integration at Kaede, I chose to use conserved exonic and UTR sequences as homology arms while also targeting the intron with my sgRNA (Fig. A.1A, targeted grey arrows). I also chose to target the

N-terminus of the coding sequence to not interfere with the T-box DNA-binding motif at the C-terminus. However, this might have led to my construct being spliced out.

Results

Method for intronic targeting

I ordered a gBlock from IDT with the following sequence: 219 bp derived from amplifying part of exon 9 and the end of exon 10 of tbx5a, with an omitted STOP codon at the end; 66 bp E2A flexible cleavable linker with double glycine at the end; 681 bp Kaede coding sequence; 41 bp 3'UTR of the tbx5a gene (Fig. A.1B). The left homology arm also contains sequence specificity for two of the three sgRNAs tested (Fig. grey arrows). After cloning the gBlock into a plasmid vector, I injected single-cell embryos with 345 ng xenopus Cas9 mRNA; 50 ng sgRNA 2, targeted to exon 10; and 300 ng donor plasmid. I found that 37% of injected embryos survived until 24 hpf, 46% of those survived did not have major developmental defects, and 65% of those had positive green fluorescence in the LPM (Fig. A.1C, F0 embryos).

Validation of the Is(tbx5a-E2A-Kaede) *insertion event and fluorescent expression*

PCR amplification on the inserted DNA sequence yielded positive results in 6 out of 11 non-fluorescent embryos analyzed. However, the T7E1 assay, which will cut the DNA at mismatched sites, did not display any cutting. I figured that were a couple of explanations for these observations. Perhaps there was retention of the non-integrated donor plasmid in the cells, so PCR amplification was yielding a false-positive results. Or the T7E1 assay was not reliable in finding precise integration events. Uncertain of the explanation, I screened out the 7 embryos with positive green fluorescence in the LPM and grew them to adulthood (Fig.

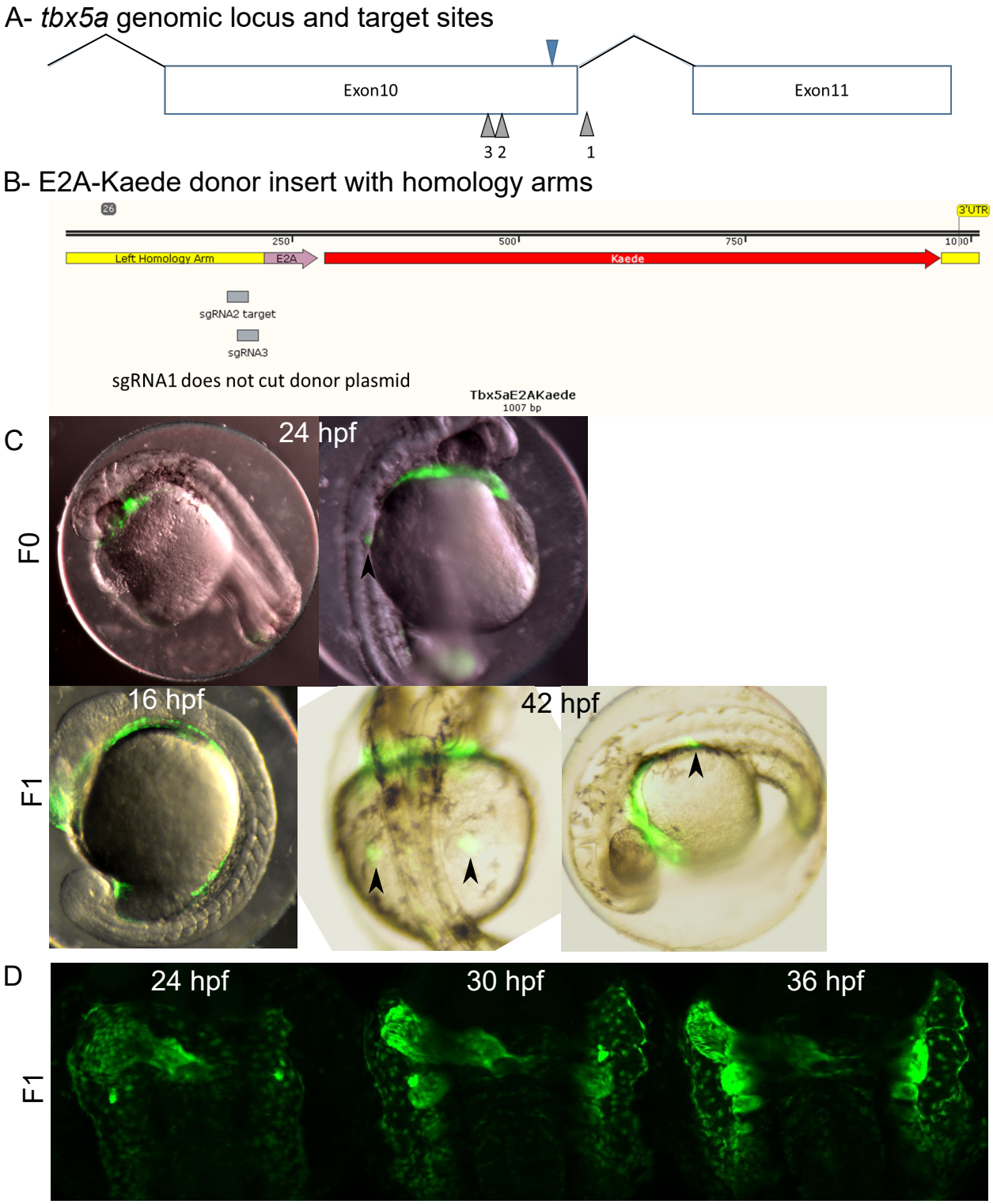

Figure A.1: **Creation of a tbx5a reporter line using CRISPR-Cas9 knock-in.** (Cont. on next page)

Figure A.1: (Continued) A- Schematic of genomic tbx5a locus at the N-terminal region. Blue arrow denotes STOP codon of the most common Tbx5a splice form. Grey arrows are three sgRNAs targeting Cas9-mediated cutting. B- Schematic of gBlock ordered from IDT to generate donor insert DNA with homology arms (yellow). Grey blocks are the sgRNA sequences (20 bp each) that will also direct cutting of the donor plasmid. C- F0 injected embryos had green fluorescence in the ALPM-derived regions. The second image also shows green fluorescence in the pectoral fin bud (black arrow head). F1 outcrossed embryos express green fluorescent in tbx5a-expressing regions. Arrowheads- pectoral fin buds. D- Lightsheet dorsal view timelapse maximum intensity projections of an F1 embryo.

A.1C, F0 embryos). I was unable to amplify and genotype the *Is(tbx5a-E2A-Kaede)* embryos, and so my nomenclature of this construct has not been definitively proven. Outcrossing Is(tbx5a-E2A-Kaede) embryos resulted in F1 embryos that expressed green fluorescence in known Tbx5a-expression domains: the developing eye at 16 hpf; pectoral fin buds; and the heart (Fig. A.1C). Under closer examination, *Is(tbx5a-E2A-Kaede)* embryos express green fluorescence similarly to Hand2-expression (Fig. 3.3.1A, A.1D). I conducted a long timelapse on the Lightsheet from 24 to 36 hpf and saw green fluorescence in the cable, heart tube, developing pharyngeal arches, eventual pericardial sac, and bilateral bright spots. However, these green fluorescent domains were not photoconvertable to red fluorescence upon exposure to UV light.

Conclusions

Since I did not validate the genetic mutation caused by CRISPR/Cas9 manipulation, discussion of the implications of the green fluorescence I observe on the endogenous expression patterns of Tbx5a is not warranted. However, since the creation of this line, Ocaña et al. (2017) published a Tg(tbx5a-eGFP) line generated from a bacteria artificial chromosome that appears similar to that which I observe [83]. Specifically, they make formal observations about Tbx5a-eGFP expression in the cable, pericardial sac, and pharyngeal arches [83]. However, they do not explicitly mention the bilateral bright spots, though I observe them in their images [83].

There are several possibilities that can explain why the green fluorescence was not photoconvertable. Since there are multiple splice forms of tbx5a, inclusion of the Kaede coding sequence could have interfered with proper Tbx5a-E2A-Kaede splicing, thereby truncating the Kaede protein, limiting its function. Alternatively, perhaps the entire Kaede coding sequence was not integrated by recombination. Successful genotyping of the inserted construct is necessary.

Tips for improvement of knock-in strategy

Today, further innovations and refinement of the CRISPR-Cas9 knock-in strategy in zebrafish would compel me to make slight variations of my approach were I to do it again in the future. Firstly, the sequence of the targeted intron must be invariable and known. Individual polymorphisms between individual parent fish might limit the ability for a sgRNA to bind specifically within the intron. Therefore, backcrossing daughters to fathers and injecting into the offspring will limit the amount of variance in the genome. Second, insertion of a heat-shock promoter hsp70 before the reporter coding sequence has been shown to increase the efficiency of fluorescent construct expression [200]. Additional strategies are discussed in a review by Albadri et al. (2017) [201].

APPENDIX B

CHIP-SEQ ALIGNMENT OF TBX5 TARGETS

Preface

The work in this section comes from preliminary data that I collected for a grant proposal titled, Exploring the function of Fgf24 in zebrafish limb bud initiation. All of the analysis done is my own, however I used publicly available ascension data from a bioChIP-seq experiment in mouse cardiac muscle cells by He et al. (2011) [150].

Rationale

I sought to provide evidence for a feed-forward mechanism of FGF regulation in pectoral fin initiation. Both knockdown of Fgf24 and inhibition of Fgf receptors with pharmacological inhibitors SU5402 and Ponatinib phenocopy the loss of cell convergence phenotype [56]. I treated somitogenesis-stage zebrafish embryos with SU5402 and Ponatinib also causes the down-regulation of Tbx5a expression (Fig. B.1), which suggests that Fgf signaling feedback might be required for maintenance of Tbx5a expression. I hypothesize that Fgf24 is necessary for the maintenance of Tbx5 and therefore limb field identity by participating in a feed forward mechanism. Further support for this hypothesis can be found in the results of a bioinformatic experiment that I conducted.

Results

I used the raw reads from biotinylated-ChIP-seq experiment of TBX5 binding regions in HL1 mouse cardiomyocyte line (GSM558908) [150]. After re-aligning the reads to the mouse (mm9) genome, I used Model-based Analysis of ChIP-Seq (MACS) analysis to identify peaks. He et al. (2011) used Sole-Search algorithm, but MACS uses a dynamic Poisson distribution

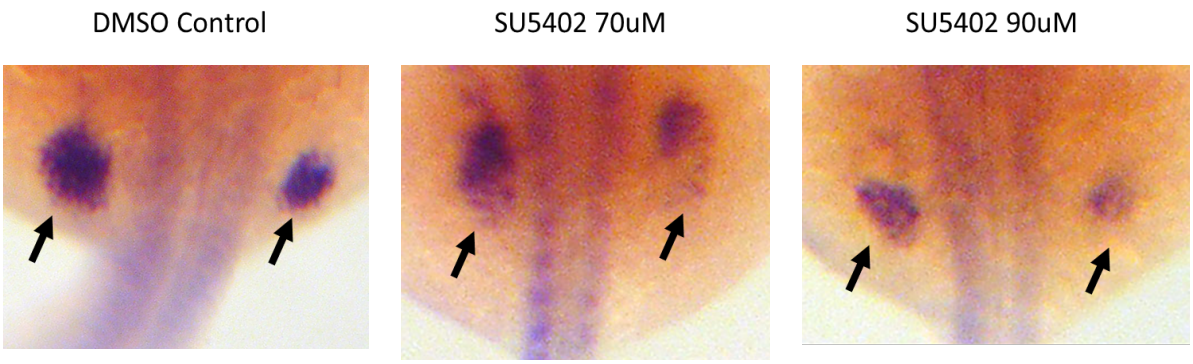

Figure B.1: **In situ hybridization of Tbx5a under FGF-signaling inhibition.** Arrows point to the limb field. Zebrafish embryos fixed at 24 hours post fertilization treated with Fgfr inhibitor SU5402 or a DMSO control. Anterior is up, dorsal view.

to capture local biases that may be within the genome, making MACS a stronger method [150, 202].

I found 47,998 peaks that had a fold-enrichment larger than 2.0. I identified genes involved in cell migration or cell signaling by Gene Ontology (GO) analysis. A short list of candidate target genes of TBX5 involved in cell migration and cell signaling is shown in Table B.1. The high enrichment values suggests that these genes are up-regulated by TBX5. Furthermore, aligned reads appear to overlap with mostly exonic regions of the genome (Fig. B.2).These candidates still need to be validated by expression in zebrafish within the LPM and then through a similar bio-ChIP-seq pulldown of biotinylated Tbx5a, which has not been done in the field.

Cell Migration Genes			Cell Signaling Genes		
Name	P-value	Fold-enriched	Name	P-value	Fold-enriched
TJP2	5 e-57	8.3	FGFR2	4 e-23	8.88
CHCHD2	4 e-12	19.11	FGFR3	1.2 e-22	11.29
ROCK1	5.6 e-21	12.93	WNT2B	2.2 e-6	18.27

Table B.1: **Candidate down-stream target genes of TBX5 protein in HL1 cells.** MACS analysis on bio-ChIP-seq data aligned to mouse genome. A sample of candidates are shown that are related to cell migration and cell signaling.

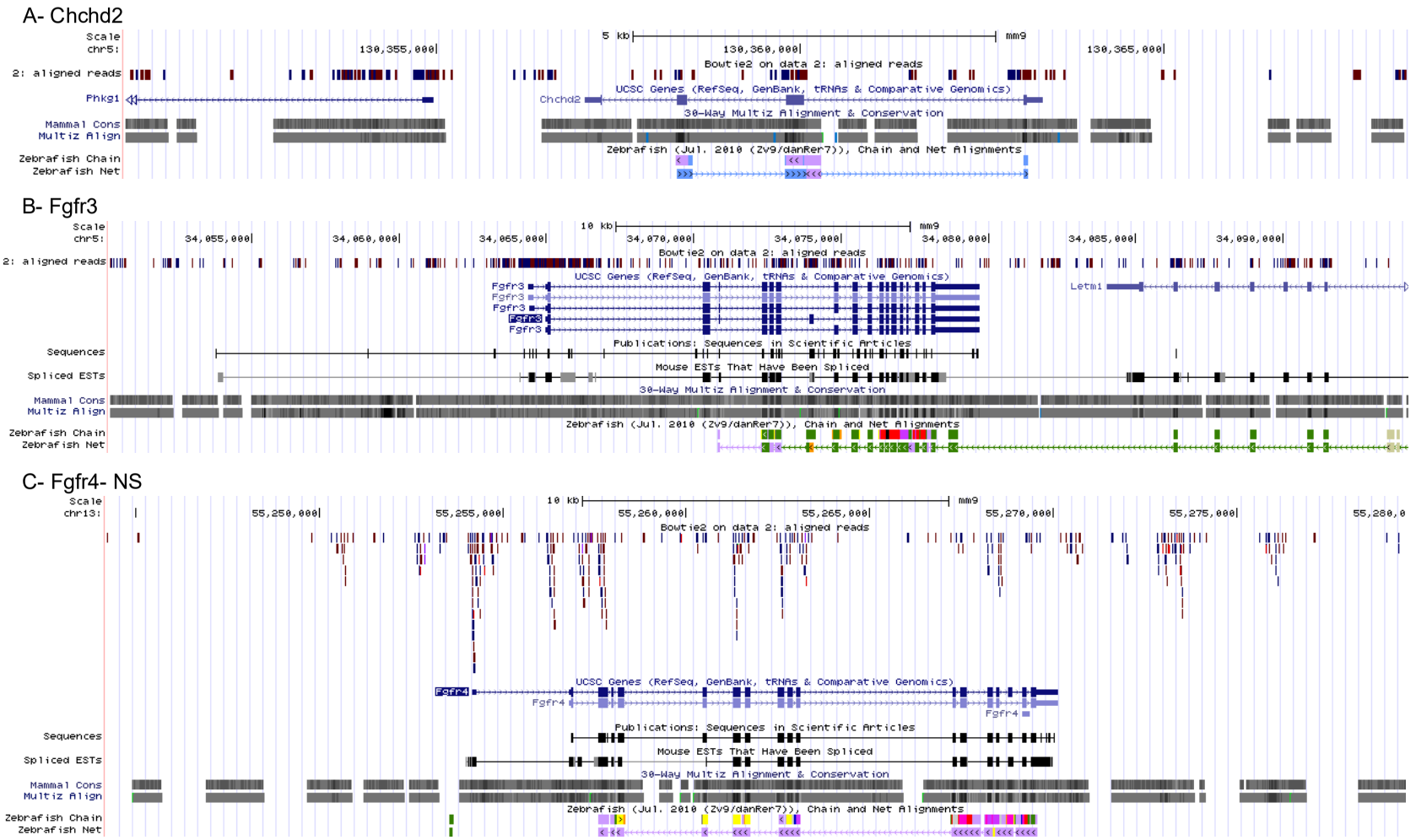

Figure B.2: **Aligned bio-ChIP-seq reads mostly lie within exonic regions of the mouse and zebrafish genomes.** Using the UCSC Genome Browser on the Mouse July 2007 (NCBI37/mm9) assembly. The aligned reads from MACS analysis with conserved regions (Mammal Cons, Multiz Align), possible splice sites (Spliced ESTs), and zebrafish Zv9. A-Chchd2 is a candidate gene for cell migration; B- Fgfr3 is a candidate gene for cell signaling; C-Fgfr4 is not significantly aligned with the exonic regions.

Conclusions

From my preliminary data, I hypothesize that downstream Fgf ligand signals back to Tbx5-expressing cells to result in up-regulation or maintenance of Tbx5a expression. These data still need to be validated to provide definitive support for a feed forward mechanism in zebrafish. In particular, support for functional dependency of Tbx5a maintenance on Fgf must be obtained. To establish that Tbx5a is being regulated by a feed forward mechanism, I would inject embryos with varying amounts of MO against Fgf24 to achieve partial knockdown. I would then assay for the expression of Tbx5a quantitatively by qRT-PCR and spatially by *in situ* hybridization. I expect to see an exponential decrease in the expression of Tbx5a with increasing doses of MO if Fgf24 participates in a feed forward mechanism.

Since the bio-ChIP-seq done by He et al. (2011) was done in cardiomyocytes, candidate genes found in this analysis have implications for *TBX5* function in cell migration and cell signaling in the heart. For further investigation, these downstream candidate target genes of TBX5 binding must be validated in developing embryos. A similar ChIP-seq analysis on 4-week old mouse hearts validates candidates by co-IP in E9.5 embryonic hearts [156].

References

[1] Arpiar Saunders, Evan Z. Macosko, Alec Wysoker, Melissa Goldman, Fenna M. Krienen, Heather de Rivera, Elizabeth Bien, Matthew Baum, Laura Bortolin, Shuyu Wang, Aleksandrina Goeva, James Nemesh, Nolan Kamitaki, Sara Brumbaugh, David Kulp, and Steven A. McCarroll. Molecular Diversity and Specializations among the Cells of the Adult Mouse Brain. *Cell*, 174(4):1015–1030.e16, 2018.

[2] Evan Z. Macosko, Anindita Basu, Rahul Satija, James Nemesh, Karthik Shekhar, Melissa Goldman, Itay Tirosh, Allison R. Bialas, Nolan Kamitaki, Emily M. Martersteck, John J. Trombetta, David A. Weitz, Joshua R. Sanes, Alex K. Shalek, Aviv Regev, and Steven A. McCarroll. Highly Parallel Genome-wide Expression Profiling of Individual Cells Using Nanoliter Droplets. *Cell*, 161(5):1202–1214, 2015.

[3] Fengzhu Xiong, Andrea R Tentner, Peng Huang, Arnaud Gelas, R Kishore, Lydie Souhait, Nicolas Rannou, Ian A Swinburne, Nikolaus D Obholzer, Paul D Cowgill, Alexander F Schier, and Sean G Megason. Specified Neural Progenitors Sort to Form Sharp Domains After Noise Shh Signaling. *Cell*, 153(3):550–561, 2013.

[4] Sung-hwan Moon, Jung Mo Kim, Ki-sung Hong, Jeong Min Shin, Jumi Kim, and Hyung-min Chung. Differentiation of hESCs into Mesodermal Subtypes : Vascular- , Hematopoietic- and Mesenchymal-lineage Cells. *International Journal of Stem Cells*, 4(1):24–34, 2011.

[5] Xuejun H. Parsons. Constraining the Pluripotent Fate of Human Embryonic Stem Cells for Tissue Engineering and Cell Therapy The Turning Point of Cell-Based Regenerative Medicine Xuejun. *Br Biotechnology Journal*, 3(4):424–457, 2013.

[6] D. Evseenko, Y. Zhu, K. Schenke-Layland, J. Kuo, B. Latour, S. Ge, J. Scholes, G. Dravid, X. Li, W. R. MacLellan, and G. M. Crooks. Mapping the first stages of mesoderm commitment during differentiation of human embryonic stem cells. *Proceedings of the National Academy of Sciences*, 107(31):13742–13747, 2010.

[7] Daniel A Fletcher and R Dyche Mullins. Cell mechanics and the cytoskeleton Daniel. *Nature*, 463(7280):485–492, 2010.

[8] Ewa Paluch and Carl Philipp Heisenberg. Biology and Physics of Cell Shape Changes in Development. *Current Biology*, 19(17):R790–R799, 2009.

[9] M. Albert Basson. Signaling in cell differentiation and morphogenesis. *Cold Spring Harbor perspectives in biology*, 4(6):1–22, 2012.

[10] Douglas R Green and Fabien Llambi. Cell Death Signaling. *Cold Spring Harbor perspectives in biology*, 7:a006080, 2015.

[11] Elena Scarpa and Roberto Mayor. Collective cell migration in development. *Journal of Cell Biology*, 212(2):143–155, 2016.

[12] Jan Hendrick Van Weerd, Kazuko Koshiba-Takeuchi, Chulan Kwon, and Jun K. Takeuchi. Epigenetic factors and cardiac development. *Cardiovascular Research*, 91(2):203–211, 2011.

[13] Rush Elliott. *A Contribution to the Development of the Pericardium*. PhD thesis, University of Michigan, 1931.

[14] C. B. Lockwood. XIII. The Early Development of the Pericardium, Diaphragm, and Great Veins. In *Philosophical Transactions of the Royal Society of London*, volume 179, pages 365–384. 1888.

[15] Eunmyong Lee, Yeon Koo, Aylwin Ng, Yongjie Wei, Kate Luby-Phelps, Amy Juraszek, Ramnik J. Xavier, Ondine Cleaver, Beth Levine, and James F. Amatruda. Autophagy is essential for cardiac morphogenesis during vertebrate development. *Autophagy*, 2014.

[16] Takashi Yoshino, Hidetaka Murai, and Daisuke Saito. Hedgehog-BMP signalling establishes dorsoventral patterning in lateral plate mesoderm to trigger gonadogenesis in chicken embryos. *Nature Communications*, 7:1–11, 2016.

[17] Laurel A. Rohde, Andrew C. Oates, and Robert K. Ho. A crucial interaction between embryonic red blood cell progenitors and paraxial mesoderm revealed in spadetail embryos. *Developmental Cell*, 7(2):251–262, 2004.

[18] Laura Ariza, Rita Carmona, Ana Cañete, Elena Cano, and Ramón Muñoz-Chápuli. Coelomic epithelium-derived cells in visceral morphogenesis. *Developmental Dynamics*, 245(3):307–322, 2016.

[19] Kinji Asahina, Bin Zhou, William T Pu, and Hidekazu Tsukamoto. Septum Transversum-Derived Mesothelium Gives Rise to Hepatic Stellate Cells and Perivascular Mesenchymal Cells in Developing Mouse LIver. *Hepatology*, 53(3):983–995, 2011.

[20] F Shalaby, J Ho, Stanford WL, Fischer KD, Schuh AC, L Schwartz, A Bernstein, and J Rossant. A requirement for Flk1 in primitive and definitive hematopoiesis and. *Cell*, 89:981–990, 1997.

[21] Brant M Weinstein, Alexander F Schier, S Abdelilah, Jarema Malicki, Lilianna Solnica-Krezel, Derek L Stemple, Didier Y R Stainier, F Zwartkruis, W Driever, and M Fishman. Hematopoietic mutations in the zebrafish. *Development (Cambridge, England)*, 123:303–309, 1996.

[22] Jeannie Karl and Blanche Capel. Sertoli Cells of the Mouse Testis Originate from the Coelomic Epithelium. *Developmental Biology*, 203:323–333, 1998.

[23] Anthony Graham and Alexa Smith. Patterning the pharyngeal arches. *BioEssays*, 23(1):54–61, 2001.

[24] Robert G Kelly, Nigel A Brown, Margaret E Buckingham, and United Kingdom. The Arterial Pole of the Mouse Heart Forms from. *DNA Sequence*, 1:435–440, 2001.

[25] D Y Stainier, R K Lee, and M C Fishman. Cardiovascular development in the zebrafish. I. Myocardial fate map and heart tube formation. *Development (Cambridge, England)*, 119(1):31–40, 1993.

[26] T. Mikawa, A. Borisov, A. M.C. Brown, and D. A. Fischman. Clonal analysis of cardiac morphogenesis in the chicken embryo using a replicationdefective retrovirus: I. Formation of the ventricular myocardium. *Developmental Dynamics*, 193(1):11–23, 1992.

[27] E. Cano, R. Carmona, and R. Munoz-Chapuli. Wt1-expressing progenitors contribute to multiple tissues in the developing lung. *AJP: Lung Cellular and Molecular Physiology*, 305(4):L322–L332, 2013.

[28] A. Ijpenberg, J. M. Pérez-Pomares, J. A. Guadix, R. Carmona, V. Portillo-Sánchez, D. Macías, P. Hohenstein, C. M. Miles, N. D. Hastie, and R. Muñoz-Chápuli. Wt1 and retinoic acid signaling are essential for stellate cell development and liver morphogenesis. *Developmental Biology*, 312(1):157–170, 2007.

[29] J. Que, B. Wilm, H. Hasegawa, F. Wang, D. Bader, and B. L. M. Hogan. Mesothelium contributes to vascular smooth muscle and mesenchyme during lung development. *Proceedings of the National Academy of Sciences*, 105(43):16626–16630, 2008.

[30] Rita Carmona, Elena Cano, Andrea Mattiotti, Joaquín Gaztambide, and Ramón Muñoz-Chápuli. Cells Derived from the Coelomic Epithelium Contribute to Multiple Gastrointestinal Tissues in Mouse Embryos. *PLoS ONE*, 8(2), 2013.

[31] Bettina Wilm, Annemieke Ipenberg, Nicholas D. Hastie, John B. E. Burch, and David M Bader. The serosal mesothelium is a major source of smooth muscle cells of the gut vasculature. *Development*, 132(23):5317–5328, 2005.

[32] J. R. Hinchliffe and D. R Johnson. *The Development of the Vertebrate Limb: an Approach Through Experiment, Genetics, and Evolution*. Clarendon Press, Oxford, 1980.

[33] Q. Mao, H. K. Stinnett, and R. K. Ho. Asymmetric cell convergence-driven zebrafish fin bud initiation and pre-pattern requires Tbx5a control of a mesenchymal Fgf signal. *Development*, 142(24):4329–4339, 2015.

[34] D Yelon, B Ticho, M E Halpern, I Ruvinsky, R K Ho, L M Silver, and D Y Stainier. The bHLH transcription factor hand2 plays parallel roles in zebrafish heart and pectoral fin development. *Development (Cambridge, England)*, 127(12):2573–82, 2000.

[35] Arne C. Lekven, Christopher J. Thorpe, Joshua S. Waxman, and Randall T. Moon. Zebrafish wnt8 Encodes Two Wnt8 Proteins on a Bicistronic Transcript and Is Required for Mesoderm and Neurectoderm Patterning. *Developmental Cell*, 1(1):103–114, 2001.

[36] Akane Tonegawa, Noriko Funayama, Naoto Ueno, and Yoshiko Takahashi. Mesodermal subdivision along the mediolateral axis in chicken controlled by different concentrations of BMP-4. *Development*, 124:1975–1984, 1997.

[37] N Funayama, Y Sato, K Matsumoto, T Ogura, and Y Takahashi. Coelom formation: binary decision of the lateral plate mesoderm is controlled by the ectoderm. *Development (Cambridge, England)*, 126(18):4129–38, 1999.

[38] B. Guner-Ataman, N. Paffett-Lugassy, M. S. Adams, K. R. Nevis, L. Jahangiri, P. Obregon, K. Kikuchi, K. D. Poss, C. E. Burns, and C. G. Burns. Zebrafish second heart field development relies on progenitor specification in anterior lateral plate mesoderm and nkx2.5 function. *Development*, 140(6):1353–1363, 2013.

[39] Koh Onimaru, Eiichi Shoguchi, Shigeru Kuratani, and Mikiko Tanaka. Development and evolution of the lateral plate mesoderm: Comparative analysis of amphioxus and lamprey with implications for the acquisition of paired fins. *Developmental Biology*, 359(1):124–136, 2011.

[40] Nicholas J. Cole, Thomas E. Hall, Emily K. Don, Silke Berger, Catherine A. Boisvert, Christine Neyt, Rolf Ericsson, Jean Joss, David B. Gurevich, and Peter D. Currie. Development and evolution of the muscles of the pelvic fin. *PLoS Biology*, 9(10):16–18, 2011.

[41] Dae Gwon Ahn, Matthew J. Kourakis, Laurel A. Rohde, Lee M. Slivert, and Robert K. Ho. T-box gene Tbx5 is essential for formation of the pectoral limb bud. *Nature*, 417(6890):754–758, 2002.

[42] Y. Gibert, Alexandra Gajewski, Axel Meyer, and Gerrit Begemann. Induction and prepatterning of the zebrafish pectoral fin bud requires axial retinoic acid signaling. *Development*, 133(14):2649–2659, 2006.

[43] Jennifer K Ng, Yasuhiko Kawakami, Dirk Büscher, Angel Raya, Tohru Itoh, Christopher M Koth, Concepción Rodríguez Esteban, Joaquín Rodríguez-León, Deborah M Garrity, Mark C Fishman, and Juan Carlos Izpisúa Belmonte. The limb identity gene Tbx5 promotes limb initiation by interacting with Wnt2b and Fgf10. *Development (Cambridge, England)*, 129(22):5161–70, 2002.

[44] Takashi Wakahara, Naoki Kusu, Hajime Yamauchi, Ikuo Kimura, Morichika Konishi, Ayumi Miyake, and Nobuyuki Itoh. Fibin, a Novel Secreted Lateral Plate Mesoderm Signal, Is Essential for Pectoral Fin Bud Initiation in Zebrafish. *Developmental Biology*, 303(2):527–535, 2007.

[45] Dae-gwon Ahn, Ilya Ruvinsky, Andrew C Oates, Lee M Silver, and Robert K Ho. tbx20 , a new vertebrate T-box gene expressed in the cranial motor neurons and developing cardiovascular structures in zebra ® sh. 95:253–258, 2000.

[46] Ilya Ruvinsky, Andrew C. Oates, Lee M. Silver, and Robert K. Ho. The evolution of paired appendages in vertebrates: T-box genes in the zebrafish. *Development Genes and Evolution*, 210(2):82–91, 2000.

[47] Ryohei Nomura, Eriko Kamei, Yuuhei Hotta, Morichika Konishi, Ayumi Miyake, and Nobuyuki Itoh. Fgf16 is essential for pectoral fin bud formation in zebrafish. *Biochemical and Biophysical Research Communications*, 347(1):340–346, 2006.

[48] H Ohuchi, Jun K Takeuchi, H Yoshioka, Y Ishimaru, K Ogura, N Takahashi, T Ogura, and S Noji. Correlation of wing-leg identity in ectopic FGF-induced chimeric limbs with the differential expression of chick Tbx5 and Tbx4. *Development (Cambridge, England)*, 125(1):51–60, 1998.

[49] J. K. Takeuchi, Koshiba-Takeuchi Kazuko, Takayuki Suzuki, Mika Kamimura, Keiko Ogura, and Toshihiko Ogura. Tbx5 and Tbx4 trigger limb initiation through activation of the Wnt/Fgf signaling cascade. *Development*, 130(12):2729–2739, 2003.

[50] S. Fischer, Bruce W. Draper, and Carl J. Neumann. The zebrafish fgf24 mutant identifies an additional level of Fgf signaling involved in vertebrate forelimb initiation. *Development*, 130(15):3515–3524, 2003.

[51] K N Michailova and K G Usunoff. *Normal Structures of serosal membranes*, volume 183. 2006.

[52] Shin-Yi Chen, Hung-Yu Shih, Sheng-Jia Lin, Chung-Der Hsiao, Zih-Cing Li, and Yi-Chuan Cheng. Etv5a regulates the proliferation of ventral mesoderm cells and the formation of hemato-vascular derivatives. *Journal of Cell Science*, 126(24):5626–5634, 2013.

[53] Virginie Lecaudey, Isabelle Anselme, Renate Dildrop, Ulrich Rüther, and Sylvie Schneider-Maunoury. Expression of the zebrafish Iroquois genes during early nervous system formation and patterning. *Journal of Comparative Neurology*, 492(3):289–302, 2005.

[54] Rebecca A. Wingert and Alan J. Davidson. Zebrafish nephrogenesis involves dynamic spatiotemporal expression changes in renal progenitors and essential signals from retinoic acid and irx3b. *Developmental Dynamics*, 240(8):2011–2027, 2011.

[55] Oscar H. Ocaña, Rebeca Córcoles, Ángels Fabra, Gema Moreno-Bueno, Hervé Acloque, Sonia Vega, Alejandro Barrallo-Gimeno, Amparo Cano, and M. Angela Nieto. Metastatic Colonization Requires the Repression of the Epithelial-Mesenchymal Transition Inducer Prrx1. *Cancer Cell*, 22(6):709–724, 2012.

[56] Q. Mao. *Spatial Dynamics and Regulation of the Zebrafish Limb Morphogenetic Field*. PhD thesis, University of Chicago, 2013.

[57] Jennifer M. Iklé, Andre L.P. Tavares, Marisol King, Hailei Ding, Sophie Colombo, Beth A. Firulli, Anthony B. Firulli, Kimara L. Targoff, Deborah Yelon, and David E. Clouthier. Nkx2.5 regulates endothelin converting enzyme-1 during pharyngeal arch patterning. *Genesis*, 55(3):1–16, 2017.

[58] C B Kimmel, Craig T. Miller, and Cecelia B. Moens. Zebrafish: An in vivo model for the study of neurological diseases. *Developmental Biology*, 233:239–257, 2001.

[59] C. Alexander, E. Zuniga, I. L. Blitz, N. Wada, P. Le Pabic, Y. Javidan, T. Zhang, K. W. Cho, J. G. Crump, and T. F. Schilling. Combinatorial roles for BMPs and Endothelin 1 in patterning the dorsal-ventral axis of the craniofacial skeleton. *Development*, 138(23):5135–5146, 2011.

[60] C B Kimmel, W W Ballard, S R Kimmel, B Ullmann, and T F Schilling. Stages of embryonic development of the zebrafish. *Developmental dynamics : an official public*, 203(3):253–310, 1995.

[61] Thomas F. Schilling, Jean Paul Concordet, and Philip W. Ingham. Regulation of left-right asymmetries in the zebrafish by Shh and BMP4. *Developmental Biology*, 210(2):277–287, 1999.

[62] Florian Razy-Krajka, Basile Gravez, Nicole Kaplan, Claudia Racioppi, Wei Wang, and Lionel Christiaen. An FGF-driven feed-forward circuit patterns the cardiopharyngeal mesoderm in space and time. *eLife*, 7:1–27, 2018.

[63] Hagen R. Witzel, Sirisha Cheedipudi, Rui Gao, Didier Y R Stainier, and Gergana D. Dobreva. Isl2b regulates anterior second heart field development in zebrafish. *Scientific Reports*, 7:1–9, 2017.

[64] Karim Mesbah, M. Sameer Rana, Alexandre Francou, Karel Van duijvenboden, Virginia E. Papaioannou, Antoon F. Moorman, Robert G. Kelly, and Vincent M. Christoffels. Identification of a Tbx1/Tbx2/Tbx3 genetic pathway governing pharyngeal and arterial pole morphogenesis. *Human Molecular Genetics*, 21(6):1217–1229, 2012.

[65] Rui Diogo, Robert G. Kelly, Lionel Christiaen, Michael Levine, Janine M. Ziermann, Julia L. Molnar, Drew M. Noden, and Eldad Tzahor. A new heart for a new head in vertebrate cardiopharyngeal evolution. *Nature*, 520(7548):466–473, 2015.

[66] Anastasia Felker, Karin D. Prummel, Anne M. Merks, Michaela Mickoleit, Eline C. Brombacher, Jan Huisken, Daniela Panáková, and Christian Mosimann. Continuous addition of progenitors forms the cardiac ventricle in zebrafish. *Nature Communications*, 9(1):1–14, 2018.

[67] Maria V D E L A Cruz, Concepcin Sanchez Gmez, M Manuel Arteaga, and Carlos Arguello. Experimental study of the development of the truncus and the conus in the chick embryo. *J. Anat.*, 123(3):661–686, 1977.

[68] Chen-Leng Cai, Xingqun Lian, Yunqing Shi, Po-Hsien Chu, Samuel L. Pfaff, Ju Chen, and Sylvia Evans. Isl1 Identifies a Cardiac Progenitor Population that Proliferates Prior to Differentiation and Contributes a Majority of Cells to the Heart. *Developmental Cell*, 5(6):877–889, 2003.

[69] Yong Zhou, Timothy J. Cashman, Kathleen R. Nevis, Pablo Obregon, Sara A. Carney, Yan Liu, Aihua Gu, Christian Mosimann, Samuel Sondalle, Richard E. Peterson, Warren Heideman, Caroline E. Burns, and C. Geoffrey Burns. Latent TGF-βbinding protein 3 identifies a second heart field in zebrafish. *Nature*, 474(7353):645–648, 2011.

[70] D. Hami, A. C. Grimes, H.-J. Tsai, and M. L. Kirby. Zebrafish cardiac development requires a conserved secondary heart field. *Development*, 138(11):2389–2398, 2011.

[71] Hajime; Fukui, Takahiro; Miyazaki, Renee Wei-Yan; Yan Chow, Hiroyuki; Ishikawa, Hiroyuki; Nakajima, Julien; Vermot, Mochizuki; Naoki, and Naoki Mochizuki. Hippo signaling determines the number of venous pole cells that originate from the anterior lateral plate mesoderm. *eLife*, 7:e29106, 2018.

[72] Vanessa George, Sophie Colombo, and Kimara L. Targoff. An early requirement for nkx2.5 ensures the first and second heart field ventricular identity and cardiac function into adulthood. *Developmental Biology*, 400(1):10–22, 2015.

[73] Christian Mosimann, Daniela Panáková, Andreas A. Werdich, Gabriel Musso, Alexa Burger, Katy L. Lawson, Logan A. Carr, Kathleen R. Nevis, M. Khaled Sabeh, Yi Zhou, Alan J. Davidson, Anthony Dibiase, Caroline E. Burns, C. Geoffrey Burns, Calum A. Macrae, and Leonard I. Zon. Chamber identity programs drive early functional partitioning of the heart. *Nature Communications*, 6(8146):1–10, 2015.

[74] Noelle Paffett-Lugassy, Natasha Novikov, Spencer Jeffrey, Maryline Abrial, Burcu Guner-Ataman, Srinivasan Sakthivel, Caroline E. Burns, and C. Geoffrey Burns. Unique developmental trajectories and genetic regulation of ventricular and outflow tract progenitors in the zebrafish second heart field. *Development*, 144:4616–4624, 2017.

[75] Jeffrey J. Schoenebeck, Brian R. Keegan, and Deborah Yelon. Vessel and Blood Specification Override Cardiac Potential in Anterior Mesoderm. *Developmental Cell*, 13(2):254–267, 2007.

[76] Serbedzija Gn, Chen Jn, and Fishman Mc. Regulation in the heart field of zebrafish. *Development*, 125(6):1095–1101, 1998.

[77] B. R. Keegan, Dirk Meyer, and Deborah Yelon. Organization of cardiac chamber progenitors in the zebrafish blastula. *Development*, 131(13):3081–3091, 2004.

[78] A. F. M. Moorman and V. M. Christoffels. Cardiac Chamber Formation: Development, Genes, and Evolution. *Physiological Reviews*, 83(4):1223–1267, 2003.

[79] Jeroen Bakkers. Zebrafish as a model to study cardiac development and human cardiac disease. *Cardiovascular Research*, 91(2):279–288, 2011.

[80] N. G. Holtzman, J. J. Schoenebeck, H.-J. Tsai, and D. Yelon. Endocardium is necessary for cardiomyocyte movement during heart tube assembly. *Development*, 134(12):2379–2386, 2007.

[81] K. Baker, N. G. Holtzman, and R. D. Burdine. Direct and indirect roles for Nodal signaling in two axis conversions during asymmetric morphogenesis of the zebrafish heart. *Proceedings of the National Academy of Sciences*, 105(37):13924–13929, 2008.

[82] Kelly A. Smith, Sonja Chocron, Sophia von der Hardt, Emma de Pater, Alexander Soufan, Jeroen Bussmann, Stefan Schulte-Merker, Matthias Hammerschmidt, and Jeroen Bakkers. Rotation and Asymmetric Development of the Zebrafish Heart Requires Directed Migration of Cardiac Progenitor Cells. *Developmental Cell*, 14(2):287–297, 2008.

[83] Oscar H. Ocaña, Hakan Coskun, Carolina Minguillón, Prayag Murawala, Elly M. Tanaka, Joan Galcerán, Ramón Muñoz-Chápuli, and M. Angela Nieto. A right-handed signalling pathway drives heart looping in vertebrates. *Nature*, 549(7670):86–90, 2017.

[84] Le A. Trinh and Didier Y.R. Stainier. Fibronectin regulates epithelial organization during myocardial migration in zebrafish. *Developmental Cell*, 6(3):371–382, 2004.

[85] Sally Horne-Badovinac, Dan Lin, Steve Waldron, Monica Schwarz, Geraldine Mbamalu, Tony Pawson, Yuh Nung Jan, Didier Y.R. Stainier, and Salim Abdelilah-Seyfried. Positional cloning of heart and soul reveals multiple roles for PKCλ in zebrafish organogenesis. *Current Biology*, 11(19):1492–1502, 2001.

[86] Randall T. Peterson, John D. Mably, Jau Nian Chen, and Mark C. Fishman. Convergence of distinct pathways to heart patterning revealed by the small molecule concentramide and the mutation heart-and-soul. *Current Biology*, 11(19):1481–1491, 2001.

[87] S. Rohr. Heart and soul/PRKCi and nagie oko/Mpp5 regulate myocardial coherence and remodeling during cardiac morphogenesis. *Development*, 133(1):107–115, 2006.

[88] Emily S. Noël, Manon Verhoeven, Anne Karine Lagendijk, Federico Tessadori, Kelly Smith, Suma Choorapoikayil, Jeroen Den Hertog, and Jeroen Bakkers. A Nodal-independent and tissue-intrinsic mechanism controls heart-looping chirality. *Nature Communications*, 4, 2013.

[89] Stefan Rohr, Cécile Otten, and Salim Abdelilah-Seyfried. Asymmetric involution of the myocardial field drives heart tube formation in zebrafish. *Circulation Research*, 102(2):12–19, 2008.

[90] Jeroen Bussmann, Jeroen Bakkers, and Stefan Schulte-Merker. Early endocardial morphogenesis requires Scl/Tal1. *PLoS Genetics*, 3(8):1425–1437, 2007.

[91] E. de Pater, L. Clijsters, S. R. Marques, Y.-F. Lin, Z. V. Garavito-Aguilar, D. Yelon, and J. Bakkers. Distinct phases of cardiomyocyte differentiation regulate growth of the zebrafish heart. *Development*, 136(10):1633–1641, 2009.

[92] Larry A. Taber, Dmitry A. Voronov, and Ashok Ramasubramanian. The role of mechanical forces in the torsional component of cardiac looping. *Annals of the New York Academy of Sciences*, 1188:103–110, 2010.

[93] Martina Burczyk, Martin D. Burkhalter, Tamara Blätte, Sabrina Matysik, Marc G. Caron, Lawrence S. Barak, and Melanie Philipp. Phenotypic regulation of the sphingosine 1-phosphate receptor miles apart by G protein-coupled receptor kinase 2. *Biochemistry*, 54(3):765–775, 2015.

[94] DY Stainier, B Fouquet, JN Chen, JS Warren, BM Weinstein, SE Meiler, MA Mohideen, SC Neuhauss, L Solnica-Krezel, AF Schier, F Zwartkruis, DL Stemple, J Malicki, W Driever, and M C Fishman. Mutations affecting the formation and function of the cardiovascular system in the zebrafish embryo. *Development*, 123:285–292, 1996.

[95] Hajime Fukui, Kenta Terai, Hiroyuki Nakajima, Ayano Chiba, Shigetomo Fukuhara, and Naoki Mochizuki. S1P-Yap1 signaling regulates endoderm formation required for cardiac precursor cell migration in zebrafish. *Developmental Cell*, 31(1):128–136, 2014.

[96] E Kupperman, S An, N Osborne, S Waldron, and D Y Stainier. A sphingosine-1-phosphate receptor regulates cell migration during vertebrate heart development. *Nature*, 406(6792):192–5, 2000.

[97] Maria Ines Medeiros De Campos-Baptista, Nathalia Glickman Holtzman, Deborah Yelon, and Alexander F. Schier. Nodal signaling promotes the speed and directional movement of cardiomyocytes in zebrafish. *Developmental Dynamics*, 237(12):3624–3633, 2008.

[98] Alexandra Lepilina, Ashley N. Coon, Kazu Kikuchi, Jennifer E. Holdway, Richard W. Roberts, C. Geoffrey Burns, and Kenneth D. Poss. A Dynamic Epicardial Injury Response Supports Progenitor Cell Activity during Zebrafish Heart Regeneration. *Cell*, 127(3):607–619, 2006.

[99] Harold E. Olivey and Eric C. Svensson. Epicardial-myocardial signaling directing coronary vasculogenesis. *Circulation Research*, 106(5):818–832, 2010.

[100] Jessica S. Plavicki, Peter Hofsteen, Monica S. Yue, Kevin A. Lanham, Richard E. Peterson, and Warren Heideman. Multiple modes of proepicardial cell migration require heartbeat. *BMC Developmental Biology*, 14(1), 2014.

[101] Jiandong Liu and Didier Y R Stainier. Tbx5 and Bmp signaling are essential for proepicardium specification in zebrafish. *Circulation Research*, 106(12):1818–1828, 2010.

[102] Fabrizio C. Serluca. Development of the proepicardial organ in the zebrafish. *Developmental Biology*, 315(1):18–27, 2008.

[103] Richard N. Bamford, Erich Roessler, Rebecca D. Burdine, Umay aplakolu, June Dela Cruz, Miranda Splitt, Jeffrey Towbin, Peter Bowers, Bruno Marino, Alexander F. Schier, Michael M. Shen, Maximilian Muenke, and Brett Casey. Loss-of-function mutations in the EGF-CFC gene CFC1 are associated with human left-right laterality defects. *Nature Genetics*, 26(3):365–369, 2000.

[104] Karen S. Kuehl and Christopher Loffredo. Risk factors for heart disease associated with abnormal sidedness. *Teratology*, 66(5):242–248, 2002.

[105] Hilde Peeters and Koen Devriendt. Human laterality disorders. *European Journal of Medical Genetics*, 49(5):349–362, 2006.

[106] Jeroen Bakkers, Manon C. Verhoeven, and Salim Abdelilah-Seyfried. Shaping the zebrafish heart: From left-right axis specification to epithelial tissue morphogenesis. *Developmental Biology*, 330(2):213–220, 2009.

[107] Jau-Nian Chen, Frauke van Bebber, Allan M. Goldstein, Fabrizio C. Serluca, Donald Jackson, Sarah Childs, George Serbedzija, Kerri S. Warren, John D. Mably, Per Lindalhl, Alan Mayer, Pascal Haffter, and Mark C Fishman. Genetic steps to organ laterality in zebrafish. *Comparative and Functional Genomics*, 2(2):60–68, 2001.

[108] Jeffrey J. Essner, Kyle J. Vogan, Molly K. Wagner, Clifford J. Tabin, H. Joseph Yost, and Martina Brueckner. Conserved function for embryonic nodal cilia. *Nature*, 418(6893):37–38, 2002.

[109] J. J. Essner. Kupffer's vesicle is a ciliated organ of asymmetry in the zebrafish embryo that initiates left-right development of the brain, heart and gut. *Development*, 132(6):1247–1260, 2005.

[110] A. G. Kramer-Zucker. Cilia-driven fluid flow in the zebrafish pronephros, brain and Kupffer's vesicle is required for normal organogenesis. *Development*, 132(8):1907–1921, 2005.

[111] Kelly A. Smith, Emily Noël, Ingrid Thurlings, Holger Rehmann, Sonja Chocron, and Jeroen Bakkers. Bmp and Nodal independently regulate lefty1 expression to maintain unilateral Nodal activity during left-right axis specification in zebrafish. *PLoS Genetics*, 7(9), 2011.

[112] Chikara Meno, Akihiko Shimono, Yukio Saijoh, Kenta Yashiro, Kyoko Mochida, Sachiko Ohishi, Sumihare Noji, Hisato Kondoh, and Hiroshi Hamada. Lefty-1 Is Required for Left-Right Determination As a Regulator of Lefty-2 and Nodal. *Cell*, 94(3):287–297, 1998.

[113] Bernard Thisse, Christopher V E Wright, and Christine Thisse. Activin- and Nodal-related factors control antero-posterior patterning of the zebrafish embryo. *Nature*, 403:425–428, 2000.

[114] S. Long, N. Ahmad, and M. Rebagliati. The zebrafish nodal-related gene southpaw is required for visceral and diencephalic left-right asymmetry. *Development*, 130(11):2303–2316, 2003.

[115] Sonja Chocron, Manon C. Verhoeven, Fabian Rentzsch, Matthias Hammerschmidt, and Jeroen Bakkers. Zebrafish Bmp4 regulates left-right asymmetry at two distinct developmental time points. *Developmental Biology*, 305(2):577–588, 2007.

[116] Ketan Patel, Alison Isaac, and Jonathan Cooke. Nodal signalling and the roles of the transcription factors SnR and Pitx2 in vertebrate left-right asymmetry. *Current Biology*, 9(11):609–612, 1999.

[117] Aimee K. Ryan, Bruce Blumberg, Concepción Rodriguez-Esteban, Sayuri Yonei-Tamura, Koji Tamura, Tohru Tsukui, Jennifer De La Peña, Walid Sabbagh, Jason Greenwald, Senyon Choe, Dominic P. Norris, Elizabeth J. Robertson, Ronald M. Evans, Michael G. Rosenfeld, and Juan Carlos Izpisúa Belmonte. Pitx2 determines left-right asymmetry of internal organs in vertebrates. *Nature*, 394(6693):545–551, 1998.

[118] Marina Campione, Herbert Steinbeisser, Axel Schweickert, Kirsten Deissler, Frauke van Bebber, Linda A. Lowe, Sonja Nowotschin, Christoph Viebahn, Pascal Haffter, Michael R. Kuehn, and Martin Blum. The homeobox gene Pitx2: mediator of asymmetric left-right signaling in vertebrate heart and gut looping. *Development*, 126(6):1225–1234, 1999.

[119] Philip J Gage, Hoonkyo Suh, and Sally A Camper. Dosage requirement of Pitx2 for development of multiple organs. *Development*, 126:4643–4651, 1999.

[120] Malcolm Logan, Sylvia M. Pagán-Westphal, Devyn M. Smith, Laura Paganessi, and Clifford J. Tabin. The transcription factor pitx2 mediates situs-specific morphogenesis in response to left-right asymmetric signals. *Cell*, 94(3):307–317, 1998.

[121] M. Elisa Piedra, Jose M. Icardo, Marta Albajar, Jose C. Rodriguez-Rey, and Maria A. Ros. Pitx2 participates in the late phase of the pathway controlling left- right asymmetry. *Cell*, 94(3):319–324, 1998.

[122] Diego Franco and Marina Campione. The role of Pitx2 during cardiac development: Linking left-right signaling and congenital heart diseases. *Trends in Cardiovascular Medicine*, 13(4):157–163, 2003.

[123] Chijen R. Lin, Chrissa Kloussi, Shawn O'Connell, Paola Briata, Daniel Szeto, Forrest Liu, Juan Carlos Izpisúa-Belmonte, and Michael G. Rosenfeld. Pitx2 regulates lung asymmetry, cardiac positioning and pituitary and tooth morphogenesis. *Nature*, 401(6750):279–282, 1999.

[124] K Kitamura, H Miura, S Miyagawa-Tomita, M Yanazawa, Y Katoh-Fukui, R Suzuki, H Ohuchi, A Suehiro, Y Motegi, Y Nakahara, S Kondo, and M Yokoyama. Mouse

Pitx2 deficiency leads to anomalies of the ventral body wall, heart, extra- and periocular mesoderm and right pulmonary isomerism. *Development (Cambridge, England)*, 126(24):5749–58, 1999.

[125] Mei-fang Lu, Carolyn Pressman, Rex Dyer, and Randy L Johnson. Function of Rieger syndrome gene in left right asymmetry and craniofacial development. *Nature*, 401(September):1998–2000, 1999.

[126] Marie Laurence Mucchielli, Salvador Martinez, Alexandre Pattyn, Christo Goridis, and Jean François Brunet. Otlx2, an Otx-related homeobox gene expressed in the pituitary gland and in a restricted pattern in the forebrain. *Molecular and Cellular Neurosciences*, 8(4):258–271, 1996.

[127] J N Chen, F J van Eeden, K S Warren, A Chin, C Nusslein-Volhard, P Haffter, and M C Fishman. Left-right pattern of cardiac BMP4 may drive asymmetry of the heart in zebrafish. *Development*, 124(21):4373 LP – 4382, nov 1997.

[128] Yasuhiko Kawakami, Ángel Raya, R. Marína Raya, Concepción Rodriguez-Esteban, and Juan Carlos Izplsúa Belmonte. Retinoic acid signalling links left-right asymmetric patterning and bilaterally symmetric somitogenesis in the zebrafish embryo. *Nature*, 435(7039):165–171, 2005.

[129] Alvin J Chin, Michael Tsang, and Eric S Weinberg. Heart and Gut Chiralities Are Controlled Independently from Initial Heart Position in the Developing Zebrafish. *Developmental Biology*, 227(2):403–421, 2000.

[130] Rebecca Powell, Ekaterina Bubenshchikova, Yayoi Fukuyo, Chaonan Hsu, Olga Lakiza, Hiroki Nomura, Erin Renfrew, Deborah Garrity, and Tomoko Obara. Wtip is required for proepicardial organ specification and cardiac left/right asymmetry in zebrafish. *Molecular Medicine Reports*, 14(3):2665–2678, 2016.

[131] Almary Guerra, Raoul F.V. Germano, Oliver Stone, Rima Arnaout, Stefan Guenther, Suchit Ahuja, Verónica Uribe, Benoit Vanhollebeke, Didier Y.R. Stainier, and Sven Reischauer. Distinct myocardial lineages break atrial symmetry during cardiogenesis in zebrafish. *eLife*, 7:1–26, 2018.

[132] Rangarajan D. Nadadur, Michael T. Broman, Bastiaan Boukens, Stefan R. Mazurek, Xinan Yang, Malou Van Den Boogaard, Jenna Bekeny, Margaret Gadek, Tarsha Ward, Min Zhang, Yun Qiao, James F. Martin, Christine E. Seidman, Jon Seidman, Vincent Christoffels, Igor R. Efimov, Elizabeth M. McNally, Christopher R. Weber, and Ivan P. Moskowitz. Pitx2 modulates a Tbx5-dependent gene regulatory network to maintain atrial rhythm. *Science Translational Medicine*, 8(354):354ra115, 2016.

[133] Lisa J. Sletten and Mary Ella M Pierpont. Variation in severity of cardiac disease in Holt-Oram syndrome. *American Journal of Medical Genetics*, 65(2):128–132, 1996.

[134] Fatima A. Sulaiman, Satoko Nishimoto, George R.F. Murphy, Anna Kucharska, Natalie C. Butterfield, Ruth Newbury-Ecob, and Malcolm P.O. Logan. Tbx5 Buffers Inherent Left/Right Asymmetry Ensuring Symmetric Forelimb Formation. *PLoS Genetics*, 12(12):1–18, 2016.

[135] A Wessels, R H Anderson, R R Markwald, S Webb, N A Brown, S Viragh, A F Moorman, and W H Lamers. Atrial development in the human heart: an immunohistochemical study with emphasis on the role of mesenchymal tissues. *The Anatomical record*, 259(3):288–300, jul 2000.

[136] Andreas Kispert and Bernhard G Herrmann. The Brachyury gene encodes a novel DNA binding protein. *EMBO Journal*, 12(8):3211 –3220, 1993.

[137] Benoit G. Bruneau, Malcolm Logan, Nicole Davis, Tatjana Levi, Clifford J. Tabin, J. G. Seidman, and Christine E. Seidman. Chamber-specific cardiac expression of Tbx5 and heart defects in Holt- Oram syndrome. *Developmental Biology*, 211(1):100–108, 1999.

[138] Ricard Albalat, Mireia Baquero, and Carolina Minguillón. Identification and characterisation of the developmental expression pattern of tbx5b, a novel tbx5 gene in zebrafish. *Gene Expression Patterns*, 10(1):24–30, 2010.

[139] Deborah M Garrity, Sarah Childs, and Mark C Fishman. The heartstrings mutation in zebrafish causes heart/fin Tbx5 deficiency syndrome. *Development (Cambridge, England)*, 129:4635–4645, 2002.

[140] Aina Pi-Roig, Enrique Martin-Blanco, and Carolina Minguillon. Distinct tissue-specific requirements for the zebrafish tbx5 genes during heart, retina and pectoral fin development. *Open Biology*, 4(APRIL):140014, 2014.

[141] Craig T Basson1, David R. Bachinsky, Robert C. Lin, Tatjana Levi, Jacob A. Elkins, Johann Soults, David Grayzel, Elena Kroumpouzou, Thomas A. Traill, Janine Leblanc-Straceski, Beatrice Renault, Raju Kucherlapati, Seidman J.G, Christine E. Seidman, Craig T. Basson, David R. Bachinsky, Robert C. Lin, Tatjana Levi, Jacob A. Elkins, Johann Soults, David Grayzel, Elena Kroumpouzou, Thomas A. Traill, Janine Leblanc-Straceski, Beatrice Renault, Raju Kucherlapati, J. G. Seidman, and Christine E. Seidman. Mutations in human cause limb and cardiac malformation in Holt-Oram syndrome. *Nature Genetics*, 15(1):30, jan 1997.

[142] Quan Yi Li, Ruth A. Newbury-Ecob, Jonathan A. Terrett, David I. Wilson, Andrew R.J. Curtis, Cheong Ho Yi, Tom Gebühr, Philip J. Bullen, Stephen C. Robson, Tom Strachan, Damien Bonnet, Stanislas Lyonnet, Ian D. Young, J. Alexander Raeburn, Alan J. Buckler, David J. Law, and J. David Brook. Holt-Oram syndrome is caused by mutations in TBX5, a member of the Brachyury (T) gene family. *Nature Genetics*, 15(1):21–29, 1997.

[143] Ariel B. Rydeen and Joshua S. Waxman. Cyp26 Enzymes Facilitate Second Heart Field Progenitor Addition and Maintenance of Ventricular Integrity. *PLoS Biology*, 14(11):1–25, 2016.

[144] G. Musso, C. Mosimann, D. Panáková, A. Burger, Y. Zhou, L. I. Zon, and C. A. MacRae. Generating and evaluating a ranked candidate gene list for potential vertebrate heart field regulators. *Genomics Data*, 6:199–201, 2015.

[145] Sarah C. Rothschild, Charles A. Easley IV, Ludmila Francescatto, James A. Lister, Deborah M. Garrity, and Robert M. Tombes. Tbx5-mediated expression of Ca2+/calmodulin-dependent protein kinase II is necessary for zebrafish cardiac and pectoral fin morphogenesis. *Developmental Biology*, 330(1):175–184, 2009.

[146] Mohamed A. El-Brolosy and Didier Y.R. Stainier. Genetic compensation: A phenomenon in search of mechanisms. *PLoS Genetics*, 13(7):1–17, 2017.

[147] Andrea Rossi, Zacharias Kontarakis, Claudia Gerri, Hendrik Nolte, Soraya Hölper, Marcus Krüger, and Didier Y.R. Stainier. Genetic compensation induced by deleterious mutations but not gene knockdowns. *Nature*, 524(7564):230–233, 2015.

[148] Christoph W. Muller and Bernhard G. Herrmann. Crystallographic structure of the T domain-DNA complex of the Brachyury transcription factor. *Nature*, 389(6653):884–888, 1997.

[149] Franziska Greulich, Carsten Rudat, and Andreas Kispert. Mechanisms of T-box gene function in the developing heart. *Cardiovascular Research*, 91(2):212–222, 2011.

[150] A. He, S. W. Kong, Q. Ma, and W. T. Pu. Co-occupancy by multiple cardiac transcription factors identifies transcriptional enhancers active in heart. *Proceedings of the National Academy of Sciences*, 108(14):5632–5637, 2011.

[151] T. K. Ghosh, F. F. Song, E. A. Packham, S. Buxton, T. E. Robinson, J. Ronksley, T. Self, A. J. Bonser, and J. D. Brook. Physical Interaction between TBX5 and MEF2C Is Required for Early Heart Development. *Molecular and Cellular Biology*, 29(8):2205–2218, 2009.

[152] Meenakshi Maitra, Marie K. Schluterman, Haley A. Nichols, James A. Richardson, Cecilia W. Lo, Deepak Srivastava, and Vidu Garg. Interaction of Gata4 and Gata6 with Tbx5 is critical for normal cardiac development. *Developmental Biology*, 326(2):368–377, 2009.

[153] Eric M. Small and Paul A. Krieg. Transgenic analysis of the atrialnatriuretic factor (ANF) promoter: Nkx2-5 and GATA-4 binding sites are required for atrial specific expression of ANF. *Developmental Biology*, 261(1):116–131, 2003.

[154] Jun K. Takeuchi and Benoit G. Bruneau. Directed transdifferentiation of mouse mesoderm to heart tissue by defined factors. *Nature*, 459(7247):708–711, 2009.

[155] Luis Luna-Zurita, Christian U. Stirnimann, Sebastian Glatt, Bogac L. Kaynak, Sean Thomas, Florence Baudin, Md Abul Hassan Samee, Daniel He, Eric M. Small, Maria Mileikovsky, Andras Nagy, Alisha K. Holloway, Katherine S. Pollard, Christoph W. Müller, and Benoit G. Bruneau. Complex Interdependence Regulates Heterotypic Transcription Factor Distribution and Coordinates Cardiogenesis. *Cell*, 164(5):999–1014, 2016.

[156] Lauren Waldron, Jeffrey D. Steimle, Todd M. Greco, Nicholas C. Gomez, Kerry M. Dorr, Junghun Kweon, Brenda Temple, Xinan Holly Yang, Caralynn M. Wilczewski, Ian J. Davis, Ileana M. Cristea, Ivan P. Moskowitz, and Frank L. Conlon. The Cardiac TBX5 Interactome Reveals a Chromatin Remodeling Network Essential for Cardiac Septation. *Developmental Cell*, 36(3):262–275, 2016.

[157] C. Rallis, Benoit G. Bruneau, J. Del Buono, Christine E. Seidman, J. G. Seidman, S. Nissim, Clifford J. Tabin, and Malcolm P.O. Logan. Tbx5 is required for forelimb bud formation and continued outgrowth. *Development*, 130(12):2741–2751, 2003.

[158] Cathy J. Hatcher, Min Su Kim, Caroline S. Mah, Marsha M. Goldstein, Benjamin Wong, Takashi Mikawa, and Craig T. Basson. TBX5 transcription factor regulates cell proliferation during cardiogenesis. *Developmental Biology*, 230(2):177–188, 2001.

[159] Cathy J. Hatcher, Nata Y.S.-G. Diman, Min-Su Kim, David Pennisi, Yan Song, Marsha M. Goldstein, Takashi Mikawa, and Craig T. Basson. A role for Tbx5 in proepicardial cell migration during cardiogenesis. *Physiological Genomics*, 18(2):129–140, 2004.

[160] Monica S. Yue, Jessica S. Plavicki, Xin Yi Li, Richard E. Peterson, and Warren Heideman. A co-culture assay of embryonic zebrafish hearts to assess migration of epicardial cells in vitro Organogenesis. *BMC Developmental Biology*, 15(1):1–9, 2015.

[161] Jiandong Liu and Didier Y R Stainier. Zebrafish in the study of early cardiac development. *Circulation research*, 110(6):870–874, 2012.

[162] T. Piotrowski, Dae-gwon Ahn, Thomas F Schilling, Sreelaja Nair, Ilya Ruvinsky, Robert Geisler, Gerd-Jörg Rauch, Pascal Haffter, Leonard I Zon, Yi Zhou, Helen Foott, Igor B Dawid, and Robert K. Ho. The zebrafish van gogh mutation disrupts tbx1, which is involved in the DiGeorge deletion syndrome in humans. *Development*, 130(20):5043–5052, 2003.

[163] Jorge N. Domínguez, Sigolène M. Meilhac, Yvette S. Bland, Margaret E. Buckingham, and Nigel A. Brown. Asymmetric fate of the posterior part of the second heart field results in unexpected left/right contributions to both poles of the heart. *Circulation research*, 111(10):1323–1335, 2012.

[164] Wenge Lu, Steven H. Seeholzer, Mingda Han, Anne Sophie Arnold, Maria Serrano, Barbara Garita, Nancy J. Philp, Cassandra Farthing, Peter Steele, Jizhen Chen, and

Kersti K. Linask. Cellular nonmuscle myosins NMHC-IIA and NMHC-IIB and vertebrate heart looping. *Developmental Dynamics*, 237(12):3577–3590, 2008.

[165] Justus Veerkamp, Franziska Rudolph, Zoltan Cseresnyes, Florian Priller, Cécile Otten, Marc Renz, Liliana Schaefer, and Salim Abdelilah-Seyfried. Unilateral Dampening of Bmp Activity by Nodal Generates Cardiac Left-Right Asymmetry. *Developmental Cell*, 24(6):660–667, 2013.

[166] Héctor Sánchez-Iranzo, María Galardi-Castilla, Carolina Minguillón, Andrés Sanz-Morejón, Juan Manuel González-Rosa, Anastasia Felker, Alexander Ernst, Gabriela Guzmán-Martínez, Christian Mosimann, and Nadia Mercader. Tbx5a lineage tracing shows cardiomyocyte plasticity during zebrafish heart regeneration. *Nature Communications*, 9(428):1–13, 2018.

[167] Luca Caputo, Hagen R. Witzel, Petros Kolovos, Sirisha Cheedipudi, Mario Looso, Athina Mylona, Wilfred F.J. Van Ijcken, Karl Ludwig Laugwitz, Sylvia M. Evans, Thomas Braun, Eric Soler, Frank Grosveld, and Gergana Dobreva. The Isl1/Ldb1 Complex Orchestrates Genome-wide Chromatin Organization to Instruct Differentiation of Multipotent Cardiac Progenitors. *Cell Stem Cell*, 17(3):287–299, 2015.

[168] Benoit G. Bruneau, Georges Nemer, Joachim P. Schmitt, Frédéric Charron, Lynda Robitaille, Sophie Caron, David A. Conner, Manfred Gessler, Mona Nemer, Christine E. Seidman, and J. G. Seidman. A murine model of Holt-Oram syndrome defines roles of the T-Box transcription factor Tbx5 in cardiogenesis and disease. *Cell*, 106(6):709–721, 2001.

[169] Timothy F. Plageman and Katherine E. Yutzey. Microarray analysis of Tbx5-induced genes expressed in the developing heart. *Developmental Dynamics*, 235(10):2868–2880, 2006.

[170] M E Horb and G H Thomsen. Tbx5 is essential for heart development. *Development (Cambridge, England)*, 126(8):1739–51, 1999.

[171] Kari F. Lenhart, Nathalia G. Holtzman, Jessica R. Williams, and Rebecca D. Burdine. Integration of Nodal and BMP Signals in the Heart Requires FoxH1 to Create Left-Right Differences in Cell Migration Rates That Direct Cardiac Asymmetry. *PLoS Genetics*, 9(1), 2013.

[172] Roman Gorelik and Alexis Gautreau. Quantitative and unbiased analysis of directional persistence in cell migration. *Nature Protocols*, 9(8):1931–1943, 2014.

[173] A. Kaufmann, M. Mickoleit, M. Weber, and J. Huisken. Multilayer mounting enables long-term imaging of zebrafish development in a light sheet microscope. *Development*, 139(17):3242–3247, 2012.

[174] Martin Behrndt, Julia Roensch, Stephan W Grill, and Carl-philipp Heisenberg. Forces Driving Epithelial Spreading in Zebrafish Gastrulation. *Science*, 338(6014):257–260, 2012.

[175] Adam D Langenbacher, Catherine T Nguyen, Ann M Cavanaugh, Jie Huang, Fei Lu, and Jau-nian Chen. The PAF1 complex differentially regulates cardiomyocyte speci fi cation. *Developmental Biology*, 353(1):19–28, 2011.

[176] Fei Lu, Adam Langenbacher, and Jau Nian Chen. Tbx20 drives cardiac progenitor formation and cardiomyocyte proliferation in zebrafish. *Developmental Biology*, 421(2):139–148, 2017.

[177] Erin A T Boyle Anderson and Robert K Ho. A transcriptomics analysis of the Tbx5 paralogues in zebrafish. *PLoS ONE*, 13(12):e0208766, 2018.

[178] Audrey Desgrange, Jean-François Le Garrec, and Sigolène M. Meilhac. Left-right asymmetry in heart development and disease: forming the right loop. *Development*, 145(22):dev162776, 2018.

[179] Nobue Itasaki, Harukazu Nakamura, Hiroshi Sumida, and Mineo Yasuda. Actin bundles on the right side in the caudal part of the heart tube play a role in dextro-looping in the embryonic chick heart. *Anatomy and Embryology*, 183(1):29–39, 1991.

[180] Francis J. Manasek, M. Beth Burnside, and Robert E. Waterman. Myocardial cell shape change as a mechanism of embryonic heart looping*1. *Developmental Biology*, 29(4):349–371, 1972.

[181] Jean François Le Garrec, Jorge N. Domínguez, Audrey Desgrange, Kenzo D. Ivanovitch, Etienne Raphaël, J. Andrew Bangham, Miguel Torres, Enrico Coen, Timothy J. Mohun, and Sigolène M. Meilhac. A predictive model of asymmetric morphogenesis from 3D reconstructions of mouse heart looping dynamics. *eLife*, 6:1–35, 2017.

[182] Meriç Bayraktar and Jörg Männer. Cardiac looping may be driven by compressive loads resulting from unequal growth of the heart and pericardial cavity. Observations on a physical simulation model. *Frontiers in Physiology*, 5 APR(April):1–15, 2014.

[183] Nandan L. Nerurkar, Ashok Ramasubramanian, and Larry A. Taber. Morphogenetic adaptation of the looping embryonic heart to altered mechanical loads. *Developmental Dynamics*, 235(7):1822–1829, 2006.

[184] Hinako Kidokoro, Masataka Okabe, and Koji Tamura. Time-lapse analysis reveals local asymmetrical changes in C-looping heart tube. *Developmental Dynamics*, 237(12):3545–3556, 2008.

[185] BM Patten. The formation of the cardiac loop in the chick. *American Journal of Anatomy1*, 30:373–397, 1922.

[186] M E Fransen and L F Lemanski. Myocardial cell relationships during morphogenesis in normal and cardiac lethal mutant axolotls, Ambystoma mexicanum. *The American journal of anatomy*, 183(3):245–257, nov 1988.

[187] Ian C. Mitchell, Timothy S. Brown, Lance S. Terada, James F. Amatruda, and Fiemu E. Nwariaku. Effect of vascular cadherin knockdown on zebrafish vasculature during development. *PLoS ONE*, 5(1), 2010.

[188] Jenher Lu, Tzuchun Tsai, Sielin Choo, Shuyu Yeh, Renbing Tang, Anhang Yang, Hsinyu Lee, and Jennkan Lu. Induction of apoptosis and inhibition of cell growth by tbx5 knockdown contribute to dysmorphogenesis in Zebrafish embryos. *Journal of Biomedical Science*, 18(1):1–10, 2011.

[189] Sophia von der Hardt, Jeroen Bakkers, Adi Inbal, Lara Carvalho, Lilianna Solnica-Krezel, Carl Philipp Heisenberg, and Matthias Hammerschmidt. The Bmp Gradient of the Zebrafish GastrulaGuidesMigrating Lateral CellsbyRegulating Cell-Cell Adhesion. *Current Biology*, 17(6):475–487, 2007.

[190] Tzu Chun Tsai, Chun Che Shih, Hsin Ping Chien, An Hang Yang, Jenn Kan Lu, and Jen Her Lu. Anti-apoptotic effects of IGF-I on mortality and dysmorphogenesis in tbx5-deficient zebrafish embryos. *BMC Developmental Biology*, 18(1):1–15, 2018.

[191] W Shoji and M Sato-Maeda. Application of heat shock promoter in transgenic zebrafish. *Development Growth and Differentiation2*, 50(6):401–6, 2008.

[192] Tomonori Deguchi, Mariko Itoh, Hiroko Urawa, Tomohiro Matsumoto, Sohei Nakayama, Takashi Kawasaki, Takeshi Kitano, Shoji Oda, Hiroshi Mitani, Taku Takahashi, Takeshi Todo, Junichi Sato, Kiyotaka Okada, Kohei Hatta, Shunsuke Yuba, and Yasuhiro Kamei. Infrared laser-mediated local gene induction in medaka, zebrafish and Arabidopsis thaliana. *Development Growth and Differentiation*, 51(9):769–775, 2009.

[193] Lindsay E. Parrie, Erin M. Renfrew, Aimee Vander Wal, Rachel Lockridge Mueller, and Deborah M. Garrity. Zebrafish tbx5 paralogs demonstrate independent essential requirements in cardiac and pectoral fin development. *Developmental Dynamics*, 242(5):485–402, 2013.

[194] Sundar Ram Naganathan, Teije C. Middelkoop, Sebastian Fürthauer, and Stephan W. Grill. Actomyosin-driven left-right asymmetry: From molecular torques to chiral self organization. *Current Opinion in Cell Biology*, 38:24–30, 2016.

[195] Christian S. M. Helker, Annika Schuermann, Terhi Karpanen, Dagmar Zeuschner, Heinz-Georg Belting, Markus Affolter, Stefan Schulte-Merker, and Wiebke Herzog. The zebrafish common cardinal veins develop by a novel mechanism: lumen ensheathment. *Development*, 140(13):2776–2786, 2013.

[196] Thomas O. Auer, Karine Duroure, Jean Paul Concordet, and Filippo Del Bene. CRISPR/Cas9-mediated conversion of eGFP- into Gal4-transgenic lines in zebrafish. *Nature Protocols*, 9(12):2823–2840, 2014.

[197] Monte Westerfield. *The Zebrafish Book*. University of Oregon Press, 5th edition, 2007.

[198] Carrie McMahon, Gaia Gestri, Stephen W. Wilson, and Brian A. Link. Lmx1b is essential for survival of periocular mesenchymal cells and influences Fgf-mediated retinal patterning in zebrafish. *Developmental Biology*, 332(2):287–298, 2009.

[199] Jia Li, Bai Bing Zhang, Yong Gang Ren, Shan Ye Gu, Yuan Hang Xiang, Cheng Huang, and Jiu Lin Du. Intron targeting-mediated and endogenous gene integrity-maintaining knockin in zebrafish using the CRISPR/Cas9 system. *Cell Research*, 25(5):634–637, 2015.

[200] Yukiko Kimura, Yu Hisano, Atsuo Kawahara, and Shin Ichi Higashijima. Efficient generation of knock-in transgenic zebrafish carrying reporter/driver genes by CRISPR/Cas9-mediated genome engineering. *Scientific Reports*, 4:1–7, 2014.

[201] Shahad Albadri, Filippo Del Bene, and Céline Revenu. Genome editing using CRISPR/Cas9-based knock-in approaches in zebrafish. *Methods*, 121-122:77–85, 2017.

[202] Reuben Thomas, Sean Thomas, Alisha K. Holloway, and Katherine S. Pollard. Features that define the best ChIP-seq peak calling algorithms. *Briefings in Bioinformatics*, 18(3):441–450, 2017.